ESTIMATING BODY SEGMENT INERTIAL PARAMETERS OF THE HUMAN BODY USING A MICROSOFT KINECT

by

Pawel Kudzia

A thesis submitted to the Department of Mechanical and Materials Engineering

In conformity with the requirements for

the degree of Master of Applied Science

Queen's University

Kingston, Ontario, Canada

October 2015

Abstract

Estimating biomechanical measures of the human body requires body segment inertial parameters (BSIP). Widely cited estimation methods (Chandler et al., 1975; Dempster, 1955) are based on an elderly population, have inherent errors (Hanavan, 1964) and may not represent subjects to which they are applied. Subject specific methods such as medical imaging or geometrical techniques can be time consuming, expensive and may require a variety of manually acquired inputs. Presented here is an alternative, subject specific approach to estimating BSIPs, requiring no manual measurements at a equipment cost of approximately $300.

A 3D scanning protocol using a single Microsoft Kinect V2 was developed. Twenty-one subjects (10 male, 11 female) were scanned 3 times with per scan durations of approximately 20-30 seconds. Each full body 3D scan was segmented in Meshlab according to a 16 segment link model defined by Zatsiorsky and Seluyanov (1983). The 3D data was analyzed in custom MATLAB software that estimated the volume, MOI, COM, length and mass of each of the link segments. Results were compared to estimates obtained using an elliptical cylinder model (ECM) (Jensen 1978) and to estimates obtained using regression equations developed from medical imaging techniques (Zatsiorsky and Seluyanov 1983).

The body volume estimates using the Kinect demonstrated high repeatability (ICC≥0.95) with a volume overestimation ranging from 0.0023 m^3 (3%) for males and 0.0038m^3 (5.1%) for females. The upper torso accounted for the majority of the overestimation of approximately 0.0019m^3 (83%) for males and 0.002 m^3 (53%) for the females. The Kinect protocol estimated COM with an average error of <2%. Segmental mass estimates were overestimated by 3.11% for males and 5.23% for females when compared to ECM. This research established that the Kinect V2 could be used as a tool for BSIP estimation. Future work should improve on the scanning posture, scanning protocol and reducing the scan duration. Furthermore, future research should investigate on methods to eliminate the manual segmentation proposed for this protocol.

Acknowledgments

I would like to thank all of the people in the biomechanical community at Queen's who have inspired me to learn and provided me with friendship and consultation along the way. Erika, for your help in acquiring my data and for general lab laughs. I am very grateful and could not have done it without you. Conte, thank you for being a great friend and always being there and supporting me in all of my endeavors. Jon, without your computer this project would have been delayed, I am very appreciative. Thanks, as well, to Dr. Rainbow, who provided me with important code and guidance along the way. Jan Sneep, thank you for the passionate conversations at all times of the day. Thank you to my colleagues at the HMRC for lab space.

Most importantly, thank you to Dr. Genevieve Dumas, your support and encouragement during the various stages of this project were critical. It's been a great experience working with you. Your dedication towards your students is incredible. Thank you so much for everything.

I am grateful to my wonderful roommates over the years (Brendan, Jon^2, Will, Dave, Sam, Liz) and for amazing friendships from Queen's First Aid, triathlon and climbing. James, for pushing me to be a better triathlete; I look forward to the Ironman. Eleanor, thank you for your endless encouragements. Dr. Deluzio, thanks for being an excellent and approachable teacher! Finally, thank you to my parents for always providing me with support and delicious food along the way.

Queen's has been an unforgettable experience filled with memories that I will always look back on very fondly. All of the wonderful people I have met over my time here have influenced me into the person that I am now. I am very grateful for this. I look forward to my next adventure and to continue the pursuit of knowledge.

If something is important enough,
even if the odds are against you,
you should still do it – Elon Musk

Table of Contents

Chapter 4 Results

Chapter 5 Discussion

Chapter 6 Conclusions and Recommendations

References

Appendices

List of Figures

List of Tables

Nomenclature

COM – Center of Mass

MOI – Moment of Inertia

ECM – Elliptical Cylinder Model

SD - Standard Deviation

BSIP – Body segment inertial parameter

BMI - Body mass index

While human ingenuity may devise various inventions to the same ends, it will never devise anything more beautiful, nor more simple, nor more to the purpose than nature does, because in her inventions nothing is lacking and nothing is superfluous

-Leonardo da Vinci

Chapter 1
Introduction

1.0 The Human Body

Differences in the environments we are exposed to, personal habits and genetics (to name a few) come to differentiate our bodies internally and externally. Consequently, it is of no surprise that human body proportions vary among people (Jensen, 1993). The diversity of human bodies makes modeling the body challenging. In biomechanics, there is a need to understand and model morphological differences amongst humans to further develop an understanding of how the body interacts with the environment around it (Damavandi et al., 2009; Wall-Scheffler, 2012).

Interest in the human body and understanding the underlying mechanics dates back as early as 1679 with work done by Borelli (Pope 2005, Clauser et al.,1969). Borelli designed experiments to determine the COM of a grown man amongst many other investigations. He showed an understanding of load distribution on the spine and of the mechanics of the musculoskeletal system (Pope 2005, Clauser et al.,1969). Our comprehension of the human body has grown greatly since Borelli's pioneering work and knowledge continues to grow with advancements in

our technology. As our understanding expands, representative models that describe a body in motion can be developed with far greater accuracy and detail than possible before.

The underlying mechanical characteristics of motion are estimated using inverse or forward dynamics. For a human body in motion we can monitor the kinematics, therefore inverse dynamics can be applied. Inverse dynamics is a process of calculating forces and moments using representative kinematic information. Examples of calculating inverse dynamics are the Newton-Euler equations, which use the kinematic and inertial inputs to solve for forces (Equations 1-2).

$$\mathrm{F_x} = \mathrm{ma_X} \quad \mathrm{F_y} = \mathrm{ma_y} \quad \mathrm{F_z} = \mathrm{ma_z}$$

Equation 1: Force components $(\mathrm{F_x}, \mathrm{F_y}, \mathrm{F_z})$; mass (m); linear acceleration components $(\mathrm{a_x}, \mathrm{a_y}, \mathrm{a_z})$ in coordinate system (CS) x-y-z.

$$M_x = I_{xx}\dot{\Omega}_{xx} + \left(I_{zz} - I_{yy}\right)\Omega_{yy}\Omega_{zz}$$

$$M_y = I_{yy}\dot{\Omega}_{yy} + (I_{xx} - I_{zz})\Omega_{zz}\Omega_{xx}$$

$$M_z = I_{zz}\dot{\Omega}_{zz} + \left(I_{yy} - I_{xx}\right)\Omega_{xx}\Omega_{yy}$$

Equation 2: Components of the sum of external moments (M_x, M_y, M_z); principal moments of inertia (I_{xx}, I_{yy}, I_{zz}); angular velocity (Ω) and angular acceleration $(\dot{\Omega})$ in CS x-y-z

The specific input parameters of interest are the body segment inertial parameters (BSIPs) and are the topic of this dissertation. BSIPs describe the inertial properties of a body in motion and of the segments (links) of the human body. BSIPs are affected by the morphological variations amongst human bodies and can be difficult to estimate (Jensen 1993). Developing an acquisition method for estimating BSIPs is the foundation and rationale of this project.

1.1 Body Segment Inertial Parameters

Biomechanics has provided insight to how the body functions and responds to movement in its environment (Pearsall & Reid, 1994). The development of models, supported by biomechanical research, has allowed for the understanding of how various body components such as muscles, tendons, ligaments and bones interact. However, accuracy in modeling the body depends on how well mechanical approximations estimate true anatomical structures (Williams et al., 2009). Amongst biomechanical input parameters, BSIPs have been shown to affect the accuracy of biomechanical estimations, especially in high velocity situations such as running or jumping (Ganley & Powers, 2004; Pearsall & Costigan, 1999) . Small percentage variations in BSIPs estimates can result in discrepancies in the joint resultants obtained from inverse dynamics (Andrews & Mish, 1996).

In modeling, the human body can be treated as a rigid multi-linked system composed of segment limbs each having different geometric and inertial parameters (Jensen 1993). Some of the differences between link segments can be accounted for by morphological variables otherwise known as BSIP's, which include: the body link segment mass, cartesian locations of the COM and the moments of inertia. Attention has been given to the process of attaining these parameters since the late 1800's, yet full documentation of BSIP variations amongst humans is ongoing and incomplete (Jensen 1993; Pearsall & Reid, 1994). Acquiring more specific data to better model the various populations is required.

BSIPs are mechanical parameters; they are influenced by the physical geometric shape and internal composition of the body. As we age and grow, our limbs change and as a result BSIPs have been shown to differ between age, gender and racial groupings (Cheng et al., 2000; Jensen

& Fletcher, 1994; Reid & Jensen, 1990). Therefore, BSIP estimates must be used with great caution. Various investigators have warned against arbitrary use of BSIP models (Chandler et al., 1975; Clauser et al., 1969; Pearsall et al., 1994). In fact, it is important to know the specific population a model, which estimates BSIPs, is based on too appropriately use it to approximate the inertial parameters of a specific subject.

The methods that have been developed to estimate BSIPs range in cost, time requirement and accuracy. BSIP acquisition methods have many similarities yet attain estimations of inertial parameters in distinct ways, with each method having underlying advantages and disadvantages. Examples of methods are: cadaveric, medical imaging (MRI, CT, and X-ray, DEXA), mathematical (geometric), surface scanning (photography, videography, infrared, laser, computer vision) and other methods (water submersion, balance board, and quick release).

Direct methods, which used cadavers, create the foundation for this field of work (Chandler et al., 1975; Clauser et al., 1969; Dempster, 1955). Medical dissections allow for body link segments to be segmented, measured and analyzed in vitro, without restriction (Dempster, 1955). Researchers have studied body tissue and determined segment density properties using cadaveric methods, yet parameters such as the distribution of tissue density across the various body segments are difficult with this technique. With advancements in technology, estimating segment density and tissue distribution has been made possible with the use of Computed Tomography (CT), Magnetic Resonance Imaging (MRI) and Dual-energy X-ray Absorptiometry DEXA (or DXA) to name a few (Bauer et al., 2007; Durkin 2003; Lee et al., 2009; Pearsall et al., 1996; Rossi & Lyttle, 2013). Although expensive and not universally available, medical imaging technology has contributed to the understanding and knowledge of estimating BSIPs. Body segments such as the thigh and trunk have been explored in detail using this technology. The

diverse tissue distribution and complex internal structures of these body segments make it difficult to compute BSIPs using methods such as cadaveric dissections (Durkin et al., 2005; Pearsall et al., 1996).

Geometrical modeling has focused on constructing the morphological properties of the segments using mathematical shapes. Modeling the body as a series of shapes gives us the opportunity to determine BSIPs non-invasively and inexpensively on living subjects. The inputs for geometrical models range to account for the different shapes of each of the body segments (examples: Hanavan 1964; Hatze and Baca 1992; Jensen 1978; Whitsett 1963; Yeadon and Morlock 1989). Mathematical inputs, termed anthropometric measurements, represent measurement information regarding the size of body segments. As with any model, the accuracy will be limited by the physical expressions of the input parameters, in this case, the anthropometric measurements. As anthropometric measurements are commonly estimated manually, there is a certain degree of inaccuracy associated with any hand measurement. With the development of technology, manual measurements are becoming outdated, as will be further discussed.

Surface imaging methods include the use of stereo photography, videography and 3D scanning to name a few. This approach intends to reduce error from manual 2measurements, which are used in estimating BSIPs by eliminating the manual nature of estimating the measurements. Surface imaging methods aim to attain volumetric information directly from a subject with the use of a camera. By applying known density values to these volumetric profiles approximations for a wide range of BSIPs are possible (examples : Clarkson et al. 2012; Gittoes et al, 2008; Lu and Wang 2008; Mcconville and Churchill 1980; Peyer et al., 2015; Wicke and Lopers 2003; Young et al, 1983). Other surface scanning techniques include the use of infrared and laser scanning, where a high degree of accuracy has been shown (Ma et al., 2011; Norton et al., 2002).

1.2 Motivation of Project

Estimating inertial properties of the human body is essential to solving many biomechanical equations. As BSIP estimations have shown to be sensitive to the chosen model, great caution has to be taken when choosing generalized input BSIPs. With subject specific modeling requiring manual measurements and time consuming experimental setups there is a need to explore an accelerated and inexpensive method of acquiring BSIPs directly from persons of interest with simplicity and reliability.

The Microsoft Kinect Version 1 (V1) (Microsoft Corporation, Redmond, USA) camera has shown to provide potential in this field of work and could provide a means of acquiring subject specific morphological information of the full body (Clarkson et al. 2012, Clarkson et al. 2014) . With the recent release of the Microsoft Kinect Version 2 (V2) (Microsoft Corporation, Redmond, USA), the ability to acquire 3D data at a higher accuracy than before has been made possible (Lachat et al., 2015). However, this has not yet been explored in detail in relation to BSIPs measurements of living human beings. Investigating the capabilities of this device as a measuring tool to acquire subject specific BSIP estimation will provide valuable insights on the technology and how it can be applied to 3D modeling of living humans.

The specific motivation of this study is to use the Microsoft Kinect V2 to determine subject specific BSIPs of living subjects and evaluate if there is potential for this device in this context. An understanding of calculating BSIPs is crucial before adopting the device for these purposes. Once a thorough understanding of estimating BSIPs is obtained, evaluation of using the Kinect to calculate BSIPs will be investigated. Establishing the feasibility of using the device and determining reliability is imperative to adopting the device into a biomechanics laboratory and

will provide valuable insight on how using this technology compares with other BSIP estimation techniques.

1.3 Objectives

The objectives of this dissertation are as follows:

1) To determine the feasibility of using a Microsoft Kinect V2 in estimating BSIPs of living subjects. This will require developing an experimentation protocol to test the use of the Kinect V2 camera in the context of estimating BSIPs. Specifically, it is of interest to estimate: volumetric parameters, mass, cartesian location of COM, moment of inertia tensors and longitudinal segment lengths using the Kinect V2.
2) To compare the BSIPs estimated using the developed protocol to those acquired using a subject specific method, which has been evaluated in the literature.
3) To compare the estimates to BSIPs estimated using a generalized model of a similar population.

1.4 Dissertation Outline

This Dissertation consists of 6 Chapters including the Introduction. Chapter Two: Literature Review is a review of the related literature detailing the various methods that have been developed to estimate BSIPs, the biomechanical relevance of BSIPs, as well as a background on body segment densities, segmentation and the Microsoft Kinect. Chapter Two gives the reader a better understanding of the importance of this field of work and background on the relevant literature. Chapter Three: Methods describes the experimental approach. An overview of the software and the application of various code written for the data collection and analysis are also presented in this chapter. Chapter Four: Results presents the findings and explanation of the collected data. Subsequently Chapter Five: Discussion provides a detailed analysis of the results and examines the comparisons of the data to other BSIP estimation methods presented in the literature. Chapter Six: Conclusions and Future Recommendations concludes on the findings and discusses recommendations for future work in this field are also presented.

Chapter 2
Literature Review

2.0 Introduction

To relate forces to motion requires the input of inertial properties. In dynamic analysis, inertial properties must be computed for kinetic investigation. When the human form is considered, these properties are commonly referred to as the body segment inertial parameters (BSIPs). Treating the human body as a multi-link system allows for each body segment (link) to be described with its own specific geometric and inertial parameters (Jensen 1993). These parameters include: body segment mass, moments of inertia (MOI) and cartesian locations of the centre of mass (COM).

2.1 BSIP Relevance

Investigation of inertial parameters of the human body and its extremities is an important part of the study of human motion (Nikolova 2010). Researchers studying the kinetics of motion

require BSIP inputs. Clinically, this may be used in identifying patterns in gait, which could help indicate distress in the joints. It can be used to inquire on sporting performance or help identify regions of high stress in joints post-trauma (as examples). There is some debate with the clinical significance of errors in BSIPs. Some researchers show inconsequential importance in BSIP uncertainties (Challis and Kerwin, 1996; Pearsall and Costigan, 1999; Reinbolt et al., 2007) while other researchers state that misestimating these measures can produce significant variations in the observed joint kinetics (Andrews and Mish, 1996; Kingma et al., 1996; Kwon 2001; Pataky et al., 2003; Silva and Ambrósio, 2004). However, the aforementioned studies compare different inertial parameters and in different sections of the body, making it difficult to make any generalizations.

In one example, Pearsall and Costigan (1999) used predictive BSIP models and incrementally altered the output BSIPs up to +/- 40%. The results showed that accuracy in BSIP estimation should be of concern when looking at open chain or high acceleration activities, such as running, but not as large of a concern when looking at low speed activities such as walking. Pearsall and Costigan also observed that fluctuating segment mass estimations, especially at the thigh, resulted in a significant change in estimated reaction forces (Pearsall and Costigan 1999). Rao et al. (2006) showed that BSIP estimates are sensitive to the predictive model that is used to estimate the parameters, with BSIP estimations (from various modeling techniques) ranging from 9.73-60% in estimation differences. This corresponds to results showing maximum differences of 20.1% in the peak extension/flexion moment of the hip, suggesting that the influence of BSIPs cannot be neglected and models must be carefully chosen (Rao et al., 2006). The work from Andrews and Mish (1996) concluded that small percentage variation in BSIPs could propagate in to larger variations in the joint resultant forces obtained from inverse dynamics. When high

accuracy is a concern in calculated joint resultants, then considerable care needs to be taken when choosing BSIP estimation methods (Andrews and Mish, 1996).

In other studies, the determination of resultant joint moments has shown to be sensitive to the estimation of the COM of the body segments (Challis & Kerwin, 1996). Segmental mass values have also been shown to influence the calculation of joint torques (Pataky et al., 2003; Pearsall, D. & Costigan, 1999). Kwon (2001, 1996) showed that the specific method of BSIP estimation significantly affected the simulation accuracy in airborne movement (high acceleration). This left Kwon to conclude that the more individualized BSIP estimation methods generally provided more accurate simulation results (Kwon 2001, 1996). However, Lee et al. (2009) found that their highly sophisticated BSIP estimation method which used MRI for geometrical data and DEXA for mass distribution only resulted in differences of less than $0.09\frac{\mathrm{Nm}}{\mathrm{kg}}$ in the hip joint moment during gait when compared against the results obtained using four simpler models from literature. The study suggested that the joint kinetic computations during gait are relatively insensitive to BSIP variations amongst methods (due to the low accelerations) (Lee et al., 2009).

Subject morphology plays a role in BSIP estimation especially when choosing a representative model. Damavandi et al. (2009) showed that on average very lean subjects (low BMI) showed MOI estimates 13.2% lower than those of average BMI. The high BMI subjects showed to be on average 17.9% higher in the MOI estimates (Damavandi et al., 2009). This only confirms the need to use subject specific estimations. There is little dispute that obtaining BSIPs, which are more representative, will provide more accurate predictive kinematic and kinetic analyses of human motion. The clinical significance of the variations and errors resulting from BSIP estimation is a subject of debate. However, influence of estimations errors is existent and should

not be overlooked in movements that generate higher accelerations than regular gait (Lee et al., 2009) and for subjects which are not well represented in the literature (Damavandi et al., 2009).

2.2 Body Segmentation

The segmentation of the body into specific segments is an important aspect of BSIP estimation. Segmentation definitions differ amongst estimation methods (examples: (Chandler et al., 1975; Dempster, 1955; Hanavan, 1964; Hatze 1980; Jensen 1978; Paolo de Leva, 1996; Yeadon & Morlock, 1989; Zatsiorsky & Seluyanov, 1983)). The trunk region is once example were the segmentation differs between authors (examples: (Erdmann 1997; Pearsall et al., 1994, 1996)). Therefore, it is important to be aware of how researchers have chosen to segment the body in their method in order to properly gather input parameters and understand the full meaning of the estimated BSIPs from a model. At this time there does not exist any segmentation standard, making it difficult to compare between differing segmentation protocols published in literature (Zatsiorsky 2002). An example of three different trunk segmentations is shown in Figure 1.

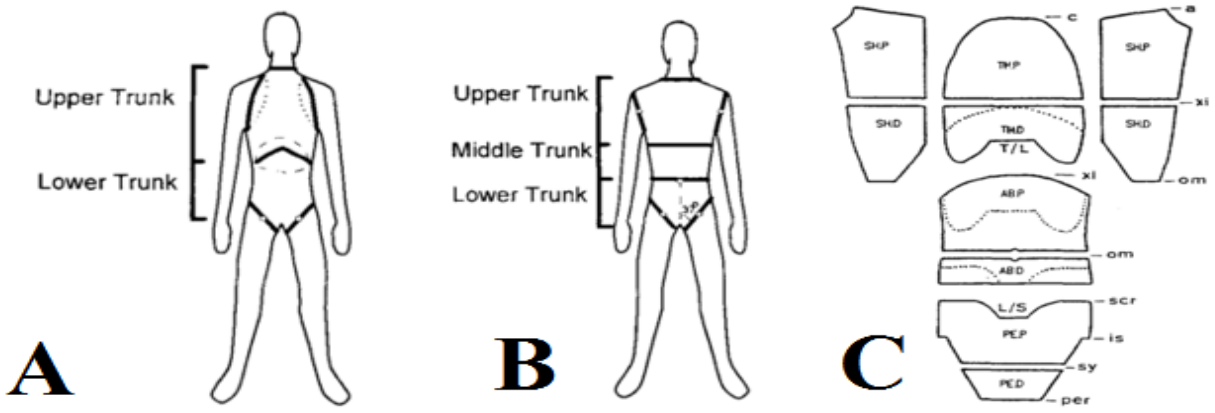

Figure 1: Differing segmentation protocol of the trunk. **A**. Dempster's (1955) two-segment trunk **B.** Zatsiorsky et al. (2002) three-segment trunk **C.** Erdmann (1997) ten segment trunk. Images A-B taken from (Pearsall et al., 1996)

2.3 Segment Density

Body segment density may be required to estimate BSIPs. Depending on the method used, (as will be described below in 2.4 BSIP Estimation Methods) the segment density is either directly estimated or a published value is used in conjunction with estimated volumetric parameters to acquire BSIP parameters. A range of body segment densities is shown in Table 1 below.

Table 1: Body segment density parameters from a variety of acquisition techniques

Technique used	**Medical Cadavers**				**CT/MRI**			**DXA**
Reference	(Harless, 1860)[1]	(Dempster, 1955)	(Clauser et al., 1969)	(Chandler et al., 1975)	(Pearsall, et al., 1994)	(Pearsall, et al., 1996)	(Erdmann, 1997)	(Wicke & Dumas, 2014)
Total Body		-	1.042±0.018	-	-	-	-	-
Head		1.11±0.120*	1.071	1.056±0.020	-	-	-	-
Full Trunk		1.03±0.065	1.023±0.032**	0.853±0.039**	0.94±0.02	0.960	1.030	-
Upper Trunk		-	-	-	0.82±0.04	0.870	0.908	-
Abdomen		-	-	-	1.01±0.01	1.020	1.043	-
Pelvis		-	-	-	1.02±0.01	1.070	1.077	-
Thigh	R:1.069±0.013 L:1.068±0.014	1.05±0.008	1.045±0.017	R:1.018±0.012 L:1.021±0.012	-	-	-	F:1.008 M:1.051
Shank	R:1.099±0.019 L:1.101±0.021	1.09±0.015	1.085±0.014	R:1.059±0.007 L:1.071±0.021	-	-	-	F:1.023 M1.074
Foot	R:1.089±0.600 L:1.089±0.010	1.10±0.056	1.085±0.014	R:1.073±0.024 L:1.069±0.024	-	-	-	-
Upper Arm	R:1.087±0.030 L:1.090±0.003	1.07±0.027	1.058±0.025	R:0.997±0.012 L:1.012±0.015	-	-	-	F : 1.055 M:1.071
Forearm	R:1.106±0.004 L:1.112±0.040	1.13±0.037	1.099±0.018	R:1.043±0.018 L:1.061±0.017	-	-	-	F:1.067 M:1.086
Hand	R:1.114±0.004 L:1.111±0.007	1.16±0.110	1.108±0.019	R:1.079±0.017 L:1.081±0.011	-	-	-	-

[1] The source is reported from [(Bjørnstrup, 1996)]

* Head +Neck **Trunk+Head+Neck

2.4 BSIP Estimation Methods

Early techniques were effective methods of estimating BSIP parameters. For example, the immersion of limbs into water is a process where the measurement of water a segment or full body displaces is related to its volume. Early work using this method was done by Harless (1960) but to this day work appears (Norton et al., 2002; Wicke & Lopers, 2003; Zatsiorsky 2002) using this as a gold standard for volume estimation (Harless (1960) taken from : Drillis et al., 1964)). Techniques such as suspending body segments (either of human cadavers or dental cast models) about an endpoint and allowing them to oscillate allowed for the MOI to be estimated from the period oscillation (Drillis et al., 1964; Hatze., 1975). Other methods, such as the quick release method, measured the deflection and force of a spring. This information was used to determine accelerations of the limb and then to estimate the MOI. In another method, the reaction board method, a board supported at 2 points (one of which is a force scale) is used to determine COM positions (based on static equilibrium) (Drillis et al., 1964). With advancements in technology, these methods are less used now but provide a foundation in developing techniques for estimating human BSIPs. Figure 2 illustrates the aforementioned methods.

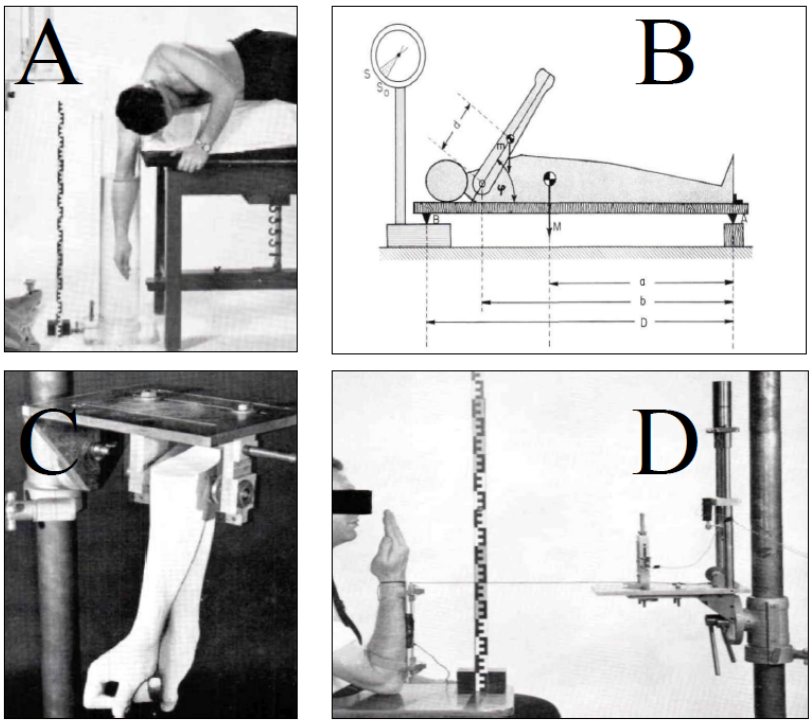

Figure 2: A. Water submersion of the arm to determine volume B. Reaction Board used to determine COM based on static equilibrium C. Oscillating a cast of an arm to determine MOI D. Quick release method of the subjects forearm used to determine MOI. (Images adapted and modified from Drillis et al., 1964)

2.4.1 Medical Cadavers

The dissection of the human body dates back to as early as the third century B.C where Greeks became some of the first scientists to perform systematic dissections of humans (Staden, 1992). Since then, dissection has provided and continues to provide very valuable medical insight on revealing anatomical details of the human body (Ogeng, 2014).

The study of cadavers for deriving biomechanical qualities such as BSIPs has been crucial for developing understanding and creating a foundation in this field of research. Work done by Dempster (1955) has been regarded as one of most extensively detailed in biomechanical

research of medical cadavers (Reid & Jensen, 1990). Dempster performed an intensive cadaver dissection of 8 elderly men with which he created tables showing body segment parameters as proportions of body height and mass. The cadavers, all Caucasian men, were reported to be smaller than the average males (Dempster, 1955). Dempster used various techniques to calculate various BSIPs as shown in Figure 3.

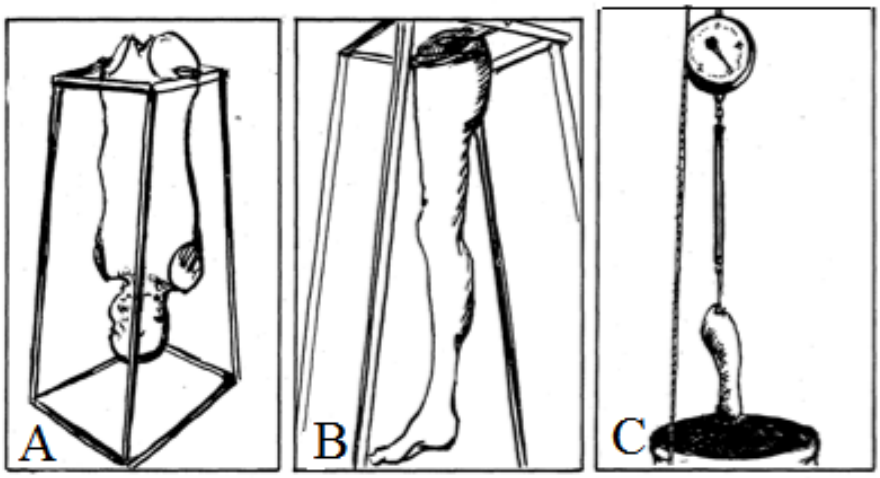

Figure 3: Various procedures associated with calculating BSIPs of disassembled cadaver. A. The trunk suspended upon a knife-edge to calculate MOI B. Lower limb suspended on knife-edge to calculate MOI C. Limb on scale to determine mass then submerged into water to determine volume. (Images adapted from: (Dempster, 1955)).

There were earlier studies done on medical cadavers, such as those presented by Braune et al. (1889) but Dempster's work was far more detailed and had a significantly larger subject pool. Shortly after, Barter (1957) put together data from Dempster along with data from studies by Braune et al. (1889) and established regression equations for predicting segment masses based on the body mass of the subject (Barter, 1957) . These regression equations have been reported as a fast and easy means of estimating segment mass, despite the many limitations and error associated with them (Clauser et al., 1969).

Clauser et al. (1969) and Chandler et al. (1975) presented tables similar to those of Dempster based on their own cadaveric experiments (Chandler et al., 1975; Clauser et al., 1969). As with Dempster (1955), their studies had small samples sizes (10 specimens from Clauser et al. (1969) and Chandler et al. (1975) dissected 6 specimens) and were based again on older Caucasian male populations. Both Chandler et al. and Clauser et al. used palpable anatomical landmarks to identify the ends of segments in contrast to the subjective determination of joint centers done by Dempster (1955). The studies by Dempster (1955), Clauser et al. (1969) and Chandler et al. (1975) represent some of the most comprehensive data based on direct measurement (Pearsall & Reid, 1994). However, extrapolating those data to represent other populations can be non representative due to different body morphologies and small cadaveric samples they are derived from (Rossi & Lyttle, 2013). Pooling data is also difficult because of differences in the segmentation patterns observed between the studies (Durkin 2003). This makes it problematic to use these equations as an accurate means of estimating subject specific BSIPs. Table 2 shows example differences seen between varying selected methods for estimating the mass of the thigh, forearm and foot.

Table 2: Example of three body segment mass equations from various sample literature based on elderly male cadaveric data W=Total Body Mass

Segment	(Dempster, 1955)	(Barter, 1957)	(Chandler et al., 1975)
Thigh	W[kg] x 0.10	W[lbs] x 0.090 + 1.60	W[kg] x 0.1027
Forearm	W[kg] x 0.016	W[lbs] x0.020 - 0.25	W[kg] x 0.0161
Foot	W[kg] x 0.0145	W[lbs] x0.010 +0.75	W[kg] x 0.0147

The use of medical cadavers has provided an important foundation in BSIP estimation. Directly measuring BSIP straight from the body is highly advantageous but comes with a variety of limitations and concerns. Cadaveric studies have been questioned for their validity in

representing BSIP measurements of living subjects. Fluid loss during segmentation, properties of deceased tissues and the age and state of the cadavers are some of the concerns from these types of studies (Durkin 2008; Lephart et al., 2014; Pearsall & Reid, 1994). In one example, Lephart et al. (2014) showed that significant differences do exist in tissue that has been thawed compared to frozen tissue. Lephart et al. also showed that body somatotypes show significant differences in tissue density and should be considered when choosing a BSIP estimation method (Lephart et al., 2014). There is difficulty in obtaining a representative pool of cadavers varying in age, gender, BMI and ethnicity and it is a major limitation with this method in acquiring representative BSIPs for a large range of people. Other limitations that exist can be cost, intricacy and ethical considerations amongst a few. This has led to the development of other techniques to estimate BSIP parameters. A summary of representative cadaveric literature is shown in Table 3.

Table 3: Summary of a variety of cadaver studies from literature used to estimate BSIPs. (Volume (V), Mass (M), Density (D), Race(R), Caucasian(C)) This doesn't not reflect the extent of full literature

Reference		Subject Pool information					Parameter					
		#	Sex	Age	R	BMI	V	M	COM	MOI	D	Comments
1955	(Dempster, 1955)	8	M	52-83	C	-	x	x	x	x	x	Water displacement to determine volume of the limbs. Caucasian elderly men
1969	(Clauser et al., 1969)	13	M	24-78	-	-	x	x	x	x	x	
1975	(Chandler et al., 1975)	6	M	45-65	C	-	x	x	x	x	x	
1972	(Liu & Wickstrom, 1972)	7	M	-	C	-	-	x	x	x	-	Only Trunk
2014	(Lephart et al., 2014)	2	M	87-94	-	-	x	x	x	x	x	Comparison of frozen to thawed tissue and the effect on BSIPs
1986	(Clarys & Marfell-Jones, 1986)	6	3M 3F	15-79	-	-		x	-	-	-	182 measurements taken off cadavers to develop regression equations which estimate mass

2.4.3 Medical Imaging

With the growing availability of medical imaging technology, the use of these techniques for directly measuring BSIPs on living humans has been shown (Durkin 2008). Attaining tissue density and mass distribution information from living subjects, which is possible with imaging methods, has been shown to overcome some of the limitations associated with cadaveric dissection, with the potential to providing more accurate measures. Medical imaging technologies that have been used in this field are: Computer Topography (CT), Magnetic Resonance Imagining (MRI), Dual Energy X-ray Absorptiometry (DEXA) and Gamma scanning to name a few.

CT has been used as a technique for BSIP estimation on living subjects (examples: (Erdmann, 1997; Huang & Suarez, 1983; Pearsall et al., 1996)). From CT scanning of biological tissue, density values can be obtained on a pixel-by-pixel basis allowing for precise determination of tissue density along the length of the body. Applying the values to volumetric estimates can provide estimates of segment mass distribution and better approximate the overall density of each of the body segments (Durkin 2008). Huang et al. (1983) described CT as an excellent approach and commented that methods have been developed to compute mass density and inertia tensors of cross sections from CT images, making CT low dosage in vivo approach for estimating subject specific BSIPs (Huang & Suarez, 1983).

In an experiment done by Erdmann (1997), 15 male subjects had their trunk segment scanned which lead to the development of predictive equations to estimate the centers of mass of the trunk. Pearsall et al. (1996) also performed CT of the trunk but of 2 males and 2 female subjects. Pearsall et al. determined mass distribution and BSIP information of the trunk along slices taken

from T1 to L5 allowing for very detailed calculation of density, volume and trunk mass. With this data Pearsall et al. were able to calculate the MOI. An example output of the volume and corresponding density is shown in Table 4. Although the results were promising, Pearsall et al. commented that the variations of boundary definitions of the trunk present in the biomechanics research community make it difficult to generalize findings (Pearsall et al., 1996).

Table 4: Example volume and density outputs along the spine from T1 to T5 calculated using CT taken from: (Pearsall et al., 1996)

Trunk Level	Volume (cc)	Density (g/cc)
T1	810(332.5)	0.99(0.06)
T2	867.1(357.5)	0.91(0.06)
T3	1125.7(134.8)	0.84(0.07)
T4	1180.3(119.8)	0.78(0.09)
T5	1230.6(110.6)	0.77(0.10)

Application of MRI in measuring BSIPs directly from living humans has also been shown as an acceptable method (examples: (Bauer et al., 2007; Lee et al., 2009; Martin et al., 1989; Pearsall, et al., 1994)). MRI offers great contrast between various tissues and is advantageous as it does not expose subjects to radiation (Heymsfield et al., 1997). Using MRI, specific determination of tissue types and distributions is determined within slices along the length of the segment as shown in Figure 4. Slice thicknesses vary, and when considered in three dimensions, the image consists of volume elements known as voxels. Each voxel has a gray scale that reflects the tissue's composition. In such a way, with both MRI and CT it is possible to discriminate between bone, skeletal muscle and adipose tissue (Heymsfield et al., 1997).

In an MRI experiment, Martin et al. (1989) showed that there was close agreement between the criterion (predicted using reaction board and oscillation techniques) BSIP estimates and those estimated using MRI on 8 baboon body segments. In a larger study, Ho et al. (2013) derived

BSIP estimates for 50 Chinese men (21.5±1.52 yr.) and the results showed to be comparable to predication based on cadavers. Ho et al. (2013) stated that the discrepancies in the segment boundaries and coordinate systems might have contributed to the differences they saw between methods. They concluded that MRI is currently the most advanced method for studying human inertia parameters (Ho et al., 2013). However, limitations such as the large associated cost and time consuming nature of estimating BSIP parameters using MRI make this method restrictive.

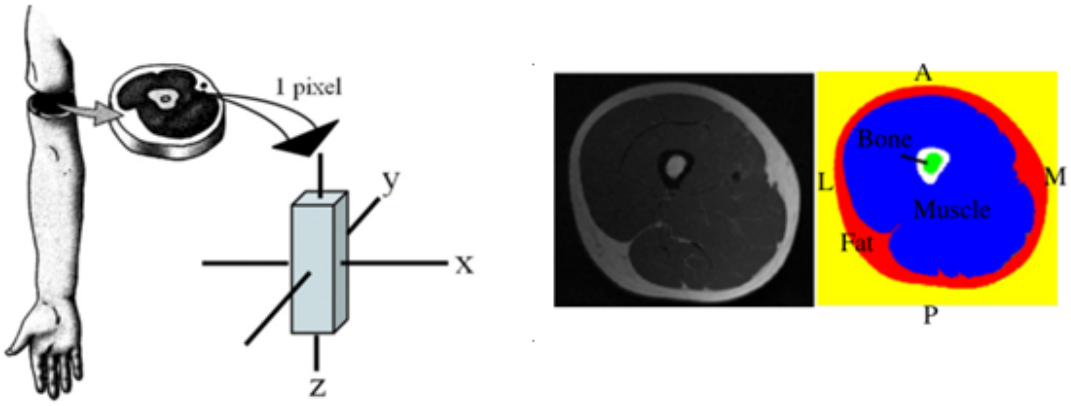

Figure 4*: Left*: MRI images are taken along the longitudinal axis of the segment (adapted from Ho et al., 2013). *Right*: Each slice shows the representative fat, bone and muscle tissues (A: Anterior, P: Posterior, M: Medial, L: Lateral) (adapted from: Lee et al., 2009)

Dual-energy X-ray absorptiometry (or DXA) is a minimal radiation low cost imaging method which can provide BSIP estimates (examples: (Durkin et al., 2002; Lee et al., 2009; Rossi & Lyttle, 2013; Wicke & Dumas, 2008)). DXA projects two X-Ray beams of different intensities on to a subject's body. Based on the attenuation of the energies as they pass through the body the mass per area unit can be evaluated. Rossi et al. (2013) showed that subject specific mass can be estimated very accurately (%RMSE of <1.5%) for the whole body in the 28 subject study. Durkin et al. (2002) found a mean percent error of whole body mass estimation using DXA

compared to scale values of -1.05%±1.32% in the 11 male subject study (Durkin et al., 2002). Similarly, Wicke and Dumas (2008) observed highly accurate estimates (error < 0.1-0.39%) of various BSIPs in the 50 participant study (Wicke & Dumas, 2008). Wicke and Dumas mentioned that 2D characteristics of the results obtained using DXA did not allow for the estimation of the MOI along the longitudinal or transverse axes or the calculations of the COM position in the sagittal plane. Shown in Figure 5 is an example DXA setup. DXA has shown to provide promising results but the technology is not widely available and can be difficult to use in large subject pools due to cost and time requirements of the method.

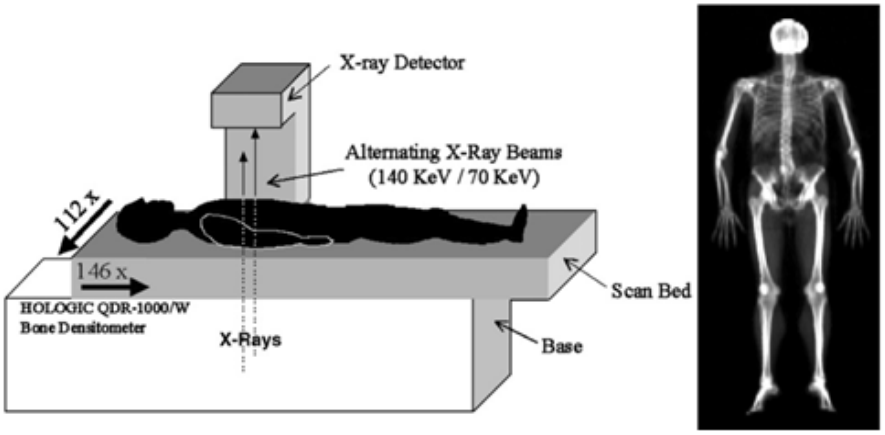

Figure 5: *Left Side:* Example DEXA setup, with each scanning less than 5 minutes. *Right Side*: Output image prior to post processing. (Durkin et al., 2002)

The medical imaging technology detailed above could serve as a means of constructing detailed databases for a wide range of populations. However, the expensive and time-consuming nature of using this technology in this context makes it difficult to acquire subject specific estimates in a lab environment. A summary of representative medical imaging literature is shown in Table 5.

Table 5: Summary of a variety of medical imaging studies from literature used to estimate BSIPs. (Volume (V), Mass (M), Density (D), Race(R), Caucasian(C)) This does not reflect the extent of full literature.

Reference		Subject Pool information					Parameter					
		#	Sex	Age	R	BMI	V	M	COM	MOI	D	Comments
CT												
1976	(Huang & Wu, 1976)	-	-	-	-	-	-	-	-	-	x	Number of samples not clear, validation study
1983	(Huang & Suarez, 1983)	-	-	-	-	-	-	-	-	-	x	Non-human
1996	(Pearsall et al., 1996)	4	2M 2F	46-68	-	-	x	x	x	x	x	Only Trunk
1997	(Erdmann, 1997)	15	M	20-40	-	-	x	x	x	x	x	Only Trunk
MRI												
1989	(Martin et al., 1989)	8	-	-	-	-	x	x	x	x	x	Baboon segments
1990	(Mungiole & Martin, 1990)	12	M	21.8-31.9	-	-	x	x	x	x	x	Athletes
1994	(Pearsall et al., 1994)	26	M	40.5±14.4	-	19.7-39.3	x	x	x	x	x	Only Trunk
2000	(Cheng et al., 2000)	8	M	26±4	Chi	-	x	x	x	x	x	Chinese Adults
2007	(Bauer et al., 2007)	10	F	9.6±0.9		18.5±1.8	x	x	x	x		Left Leg
2013	(Ho et al., 2013)	15	M	21.5±1.52	Chi	27.3±2.1	x	x	x	x	x	Full body into 14 segments Chinese Adults
DEXA												
2002	(Durkin et al., 2002)	11	M	76.04±6.41	-	23.9±1.8	x	x	x	x	x	Length was also determined for each segment
2008	(Wicke & Dumas, 2008)	50	25F 24M	F:22.2±4 M:22.5±4.7	-	F:22.4±1.5 M:23.9±3.1	x	x	x	x	x	Full body
2009	(Lee et al., 2009)	4	M	27.5±4.6	-	-	x	x	x	x	x	Full Body
2013	(Rossi & Lyttle, 2013)	28	20M 8F	M:26.2±4.0 F: 21.1±5.8	C	-	x	x	x	x	x	18 competitive swimmers and 10 healthy non-swimmers. All Caucasian
2004	(Ganley & Powers, 2004)	20	10M 10F	23-50	-	-	x	x	x	x	x	
Gamma Scanner												
1975	(Brooks & Jacobs, 1975)	3	-	-	-	-	x	x	x	x	x	Legs of lamb
1983	(Zatsiorsky & Seluyanov, 1983)	115	100M 15F	M:23.8±6.2 F: 19.0±4.0	-	-	x	x	x	x	x	Female subjects were national athletes

2.4.2 Mathematical Models

Geometric modeling is a mathematical approach in which shapes are used to represent individual segments of the body. This can be as simplistic as modeling the body as a combination of cylinders and spheres (Hanavan, 1964) or as complex as functions that take into account the complex geometry of individual body segments (Wicke & Dumas, 2010). Whether the model of the body is simple or complicated, geometric models require anthropometric measures, which represent the size of the body at various locations, allowing for individualized estimations.

Early work in geometric modeling appeared in the work done by Simmons et al. (1960) who approximated the body as a set of cylinders and spheres (taken from: Chandler et al., 1975). Later both Hanavan (1964) and Whitsett (1963) refined the model by Simmons et al. (1960) and represented the body composed of 16 and 14 segments respectively (Figure 6). The models used the mass regression equations developed by Barter (1957), which were based on cadaver studies, for density estimations to solve for the BSIPs. Although the models were rudimentary with many approximations, these researchers presented straightforward approaches which have served as a foundation for geometric modeling in this research context (Hanavan, 1964; Whitsett, 1963).

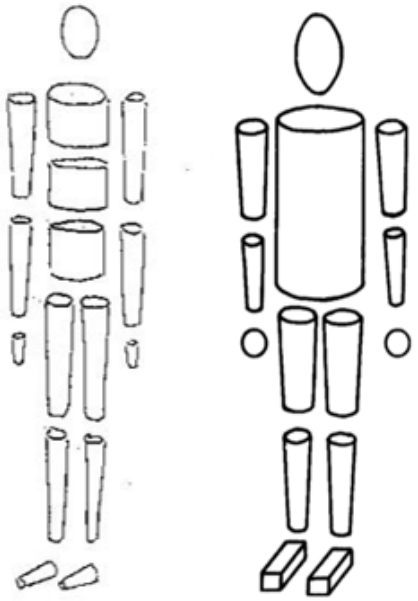

Figure 6: Geometric models using cylindrical and spherical shapes. These models had a high degree of estimation resulting in large errors in BSIP estimations. *Left Side*: 16 segment model (Hanavan, 1964). *Right Side*: 14 segment model (Whitsett, 1963)

Some years later, Jensen (1978) presented a geometric model, which used elliptical zones stacked on top of one another to represent the body. Jensen's method follows contours of the body well as shown in Figure 7. Jensen's model was based on some of the ideas proposed by Weinbach (1938) of which Dempster (1955) evaluated to be quite suitable for volume estimation (Jensen 1978). With the Elliptical Cylinder Model (ECM), which Jensen developed, the body was segmented into 16 segments. The estimated total body mass using ECM resulted of errors of less than 1.5% when compared to scale measures. Jensen's experiment showed that he was able to reduce mass estimation error by approximately 10% compared to the results determined using the model by Hanavan (1964).

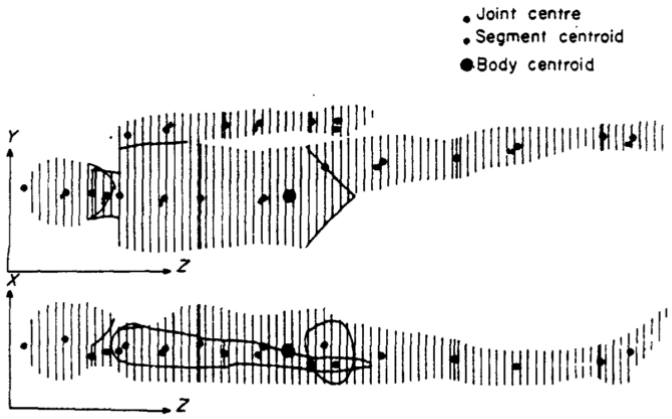

Figure 7: The Elliptical Cylinder Model (ECM) proposed by Jensen (1978). The model is designed to be adaptive to a range of body morphologies. Shown is a manually digitized human subject. The elliptical shapes are based on the counters of the body and adapt to a range of body morphologies (Jensen, 1978).

In recent years, the ECM model has been used to estimate BSIP of pregnant woman (Figure 8), a population that is not well represented in biomechanics. The versatility of the ECM model provides the possibility of estimating BSIPs, without a large amount of training from the operator or researcher (Dumas et al., 2013; Yessoufou et al., 2014).

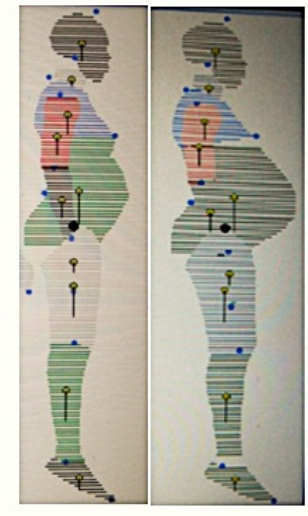

Figure 8: Image shows early pregnancy (left) and late pregnancy (right) with the abdomen region significantly increased in size. The ECM is adapted to estimate BSIPs (Yessoufou et al., 2014).

A more rigorous model by Hatze (1980) presented a geometrical model requiring 242 anthropometric inputs subdividing the body into 17 segments. The model used gender dependent density values and did not assume segment symmetry. Hatze used the same body segments as Hanavan (1964) but modified the shoulder, trunk and buttocks segments to more accurately describe these locations. Although Hatze's model is mathematically rigorous however, most of the calculations can be programed and only the 242 anthropometric input parameters are needed to evaluate the numerical solutions. An important aspect of the model is that no assumptions about the coronal symmetry of the abdominal-pelvic or abdominal-thoracic segments are made. As a result, any severe non-symmetry in the regions such a breasts or large stomach (e.g. pregnancy or high/low BMI subjects) are accounted for in the parameters, allowing for personalization. This robustness was to allow for modeling subjects with more pronounced traits in the torso and abdomen regions, allowing for highly tailored subject specific estimations (Hatze, 1980). Hatze's model reports the lowest error between measured and predicted total body mass (error < 0.5%), but has rarely been used by researchers likely due to the 242 measurement inputs (Robertson, 2013). Figure 9 shows the model alongside a computerized version that has been proposed by Robertson (2013), which has not yet been evaluated in detail.

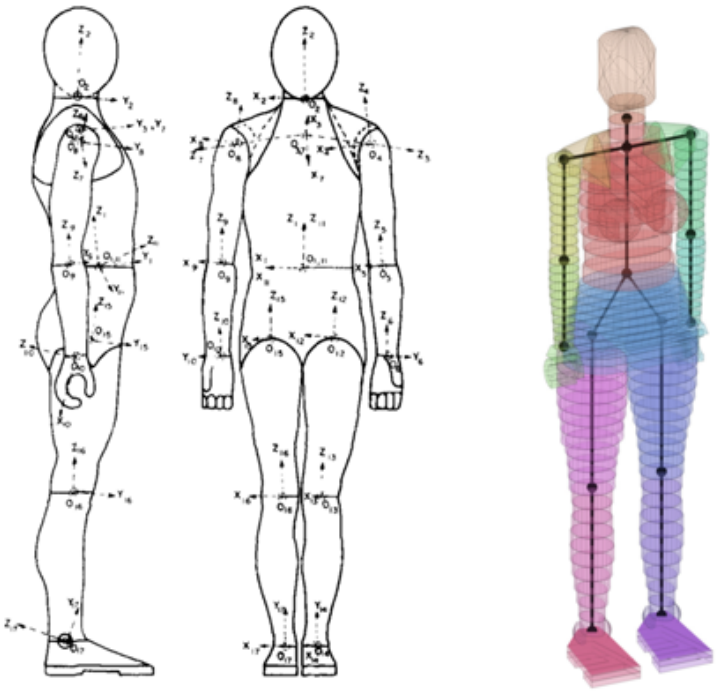

Figure 9: *Left Side*: The model presented by Hatze requiring 242 measurements of the body to be taken *Right Side*: A proposed computerized model of Hatze's (1980) model. (Hatze 1980; Robertson, 2013)

Yeadon (1990) proposed a geometric model composed of 20 body segments and requiring 95 anthropometric inputs for evaluation. Yeadon contended that using ellipses to model the body (such as those in Jensen (1978)) is done because it is mathematically convenient to do so. Yeadon proposed stadium solid shapes, a blend of rectangles and semi circles to more accurately model the segments of the body. Yeadon's model estimated total body mass with maximum error of ~3% (Yeadon 1990). Yeadon commented that this error is sufficient due to the reduced measuring time of 30-40 min compared to 90+ min for Hatze (1980). In both Hatze's (1980) and Yeadon's model the cumbersome demand of 95-242 anthropometric measurement inputs is problematic. Time requirements and errors association with anthropometric measurements are some of the inconvenient demands of these techniques.

Geometric models present a method of estimating BSIPs. With adjustability, the input parameters for mathematical models can be easily manipulated. For example, tissue density and anthropometric measurement inputs are in the control of the operator; this however, requires assumptions to be made on density values. In the aforementioned models, the input density data was based on Dempster (1955) and Chandler et al. (1975). However, density values can be used from other sources such as medical imaging. A limitation of mathematical models is that they will only be as accurate as the extent to which they model the physical morphology. Other limitations such as manual measurement requirements and assumptions made on segment shape must also be considered. A summary of selected mathematical techniques is shown on Table 6.

Table 6: Summary of a variety of mathematical techniques used to estimate BSIPs.

Year	Reference	# Segments	# Inputs	Shape	Comments
1963	(Whitsett, 1963)	14	-	Cylindrical shapes	
1964	(Hanavan, 1964)	15	25	Cylindrical shapes	
1978	(Jensen, 1978)	16	-	Elliptical cylinders stacked onto each other.	Inputs are obtained from digitization
1980	(Hatze 1980)	17	242	Vary for every segment	
1990	(Yeadon 1990)	20	95	Stadium solid	
2007	(Nikolova et al., 2007)	16	33	Cones, Cylinders and Spheres	Based on Bulgarian population

2.4.4 Surface Imaging

A photogrammetric approach of obtaining body surface information has been applied and under investigation since the turn of the 20th century (example: Weinbach, 1938). With the complexity in the analysis of biomechanical properties increasing, manually extracting parameters such as anthropometric measurements can be impractical and cumbersome in practice. Photographic methods obtain important surface measurements using a computer or camera vision based system. The acquired measurements can be used as a means of estimating BSIP of body segments and extracting anthropometric information. When used in conjunction with density estimates, a variety of BSIPs and anthropometric measures can be estimated with this technique. Additionally, photographically acquired anthropometric measurements can be applied to mathematical models or regression-based equations, possibly reducing manual estimation errors associated with human measurement (Stancic et al., 2009).

Photogrammetric work first appeared in the work of Weinbach (1938). By taking photographs of subjects (front and side view) Weinbach estimated whole body MOI and center of gravity. He did this mathematically by constructing curves based on the body surface-area measurements taken from the photographs and developing the MOI estimations about the soles of the feet (Weinbach 1938). However, the technology was limited to film cameras requiring the operator to manually identify and measure body parameters, potentially limiting the accuracy of the results.

More sophisticated work was presented by Jensen (1978) who used a photogrammetric method to acquire the necessary inputs used for his geometric model (the ECM) (Jensen 1978). From a frontal and sagittal image, Jensen estimated the volume of the body and manually sectioned the body into different segments by digitizing the images. Using this information, Jensen showed

that a variety of inertial parameters such as mass, MOI, and COM could be estimated. For example, the MOI of each segment is calculated about each of the anatomical axes (which are based on landmarks placed on the subject by the researcher) and determined by summing the local and remote terms of each ellipse by applying the parallel axis theorem. Wicke and Lopers (2003) published a validation study on Jensen's method where Wicke and Lopers applied the acquisitions techniques on 20 subjects. They compared subject volume estimations from Jensen's ECM to data obtained using water submersion of the subject's extremities and full body. Wicke and Lopers concluded that when using a high image ratio in the photographs (taken image to actual measured size ratio of 1:5) and taking a high degree of precaution is taken during the digitization of the images, the model by Jensen provides an accurate means of estimating segment volume of the body (total body volume error of 2.01+/- 2.17%). Wicke and Lopers noted that a high degree of variance is reduced when the digitizing operator has performed the digitization procedure at least 10 times (Wicke & Lopers, 2003).

With advancements in photographic technology, Baca (1996) used video recording to determine the anthropometrics of body segments. Baca applied the developed video-metric method, using a video camera, to obtain the required anthropometric inputs for the geometric model developed by Hatze (1980). The researchers found that anthropometric measurements using the video method did not significantly differ much from direct measurements, an encouraging find (Baca 1996; Hatze & Baca, 1992). When estimating total body volume, the method had an overall reported error of 9 %, higher than Jensen's (1978) ECM model. An important drawback that Baca (1996) discussed was that attaining the 242 inputs required for the geometric model from the video was cumbersome. With the 242 inputs, the probability of error in the estimations only increases.

Norton et al. (2002) used a 3D laser scanner to estimate the mass and COM of the legs. The results showed leg volume estimates for subjects were all within 1% to that attained using a water submersion technique and within 2.5% in COM estimations. Attaining leg volume to such a high degree of accuracy was very promising but at a cost of $120,000 for the scanner the method is too costly to be widely adapted (Norton et al., 2002).

Stancic et al. (2009) demonstrated the use of computer vision as a means of estimating anthropometric parameters for use in conjunction with geometric models. An algorithm was constructed using a 3D computer model of each subject from 2D photographic images as inputs. The method required no experience in anthropometric measurement acquisition. Results were compared to that of anthropometric tables obtained from Winter (1990) and to manual measurements taken by the researchers. The researchers showed that the computer based results for segment lengths were more personalized than values based on generalized proportion tables showing the possibility of eliminating the need for manual anthropometric measurements (Stancic et al., 2009).

As computer vision and laser technology have surged over the recent decade, devices have come down in price. In one example, Clarkson et al. (2012) used four Microsoft Kinect's (Version 1, 2010) to estimate the volume of the trunk of a manikin. With an array of Kinect devices surrounding the manikin torso, Clarkson et al. were able to recreate a 3D point cloud of the torso in less than 3 seconds. The obtained volumetric results were compared to Yeadon's (1990) geometric method and to a gold standard laser scan. The results showed volumetric estimations with a mean error of 0.04 % and a standard deviation of 2.11%, suggesting the Kinect provided results of greater accuracy then commonly used geometric models (Clarkson et al., 2012).

With a growing worldwide interest in the Kinect and its wide availability, Clarkson et al. (2014) assessed the suitability of using four Kinect's for estimating the volume of the trunk on living subjects. The findings were compared to that obtained using Yeadon's (1990) model once again. The scanning system on average underestimated volume of the trunk when compared to Yeadon's model. Clarkson et al. (2014) speculated that this could have been due to the limitations of Yeadon's model in accurately modeling the shape, leading to a consistent overestimation of the volume. This was only speculation as no gold standard volume estimates were available for the comparisons in this study. Clarkson et al. found that the Kinect system did show a promising reliability with an intraclass correlation coefficient (ICC) for 3 repeated scans across 12 participants of 0.997, higher than that of Yeadon's geometric model (average ICC of 0.887) deeming it acceptable for use in a healthcare environment where the typical necessary ICC is greater or equal to 0.70 (Clarkson et al., 2014). The results although promising, were only for one body segment, the torso, limiting the conclusions that can be made with the use of the device in this field.

Surface imaging methods have shown to be a promising approach of acquiring volumetric and anthropometric subject specific approximations to solve for BSIPs. When used in conjunction with density estimations acquired from other methods, it is possible to use surface imaging to obtain very personalized BSIPs at a low cost. With the rapid advancement in technology, using surface imaging technology could potentially eliminate the need to ever take manual measurements. With the aforementioned success of the Kinect, the device used in conjunction with other models to estimate BSIPs of living subjects should be investigated. Table 7 shows a brief summary of surface imaging from literature not all sources mentioned in text.

Table 7: Summary of a variety of surface imaging studies from literature used to estimate BSIPs. (Volume (V), Mass (M), Density (D), Race(R), Caucasian(C), Japanese (J)) This does not reflect the extent of full literature.

Year	Reference	Subject Pool information					Parameter					Method	Comments
		#	Sex	Age	R	BMI	V	M	COM	MOI	L		
1938	(Weinbach 1938)	8	M	-	-	-	-	-	x	-	-	Photogrammetric	
1978	(Jensen 1978)	3	M	8-11	-	-	x	x	x	x	x	Photogrammetric	3 Different Somatotype of young boys
1986	(Yokoi et al., 1986)	25 5	M: 132 F: 123	3-15	J	-	x	x	x	x	-	Photogrammetric	Japanese Children
1993	(Sarfaty & Ladin, 1993)	3	M	23-28	-	-		x	x	x	-	Video System	
2002	(Norton et al., 2002)	9	M: 5 F: 4	-	-	-	x	x	x	-	-	Laser Scanner	Scanner cost ($120,000)
2008	(Gittoes et al., 2008)	5	M	22.8±2.6	-	-	-	x	-	-	-	Photogrammetric	Athletes
2009	(Stancic et al., 2009)	3	M: 2 F: 1	-	C	-	x	x	-	-	x	Photogrammetric via Computer	Mainly for anthropometric parameters
2014	(Clarkson et al., 2014)	12	M	22	-	24±3	x	-	-	-	-	Kinect V1 Sensor	Only scanned trunk
2015	(Sanders et al., 2015)	11	F: 9 M: 2	-	-	-	x	x	x	x		Reliability study	Swimmers
2015	(Peyer et al., 2015)	6	M: 4 F: 2	-	-	-	x	x	x	x	-	Pi Camera	18 Raspberry Pi camera module

2.6 Microsoft Kinect

The Microsoft Kinect V1 sensor has a build-in color camera, depth camera and infrared emitter. Released in 2011 specifically for the Xbox 360 gaming console, it has become one of the most widely available 3D cameras (at a cost of ~$200). There is a large amount of open-source code and function libraries freely available that provide potentials for the camera is a wide range of applications. Microsoft has designed many functions for the Kinect. One particularly relevant feature is *Player Recognition & Joint Tracking*. With *Player Recognition* the Kinect is able to detect people in its view sight then applying *Joint Tracking* it is able to determine a silhouette of the person and estimate approximate joint locations.

In recent years there has been much research published in the field of biomechanics using the Kinect as a quantitative measuring device (examples: Bonnechère et al., 2014; Espitia-Contreras et al., 2014; Huang, Zhenhao et al., 2013; Ning et al., 2013; Oh et al., 2014; Weber et al., 2011). The Kinect has also been used as a means of developing 3D avatars of people (Barmpoutis, 2013; Tong et al., 2012) and for determining subject specific anthropometric data for electronic based fitting rooms (Chang et al., 2013). Clarkson et al. (2012) demonstrated the possibility of using multiple Kinect V1 cameras for BSIP estimations of the trunk. Clarkson et al. (2014) demonstrated that using the Kinect for estimating BSIPs of the trunk of living subjects was reliable and comparable to results produced by geometric modeling (Clarkson et al., 2014). Acquiring 3D scans of humans and various other objects has also been shown as feasible with the Kinect as well (Doumanoglou et al., 2013; Lachat et al., 2015; Smisek et al., 2011; Tong et al., 2012). In 2015 Microsoft released a newer version of the Kinect (Version 2, 2015) capable of

higher accuracy scanning (Figure 10). A quick comparison of the specs between Kinect V1 and V2 is shown in Table 8.

Figure 10: Microsoft Kinect V1 (2011) and Microsoft Kinect V2 (2015). The infrared camera and projector (depth sensor) as well as the RGB camera are shown for both devices.

One of the most important changes between the Kinect V1 and the Kinect V2 is the depth-sensing module (which acquires 3D information). The Kinect V1 uses a structured-light method whereas the Kinect V2 uses Time-of Flight, which uses active sensors to measure the distance of a surface by calculating the round-trip time of a pulse of light (Kolb et al., 2009).

Table 8: Equipment Specs of the Kinect V1 and the Kinect V2 (Microsoft Corporation, 2015)

Feature	**Kinect V1**	**Kinect V2**
Colour stream (resolution)	640×480	1920×1080
Depth stream (resolution)	320×240	512×424
Infrared stream (resolution)	None	512×424
Depth range	0.4m → 4.0m	0.5m → 4.5m
Horizontal Field of View	57°	70°
Vertical Field of View	43°	60°
Skeleton Joint Defined	20	26
USB	2.0	3.0
Operating System	Windows 7,8	Windows 8

2.6.1 Accuracy and Precision

Shin et al. (2013) characterized the spatial accuracy and precision of the Kinect V1 for creating 3D images for use in medical applications. The experiment involved comparing the measured distances between points on a flat and curved surface with control measurements taken with a ruler, caliper and CT. The findings showed that on a flat surface the Kinect was able to measure the distances with errors of less than 2mm and on a curved surface less than 3mm consistently (Shin et al., 2013). Choppin et al. (2013) calculated breast implant volume with the Kinect V1 and found that volume was overestimated 30.3% for 400g (small implants) and 13.9% for 600g (large implants). The results suggested that the Kinect V1 might not be the best application for small object scanning with the smaller implant shown to have a greater overestimation then the larger one (Choppin et al., 2013). Similarly, Henseler et al. (2014) found that breast volume was overestimated by the Kinect V1 never more than 10% from the ground truth volume of the implant. Henseler et al. (2014) found that the reproducibility was high for 4 of the 9 breast implants scanned but found differences of approximately 10% for the other 5 implants (Henseler et al., 2014). Meister et al. (2012) scanned a statue with a high accuracy laser scanner and compared the results to the Kinect V1. Findings suggested that flat surfaces were within a 5-10mm error (to the true length). Curved surfaces were generally underestimated in volume and sharp corners showed to be smoothed out (less detail in the scan when compared to laser data) (Meister et al., 2012). The authors suggested a general resolution of approximately 10mm in absolute world coordinates for the Kinect V1. Shown in Figure 11 is an example of the scanned statue.

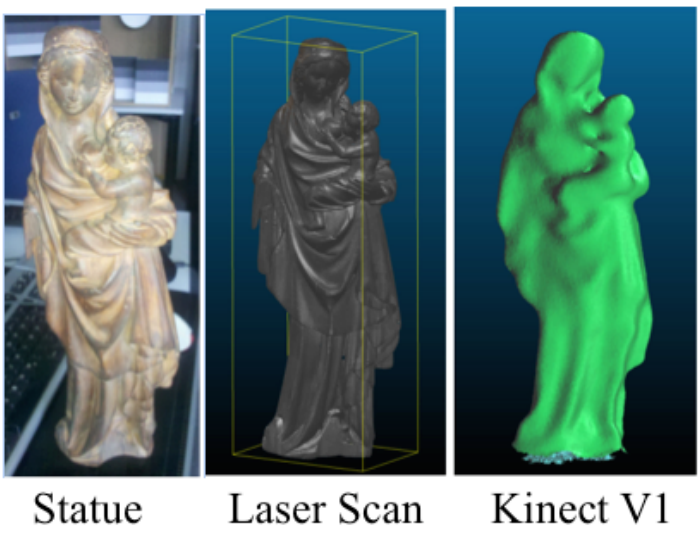

Figure 11: Left: Statue to be scanned Middle: 3D laser scan showing small detials of the statue Right: Kinect V1 Scan showing less detail (Meister et al., 2012)

With the release of the Kinect V2, Lachat et al. (2015) showed that the Kinect V2 achieved more accurate measurement results than the Kinect V1. Kinect V2 estimated distances compared to measured distances showed a correlation of r =0.99 with standard deviations of around 4mm when the Kinect V2 was <1.5m to the object and up to 16mm with the Kinect V2 4.5 meters from object (Lachat et al., 2015). Lachat et al. (2015) also found that the Kinect V2 was much less sensitive to sunlight, suggesting the possibility of using the device outdoors. Yang et al. (2015) found similar results showing that the depth accuracy of the Kinect V2 depended on the scanned objects distance away from the device with general error of less than 2mm within a 2m distance (Yang et al., 2015). Shown in Figure 12 are the estimated errors at varying physical distances away from the Kinect as well as varying degrees from the optical lenses of the Kinect V2.

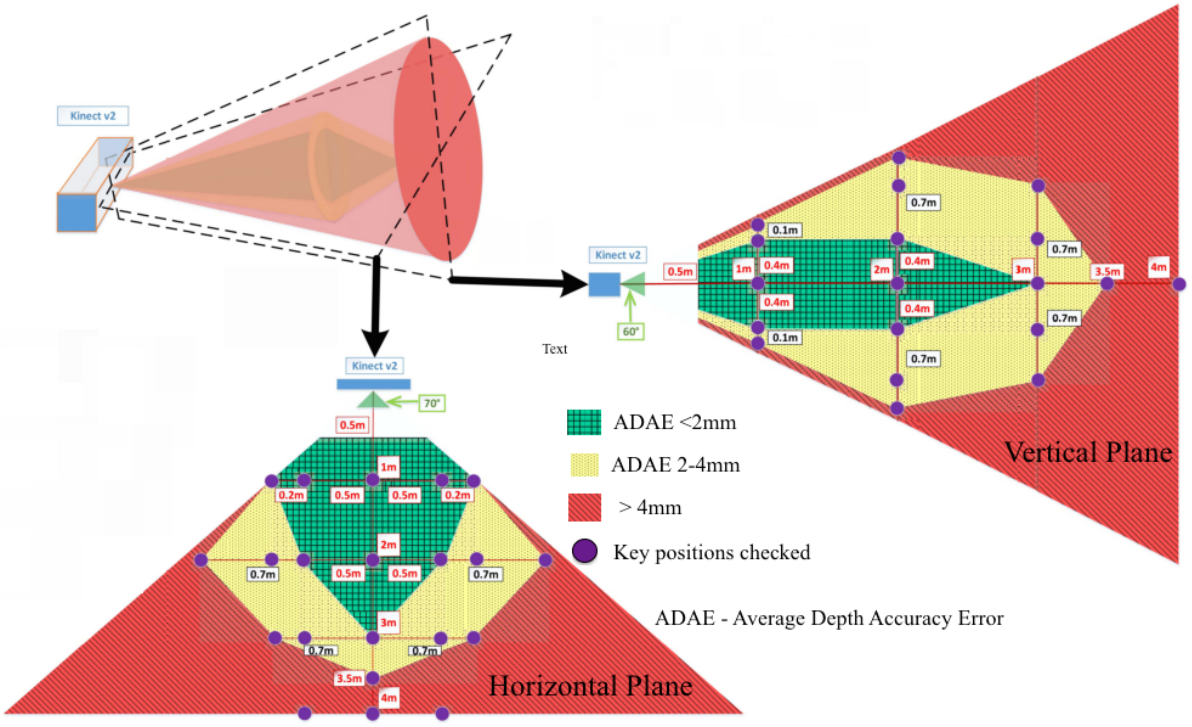

Figure 12: The field of view of the Kinect V2 and the associated measurements errors reported by Yang et al. (2015). At a distance of 1-3 m along the optical view of the lens the error is lowest (<2mm). (Image modified from original taken from: Yang et al., 2015)

2.7 Summary

The importance of acquiring accurate BSIP measures has been established in the literature. Cadaveric dissection has provided invaluable preliminary information regarding the shape, size and BSIP estimates of human body segments. Medical imaging had made it possible for extracting tissue information from living subjects, paving the way for modeling the internal composition of the body without the use of cadavers. Geometrical models and regression equations have proven potential in estimating the shapes of body segments using anthropometric measurements acquired directly from the subject of interest. However, these techniques can require a large amount of time and or money. Researchers seeking highly subject specific

estimates or seeking to model a population of subjects that is not well represented by the aforementioned modeling techniques (example: pregnant women, children, high/low BMI subjects, amputees) have limited options that are quick and inexpensive.

Using surface imaging methods researchers can acquire representative images of persons of interests from which geometric properties can be extracted. However, highly acceptable methods such as laser scanning require expensive equipment and can require a sufficient amount of space. With the development of portable scanners such as the Microsoft Kinect V1 and V2, there exists potential for subject specific BSIP estimations overcoming some of the limitations seen in aforementioned studies. With the potential of rapidly acquiring 3D scans of subjects, there is also potential of using the Kinect as a means of rapidly estimating BSIPs of subjects with virtually no morphological restrictions and minimal invasiveness. With the Kinect V2 shown to be more accurate at acquiring quantitative measurement results, exploring the use of this device in the context of subject specific BSIPs is necessary. The upcoming section, Chapter 3, presents a experimentally developed method, which utilizes the Kinect V2 as a research tool for estimating subject specific BSIPs.

Chapter 3
Methods

3.0 Subjects

Subjects were recruited from Queen's University campus by the use of posters and word of mouth. Before testing, participants read and signed an information package and consent form approved by Queen's University's Ethics Board which is shown in Appendix A. All participants were explained the Kinect and ECM protocol and the purpose of the study prior to data collection. Ten male and eleven female participants were recruited for the study. Participants were asked to wear form-fitting attire such that the contours of their body could be easily determined. Specifically, male volunteers wore forming-fitting shorts and either a forming-fitting shirt or no shirt at all. Female volunteers were given the option between wearing long or short forming-fitting pants and a sports bra or a form-fitting workout shirt. All participants were asked to wear a swim cap on their head to control hair. There were no exclusion criteria for the participants. Each participant was weighed three times on a calibrated medical scale and the

average mass was recorded. Mean age and morphological measures of the subjects was collected and is shown in Table 9.

Table 9: Average and standard deviation for age, height, weight, and body mass index (BMI) of the participants

Subjects	Age (Years)	Stature (m)	Mass (kg)	BMI (kg/m²)
Males (n=10)	23.4(1.7)	1.79(0.06)	75.66(4.5)	22.65(2.14)
Females (n=11)	22.3(2.4)	1.73(0.09)	70.18(7.8)	23.3(2.25)

3.1 Experimental Setup

3.1.1 Anatomical Land Marking

Anatomical landmarks were determined through direct palpation of the body. Once the operator determined each landmark a marker was placed on the surface for reference. Non-reflective color markers were used for this. Reflective markers such as those commonly used in gait studies were dismissed because interference between the markers and the Kinect was observed (Figure 13). In order to be able to identify the markers in the post processing stage of the experiment, markers with a high color contrast with the subjects skin were used (2cm diameter). This required that subjects be scanned in full color, a feature available with the Kinect (Microsoft Corporation, 2015).

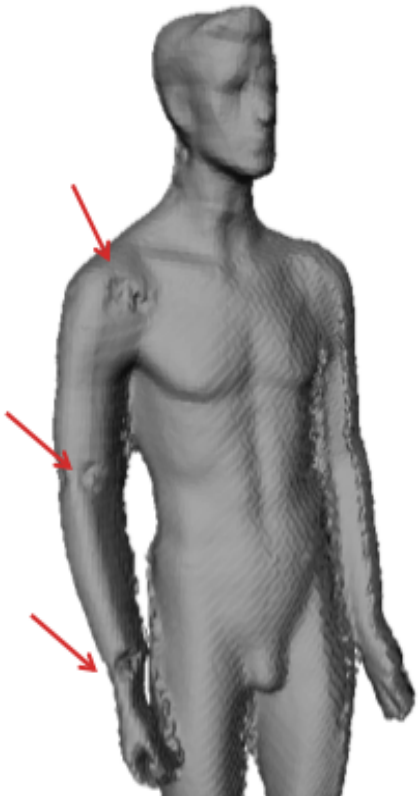

Figure 13**:** Example of interference caused by reflective markers shown on a manikin subject

The specific anatomical landmarks and respective definitions are shown in Table 10. After the landmarks were identified in the frontal and sagittal planes on the body, a thin band of adhesive tape (duct tape) was wrapped around the limb at the specific location connecting the two markers (frontal and sagittal). This was done for each set of landmarks. These bands (of tape) defined the proximal and distal boundaries for body segment segmentation. Tape was used because it is non reflective, adheres well to the body, does not affect volume measurements, and comes in a variety of contrasting colors which show up well on the scans. Figure 14 illustrates a subject outfitted with the color markers and tape approximating segmentation boundaries and anatomical landmarks.

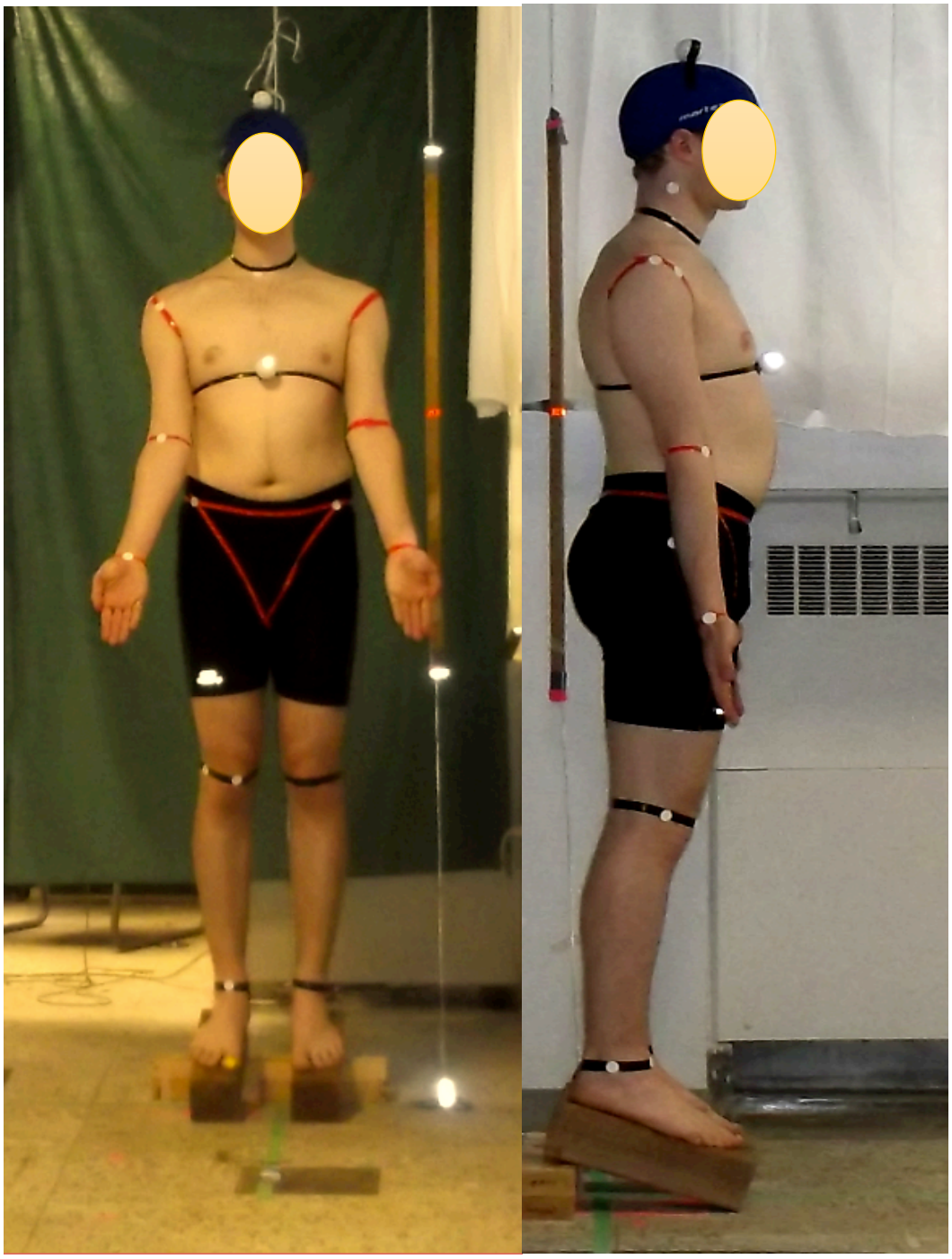

Figure 14: Example of subject outfitted with anatomical segmentation boundary tape and non-reflective tape for anatomical landmark identification

Table 10: Body Segment definitions used for anatomical segmentation. Bony landmarks were marked with high contrast tape in the front and right side view of the subject. A total of 26 marks were used to indicate landmarks.

Landmarks				Segmentation Boundaries		Comments
Body Segment	**Front View**	**Right Side**	**Segment Name**	**Proximal or Ventral**	**Distal or Caudal**	
Head + Neck	1. Apex of the Head	2. Apex of the Head	**Head**	Apex	Frontal plane at height of C7	Segmentation on the transverse plane at the cervical C6-C7 landmark defined in frontal plane
	3. Tip of the Chin (at C1 level)	4. Right Side view along Chin line	**Neck**			
Torso	5. Front at level with C6-C7	6. Centre of torso at level with front	**Upper Trunk**	Frontal plane at height of C7	Xiphoid	
	7. Xiphoid 8. Umbilicus (L3-L4)	9. Xiphoid	**Abdomen**	Xiphoid	Umbilicus	
	10. Iliac Crests 11. Pubis		**Pelvis**	Umbilicus	Plane roughly through the iliospinales at an angle of 37° to the midsagittal plane	See Figure 25
Arm	12. Tip of 3rd digit	13. Tip of 3rd digit	**Hand**	Stylion	-	
	14. Center of Styloid 15. Center of Elbow Joint	16. In line with Styloid 17. In line with elbow joint	**Forearm**	Radial	Stylion	
	18. Acromion		**Upper Arm**	Acromion*	Radial	Segmentation through the acromion by sagittal plane with arm abducted at 90°
Leg	19. At level of Greater Trochanter 20. Patella at level of femoral condyle	21. Greater Trochanter 22. At level with femoral condyle	**Thigh**	Plane roughly through the iliospinales at an angle of 37° to the midsagittal plane	Tibiale	Distal cut is at approximate plane defined by Femoral condyles
	23. At level of lateral malleolus	24. Lateral malleolus	**Shank**	Tibiale	Sphyrion	
	25. Tip of the longest toe	26. Tip of the longest toe	**Foot**	Sphyrion	-	

* based off of boundaries definitions from Zatsiorsky and Seluyanov (1983)

3.1.2 3D Scanning

The Microsoft Kinect V2 camera sampling at 30Hz rested on a height adjustable tripod (Manfrotto Professional Tripod). The Kinect was connected via USB 3.0 to a system operating Window 8.1 (Graphic Processor Unit: GeForce GTX 970, Motherboard: Z97 Gaming 3 Intel). To allow for a greater distance between the camera and the computer, a 30-foot active USB 3.0 extension cord (SuperSpeed USB 3.0 Active Extension) was used. Acquisition software, 3D Builder (Microsoft Cooperation, 2015), available freely through the Microsoft App store, was used as an acquisition tool in this project. Other software was explored and custom software was also written but due to its reliability and overall ease of use, 3D builder was deemed as the best choice for the project requiring minimal training and being easily accessible. Shown in Table 11 is a brief comparison of software that was explored for data acquisition.

Table 11: Software explored for 3D data acquisition using the Kinect

Software	Positive	Negative	Price
Microsoft 3D Builder	▪ Color scanning ▪ User friendly	▪ Restrictive settings ▪ Minimal features	▪ Free
Kinect Fusion	▪ High level of adjustability ▪ Many features	▪ Consistent crashing ▪ Inconsistent scan outputs ▪ Color scanning was inconsistent	▪ Free
Custom MATLAB Software	▪ Full range of adjustability	▪ License required ▪ Complex no GUI	▪ Large time requirement

All of the 3D scanning was performed in private lab environment free of distractions. Each subject was asked to stand in a specially marked location. A circle drawn on the floor indicated the scanning path of the camera. The subject was asked to stand at the centre of the circle on top of an elevated transparent platform. This platform served as a means of separating the subject's

feet from the ground because it was elevated. Secondly, the platform eased segmentation of the feet because the point cloud data from the floor would not be captured together with the feet. As the platform was transparent it did not show up in the scans. The subject was asked to stand in such a way that their feet were at the furthest edges of the platform and their arms abducted approximately 90° to the torso as shown in Figure 15. This posture was chosen as it allowed for visibility for the camera to capture beneath the arms and in between the thighs, maximizing the potential accuracy of the scan. With the arms and legs closer to the body inaccuracies were visible in the scans (small gaps between adjacent body segments were not well represented) as shown in Figure 16. A similar phenomenon was observed with the hands. When the hand was scanned and not fully extended meaning there was 'cupping' in the palms, which resulted in additional points being estimated in the area. Similar observations were noted by other researchers as well when using surface imaging techniques (Peyer et al., 2015; Wicke & Lopers, 2003). As a result, subjects were asked to keep their palms fully extended during scanning to reduce any errors.

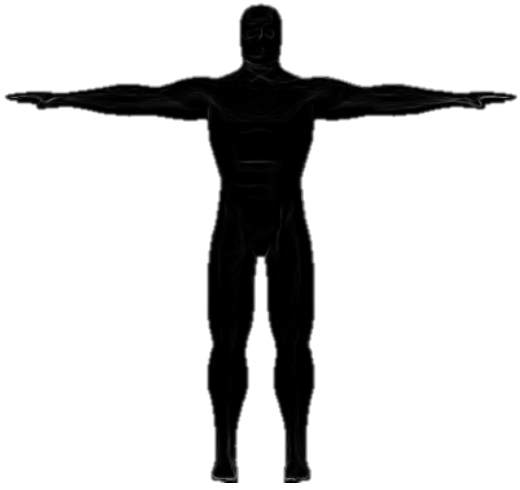

Figure 15: Pose adopted for 3D body scanning. Abducting the arms and legs allowed for minimum visual inaccuracies in the scans.

Once the subject was ready, they were alerted that during the duration of the scanning process they were to remain as still as possible. Subject limb movement, specifically of the arms swinging, created noticeable scanning errors. As result each subject was asked to breathe shallowly during the duration of the scan and try to stay as still as possible avoiding swinging their arms.

Figure 16: 3D scan of manikin showing visual inaccuracies under the arm and by the hand

To begin the scanning protocol, the Kinect was placed in front of the subject at a distance of 1.5 meters, within a minimum error range ((error < 2mm from: (Yang et al., 2015)) . This also ensured that the whole subject was visible to the camera. An assistant operating the computer began the data acquisition in 3D Builder to ensure that everything was running. Data acquisition *Size* was set to one step below large and *Detail* set to maximum. This setting allowed capturing

at maximum resolution without capturing too much of the environment around the subject. A link to a video of the scanning process is provided (https://youtu.be/s1cVydFvFp8). Once the camera was running, a vocal count down was used to prepare the subject for the scan. Another operator then began to revolve the Kinect by walking around the subject in a clockwise direction at a height of approximately 1 meter from the ground following the circular path outlined on the floor. During this process the camera was held in such a way that the lens was facing towards the subject with the subject central to the focal point, minimizing distortion. Once one full revolution was complete the camera was manually elevated to approximately 2 meters from the ground and a counter-clockwise revolution around the subject was then performed. Once the camera was back to its original starting position (after 1 full clockwise revolution and 1 full counter clockwise revolution) the computer operator clicked save and the scan was finished. The subject was immediately notified that they could move again. The scan duration on average took 20-30 seconds.

Following each scan the data was reviewed to ensure no major errors occurred during this process. Once the scan was deemed adequate, meaning without any obvious visual inaccuracy, it was saved in the polygon file format (.ply). The scanning process was then repeated until three adequate scans of the subject were acquired. Most subjects required five scans before three acceptable scans were saved. Polygon file format ensured that a variety of properties could be stored including: color, transparency and the texture coordinates. Each subject scan was given a unique identifying code to ensure subject anonymity. Shown in Figure 17 is an example of a raw output scan following protocol. Figure 18 shows a schematic of the full setup, which was described above.

Figure 17: 3D body scan of a subject identifying anatomical segmentation boundaries and landmarks.

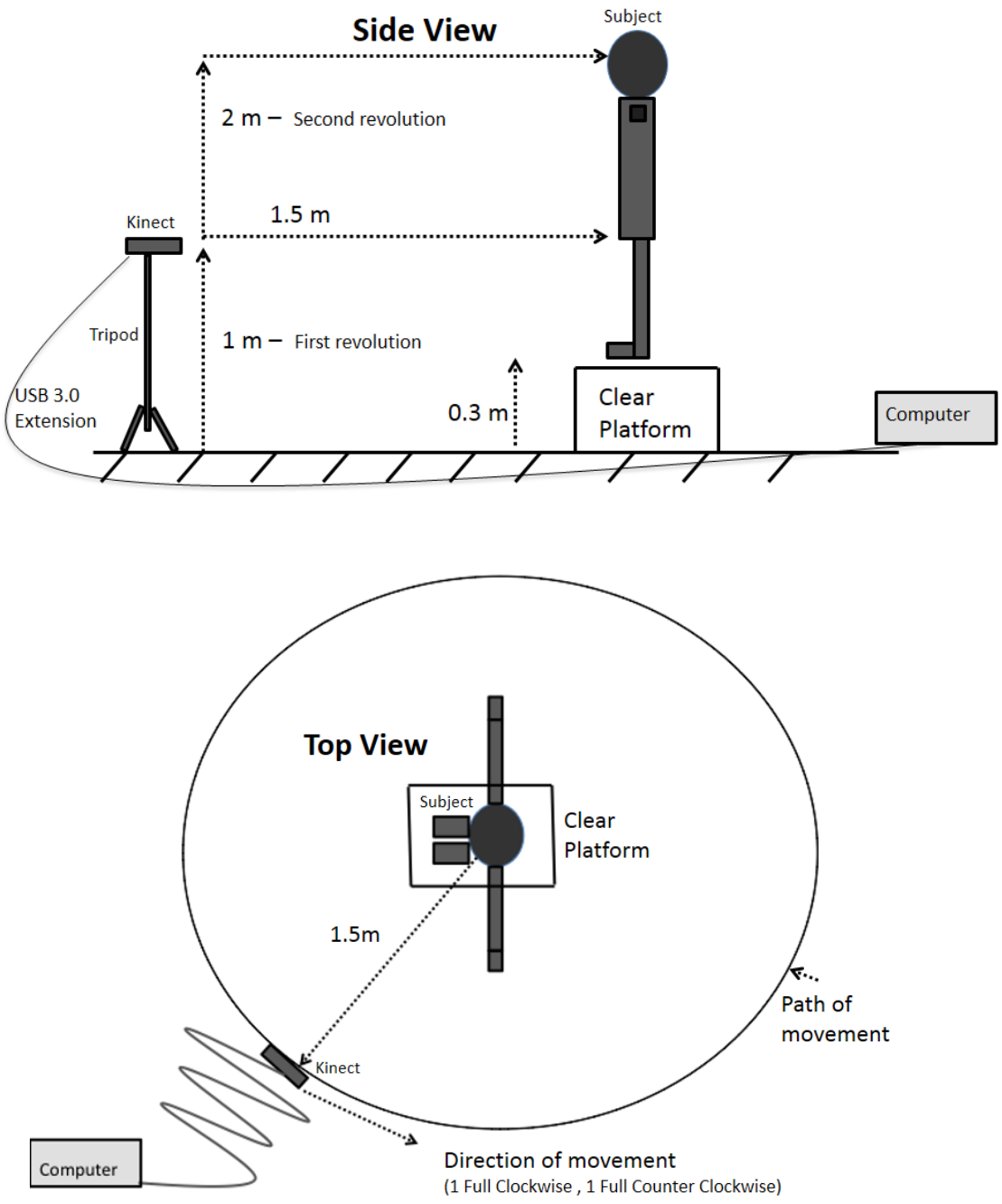

Figure 18: Setup schematic for Kinect scanning protocol. The Kinect followed a circular path of movement around the subject starting in a clockwise direction (at 1m off the ground). Once a full loop was complete the Kinect was walked back in counter clockwise direction at an elevation of approximately 2m (1m higher).

3.1.3 Elliptical Cylinder Model

The photographic method based on the elliptical cylinder model (ECM) developed by Jensen (1978) was used as a comparison tool in this project. The subject specific ECM has been evaluated by Wicke and Lopers (2003), with reported total body mass errors of less than 2% when compared to water submersion techniques (gold standard technique). The *Slicer* software written by McIlwain (McIlwain 1998) implements the model using two orthogonal photographs as inputs. The minimal training required and subject specific nature of the outputs will allow for an appropriate comparison to be made to that of the results collected using the Kinect.

Two digital cameras (Fujifilm Finepix AX 660) were placed 5 meters from a designated platform at which the subjects stood. The shooting mode was set to 'auto' on both cameras and the image size adjusted to 4608x3440 shooting at 16 mega pixels. The first camera was positioned in front of the participant, with the camera parallel to the frontal plane of the subject. The second camera was positioned to the right of the participant, with the camera parallel to the sagittal plane of the subject. Commercial meter sticks with reflective tape on the ends were hung in the sagittal and frontal planes and reflective markers were placed 1m apart on the floor. The meter sticks and markers served as a mean of scaling the photographic images in the post processing part of the experiment. A full experimental schematic is shown in Figure 19.

Each participant was asked to stand on a small platform which was angled 20° to the floor. This allowed for maximum exposure of the feet to the optical view of the camera. To make sure the hand was positioned properly, participants were asked to keep their fingers together and flex them to the point before hyperextension, as recommend by Wicke and Lopers (2003). The participants were also asked to internally rotate their hands until the minimal amount of area

could be seen in the right side view (as shown in Figure 20-B). Two operators were required to capture the photographs. This was to ensure that the photographs were taken as close as possible to the same instant. Once the participant was appropriately positioned a verbal countdown was issued and the photographs were taken. This was repeated 3 times to ensure that an adequate set of photographs was captured. Anatomical markers, which were in both the frontal and sagittal plane (as described in Table 10), were used later for the digitization and segmentation in post processing. Before the subject was asked to step off the platform the photos were quickly inspected for any visual imprecisions, none where rejected.

The subject images were imported to the computer and given a unique identifying code to ensure that each set of frontal and side images were appropriately matched. The photographs were then cropped to include only the subject and the meter sticks in the image. The cropping was done in such a way that all of the photographs maintained an aspect ratio of 4x3, based on the recommendations by Wicke and Lopers (2003). One set of photographs (frontal and side view) was chosen for each subject and imported into Slicer. Once in *Slicer* the digitizing process is simply the process of using a mouse to click around the contour of each segment. The operator's experience level is considered negligible relative to between-operator variations (Wicke and Lopers 2003). Therefore, a single trained operator digitized all of the participants to ensure consistency. The segmentation boundaries are detailed in Table 10. For the segmentation of the pelvis a computerized protractor was used to ensure that a 37° boundary from the pubis along the midsagittal plane was defined. Once all digitizing was completed, the segments BSIPs (volume, MOI, COM and length) were computed as in Jensen (1978). An example of a fully digitized participant can be seen in Figure 20.

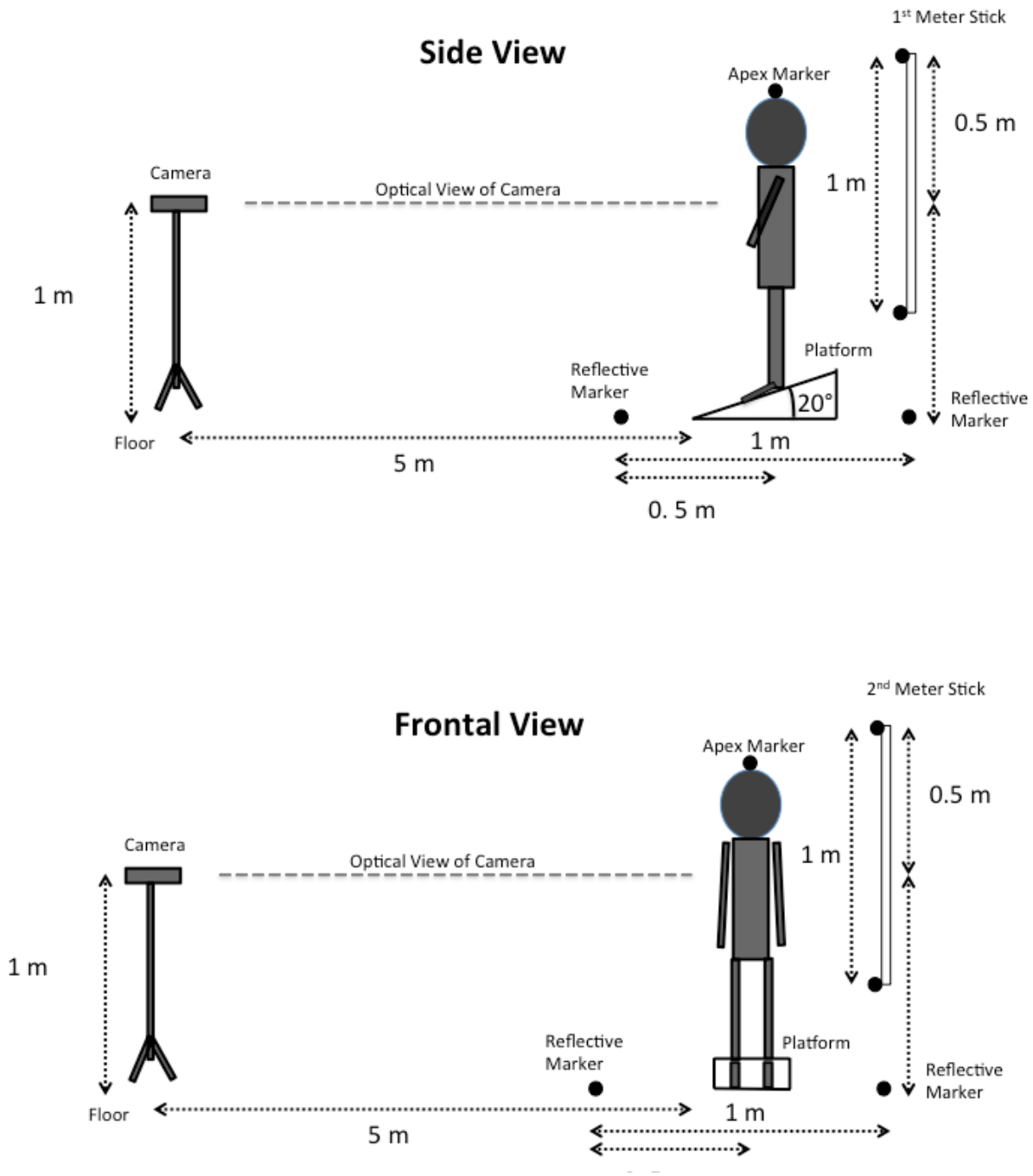

Figure 19: Side and Front view of Jensen 1978 ECM photographic method setup used for estimating subject specific BSIP. Participants stood on the platform (not to scale).

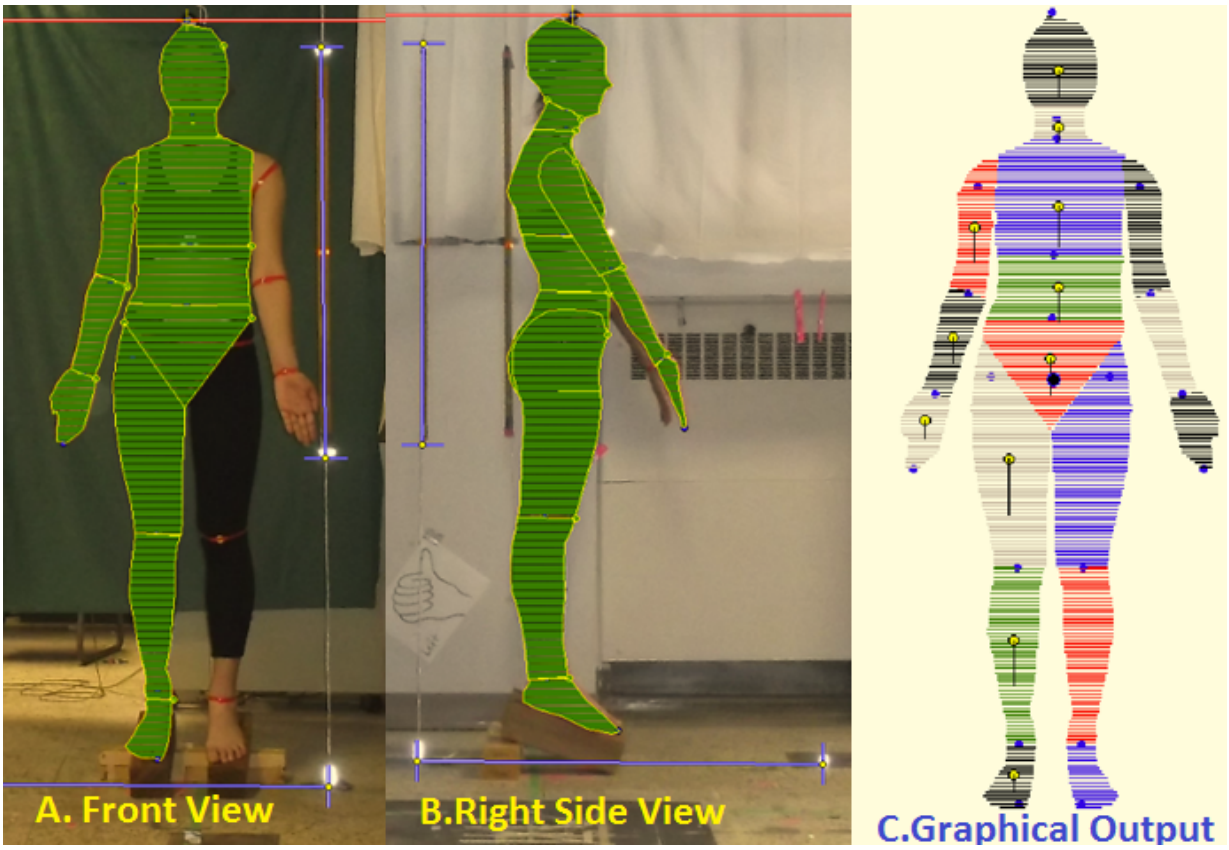

Figure 20: A. Front and B. Side view showing manual segmentation outlines defining segment boundaries. C. Graphical output from Slicer software showing segment centers of mass (yellow) and proximal and distal landmarks (blue)

3.2 Post Processing

3.2.1 Software

The Kinect data post processing was done using Meshlab (64 Bit Version 1.3), Natfabb (Basic Version 5.2) and custom MATLAB (2012 Version A) Code. Meshlab was chosen because the software allowed for easy GUI manipulation of point clouds and has been widely used by researchers (Kramer et al., 2012; Shin et al., 2013; Wheat et al., 2011). The open source nature of Meshlab as a mesh process tool was another reason that the software was chosen. The widely cited algorithms within Meshlab permit for easy reference to literature from GUI functions. This

enables for free access to the software with minimal training required (Cignoni et al., 2008). Netfabb, which is also a widely available free of charge software, was used only in the first step of mesh editing explained in Section 3.2.2. Custom dedicated MATLAB script was written for extracting specific triangular mesh information which otherwise would be time consuming and difficult to do for a large amount of scans although possible to compute in Meshlab.

3.2.2 Mesh Editing

In raw form each 3D Kinect scan had small holes within the point cloud data, which needed to be filled in prior to any analysis. Creating a mesh to enclose a cloud of points is a common step when working with point clouds. Meshlab has a variety of reconstruction algorithms, which create a triangular mesh of the imported point cloud, filling in all small holes. Under *Filters> Remeshing, Simplification, and Reconstruction* there is a wide range of options to choose from. An example is a Poisson reconstruction created by Kazhban et al. (2006). However, in some cases surface reconstruction can take away important details from the scans such a facial features (Shin et al., 2013). Minimal reconstruction of the point cloud will provide the clearest idea of the accuracy of the results obtained from the Kinect. Meshlab offers an option to *Fill Holes*. This process triangulates together the points in a cloud forming a mesh, effectively enclosing the point cloud to be a watertight mesh meaning no spaces or gaps exist between points. Meshlab does not allow for an automated process of filling in holes, each hole must be selected manually. This would require a large amount of time and would be impractical. Netfabb provides a function *Close Trivial Holes* under *Repair->Actions->Close Trivial Holes,* which performs this action automatically. The scans were all imported into Netfabb and trivial holes were closed. All of the files were saved as .ply files

3.2.3 Alignment

After the scans had a triangular mesh from the *fill hole* procedure, each subject scan was individually imported into Meshlab. However, importing the raw scans resulted in the scans not being aligned to any particular meaningful axis, making it difficult to segment the body in any meaningful way (Figure 21-A). The solution to this was to align each scan in such a way that any cuts that would be made would be perpendicular to the frontal plane of the body. The simplest solution was to align the scans to a principal axis about the body's COM. In the menu under *Filters> Normal, Curvatures and Orientation> Transform: Move, Translate, Center* moved the center of the mesh to a global axis that was central to the geometry of the object. Check marking *Translate center of box to the origin* and *Freeze Matrix* then clicking apply shifts the scan (Figure 21-B). Next under *Filters> Normal, Curvatures and Orientation> Transform: Align to Principal Axis* and checking *Use vertex* and *Freeze Matrix* aligns the z-axis along a longitudinal plane of the body scan (Figure 21-C). Shown in Figure 21 is an example of this full process. Once the scan has been aligned it was possible to begin segmentation.

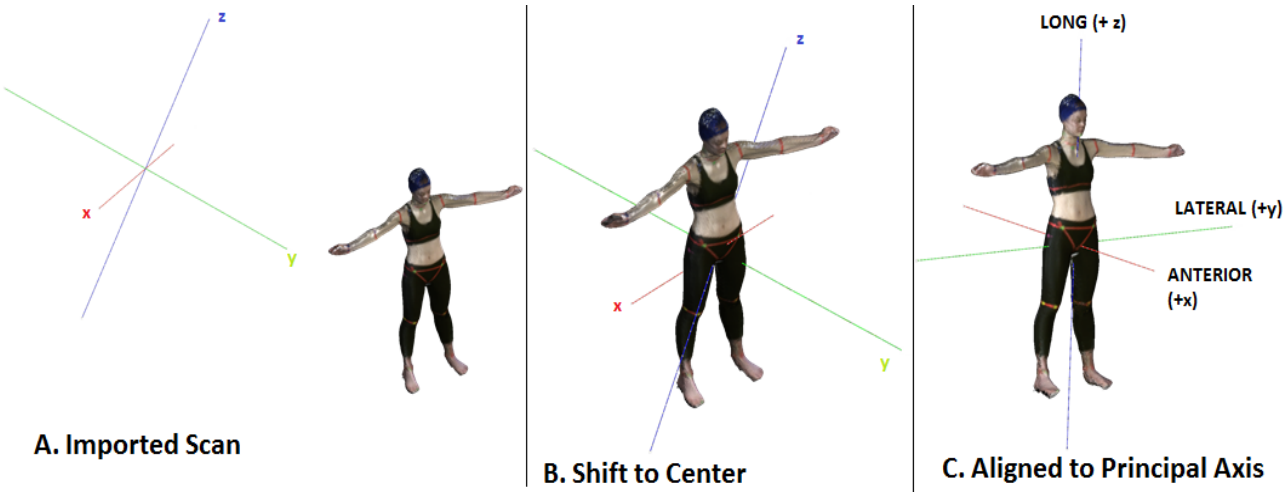

Figure 21: **A.** Imported Raw Scan **B**. Shift to Center of Meshlab Global Axes **C.** Alignment to Principal Axis of the scan about the COM.

3.2.4 Segmentation

Body segmentation for the 3D data was performed in Meshlab using the *Select Vertices* option. Referring to the anatomically marked locations on the subject (detailed in Table 10), manual segmentation was possible based on these visual cues. The tape bands were visible in the scans and were used as boundary guidelines for segmentation. Prior to segmentation the camera view was adjusted under *Windows>View From>Top* in order to ensure that the view on the screen was such as that of Figure 10. Such view, with the scan perpendicular to the cutting plane, made the segmentation procedure possible and intuitive, as demonstrated in Figure 22 where an example of the middle trunk segmentation is shown. Using the *Select Vertices* feature, vertices were selected and deleted using *Delete Selected Vertices* until the desired segment remained.

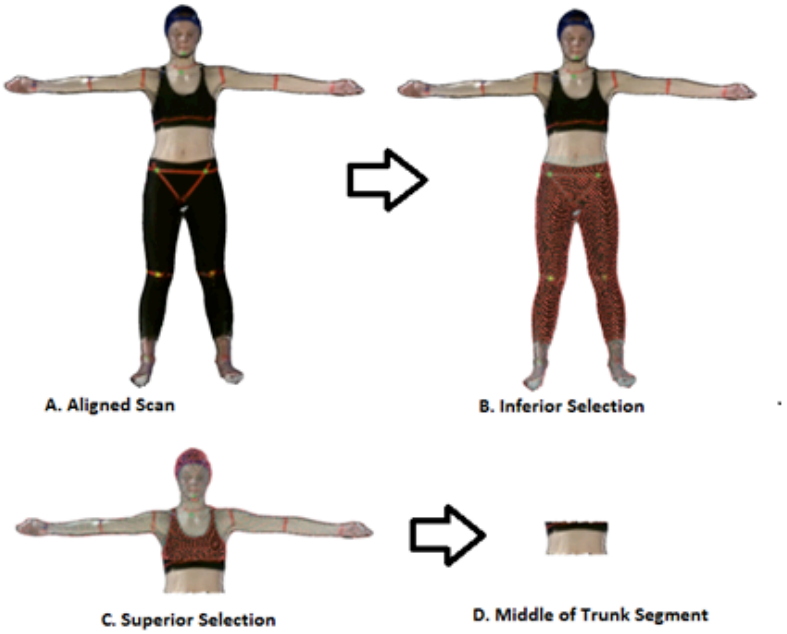

Figure 22: **A.** Raw Scan Aligned to Principal Axes showing tape which defined cutting location **B.** Vertices Selection of Lower Limbs. **C.** Lower Vertices Deleted and Upper Body Vertices Selection **D.** Segmented Middle Torso Segment.

Body segmentation always resulted in the shape to be hollow as shown by Figure 23-A. Using the holes filling algorithm found under *Edit>Fill Hole,* simple holes resulting from segmentation were easily filled, a necessary step required for calculating volume and inertial parameters later in steps of the protocol.

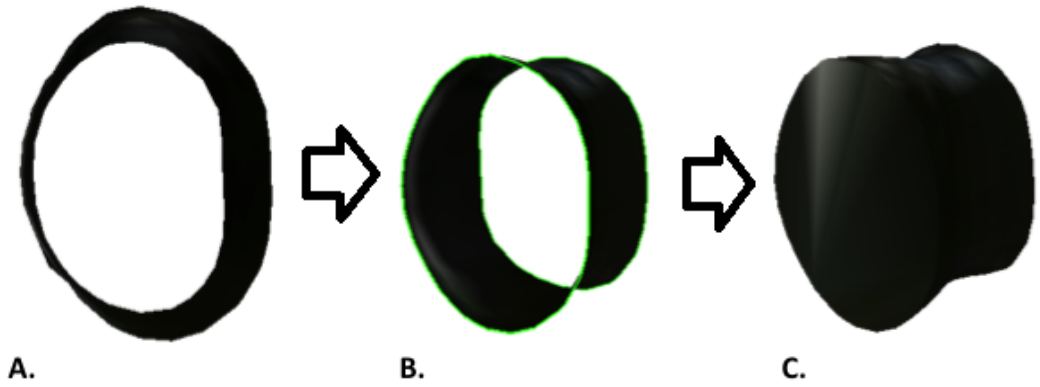

Figure 23: Lower Trunk Segment **A.** Hollow from segmentation **B.** Selecting holes to fill **C**. Holes filled.

A specific segmentation order was followed to ensure consistency between scans. The order was based on first segmenting the segments which were on the extremities of the body then moving inwards, as detailed in Table 12. The pelvis and upper torso were not segmented rather they were the last two segments remaining after all of the other segments were cut.

Table 12**:** Body segmentation order starting with the 1st and moving towards to the 3rd

Order	Body Segment	
1st	Head, Hand and Foot (Right and Left)	[5 segments]
2nd	Abdomen, Forearm and Shank (Right and Left)	[5 segments]
3rd	Thigh and Arm (Right and Left)	[4 segments]

To ensure that segmentations did not overlap with one another a specific system was developed. Following the order of segmentation detailed in Table 12, the first 5 segments would be dyed a different color and imported back into the scan then deleted. A detailed example of this is shown in Figure 24.

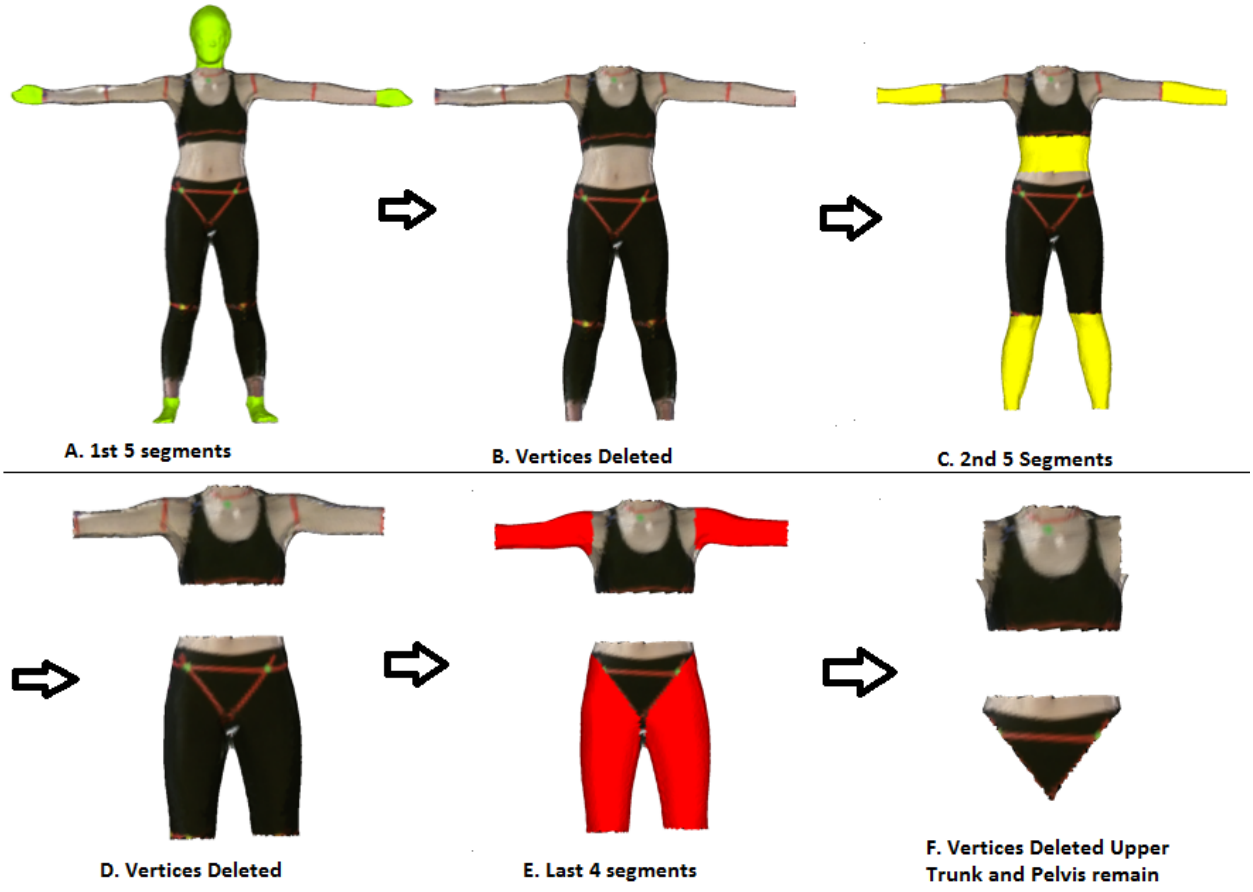

Figure 24**:** Body segmentation protocol following segmentation order detailed in Table 12. **A.** The first 5 segments **B.** Vertices deleted **C.** Second 5 segments **D.** Vertices Deleted **E.** Last 4 segments to be imported and dyed **F.** Vertices deleted and the trunk and pelvis remain.

Each body segment was given a unique identifying code. To dye the segment under *Edit->Z-Painting* each body segment was dyed a specific color. Once the segments were ready to be imported back onto the original scan the original scan was opened in Meshlab and the segments dragged into the software. Next under *Filters->Vertex Attribute Transfer* the color from each

segment was transferred to the original scan (such as in Figure 24-A). *Max Dist Search,* an option in the pull down menu, samples points within a specified distance of the imported segment being transferred. This was set at 0.01%. Once each segment color was transferred to the original scan the color vertices were selected. Under *Filters->Select Face by Color* the specific segment color was selected and then the vertices were deleted using *Delete Selected Vertices* (Figure 24-B). This process was repeated as depicted by Figure 24 A-F.

The 37° plane cut which is made at the upper thigh region was done by rotating the scan 37° (*Filters->Normals, Curvatures and Orientation->Tranform:Rotate)* about the anterior-posterior axis (x-axis defined in Figure 25). Then with the *Select Vertices* option the cut was made from the pubis. The resultant body scans after segmentation resembled that of Figure 25.

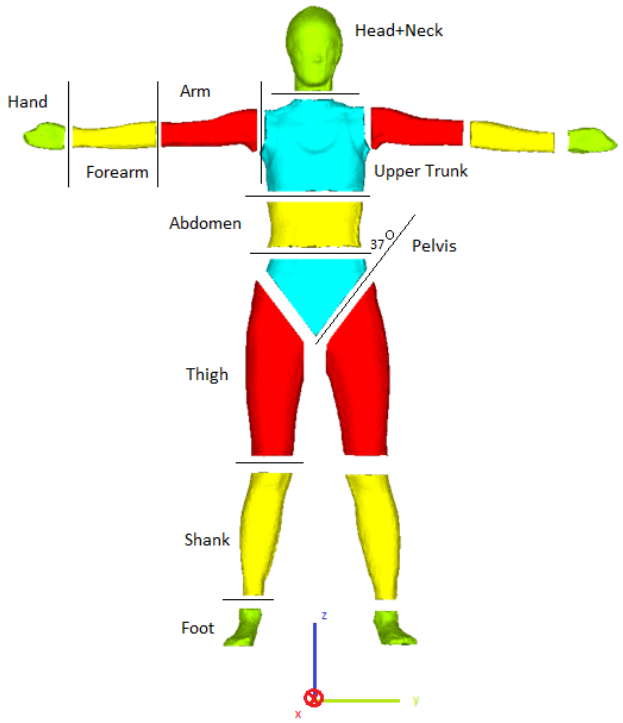

Figure 25 : Body scan post-segmentation. A total of 16 body segements are shown.

3.3 BSIP Evaluation

The volume, mass, COM, MOI and segment lengths were all evaluated as an average between the left and right side of the limbs, meaning all of the BSIPs were calculated for each 16 segments but the average value of the left and right side for the BSIPs was reported in the results. The following section overviews how the BSIPs were acquired in post processing.

3.3.1 Import STL

All of the .ply files were converted to sterolithography files (.stl) for the purpose of analyzing in Matlab. Each subject had 16 separate .stl files representing the 16 body segments. Open source code by Adam H. Aitkenhead (READ_stl from Matlab Community) was used to import the .stl files into Matlab structures. A link to the code file is provided in the Appendix B. Once the scan was imported into Matlab, the BSIP were evaluated.

3.3.2 Segment Volume

The volumes of the point clouds were calculated based on the method detailed in Eberly et al. (1991) using divergence theorem from calculus as represented by Equation 3. Integration of an area over the boundary of the region formed by the triangular mesh is used to solve for volume. Code written by Anwar M. Upal was modified and implemented into the BSIP calculation software.

$$\iint_S F \cdot dS = \iiint_W div\, F dV$$

Equation 3: Divergence theorem relates surface integral to a triple integral. S is the boundary of solid W

3.3.3 Segment Mass

Determining the mass of each segment ($m_{segment,i}$) required multiplying the found volume of each segment ($V_{segment,i}$) by an assumed corresponding density ($p_{density,i}$), as depicted by Equation 4. The densities, which were used to solve for mass estimates, are shown in Table 13.

$$m_{segment,i} = V_{segment,i} \cdot p_{density,i}$$

Equation 4: Segment mass equation to solve for the mass of each segment

Table 13: Body segment densities used in the experiment.

Body Segment	Density $[kg/m^3]$	References
Head+Neck	1070*	(Clauser et al., 1969)[1]
Upper Trunk	820	(Pearsall et al., 1994)[2]
Abdomen	1010	
Pelvis	1020	
Arm	1060	(Clauser et al., 1969)[1]
Forearm	1100	
Hand	1105	
Thigh	1040	
Shank	1080	
Foot	1080	
*This density measure reported is for the head not the head+neck		

[1] Taken from cadaver measurements (n=13)

[2] Taken from MRI measurements (n=26)

Each segment mass was presented as percentage of total body mass calculated using equation 5.

$$\%m_{total} = \frac{m_{segment_i}}{\sum\left(m_{segments_i}\right)} \cdot 100\%$$

Equation 5: Equation for percentage body mass

3.3.4 Moment of Inertia

The MOI was solved about the COM of each of the segments about axes that represented the principal axes of the segments. This resulted in an inertia matrix with only diagonal terms Ixx, Iyy, Izz, the principal moments. As constant density was assumed throughout all of the body segments the principal axis also represents the axis of rotational symmetry of the segment (Kibble & Berkshire, 2004). To calculate the moment of inertia, code written by Anwar M. Upal was used which is also based on the Divergence Theorem of Calculus. After the MOI was evaluated, the matrix was multiplied by the estimated density value of each segment.

3.3.4.1 Meshlab

Alternatively, Meshlab provides a function to compute the volume, inertial tensor, and cosine matrix (inertial axes definitions) of a 3D mesh. This information can be found under *Filters>Quality Measures and Computations>Compute Geometric Properties*. In order to view the information the Layer Dialogue window has to be opened under *View>Show Layer Dialogue*. In Meshlab, outputs are all displayed in centimeters units as opposed to meter. Caution needs to be taken, as the numerical display is limited to 8 digits.

Inertial estimations determined using Meshlab assume a density value of 1, as such the estimated inertial parameters ($I_{mesh,i}$) need to multiplied the by the corresponding density of each body segment. The results obtained using Meshlab were identical to the estimates from Matlab.

3.3.5 Length and Center of Mass

The centroid was determined by calculating the geometric centre of the cloud of points representing each segment. This assured that the centroid is not simply an average of all of the points within the cloud. Taking the average is an alternative approach but caution should be taken because the average will not always represent the true center of the point cloud. If for example the point distribution (density) was not even throughout, meaning there is a higher pool of points in certain locations of the cloud, then this would pull the centroid towards this direction. By estimating a physical centroid based on the geometry rather then the average of the points in a point cloud, the outcome is a better representation of the center. An example of the geometrical centroid of a forearm segment compared to the mean location is shown Figure 26.

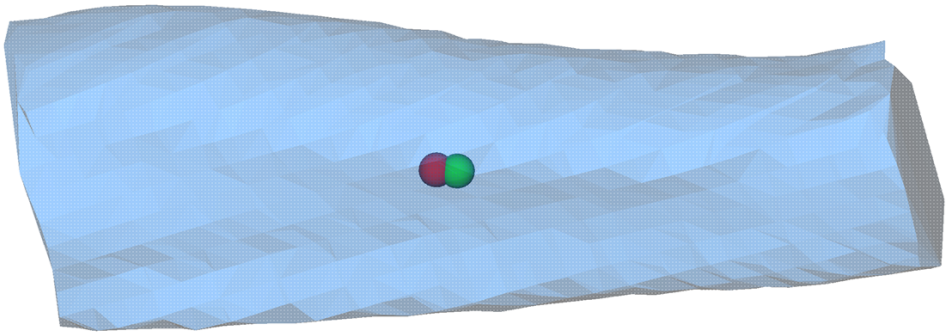

Figure 26: Forearm segment showing geometric centroid (red) and centroid based on the average of point cloud points (green)

To determine a relative distance of the COM from a segment endpoint, an algorithm was constructed. The eigenvectors of the principal MOI of each segment were determined. Next, using the axis, which represented the longitudinal axis of the segment (defined as Izz), a vector along this axis was projected until the vector intersected the boundary of the segment. This was done in the positive (+Izz) and negative (-Izz) direction such that two segment endpoints were determined. An example of this is shown for the thigh in Figure 27 where the distal intersection point and proximal intersection point of the long axis are visible. A length calculation based on the distance between two points in 3D space was applied (Equation 6).

$$\text{Length}_{\text{Segment}_i} = \sqrt{\left(x_{\text{proximal}_i} - x_{\text{distal}_i}\right)^2 + \left(y_{\text{proximal}_i} - y_{\text{distal}_i}\right)^2 + \left(z_{\text{proximal}_i} - z_{\text{distal}_i}\right)^2}$$

Equation 6: Equation used to calculate distance between points in 3D

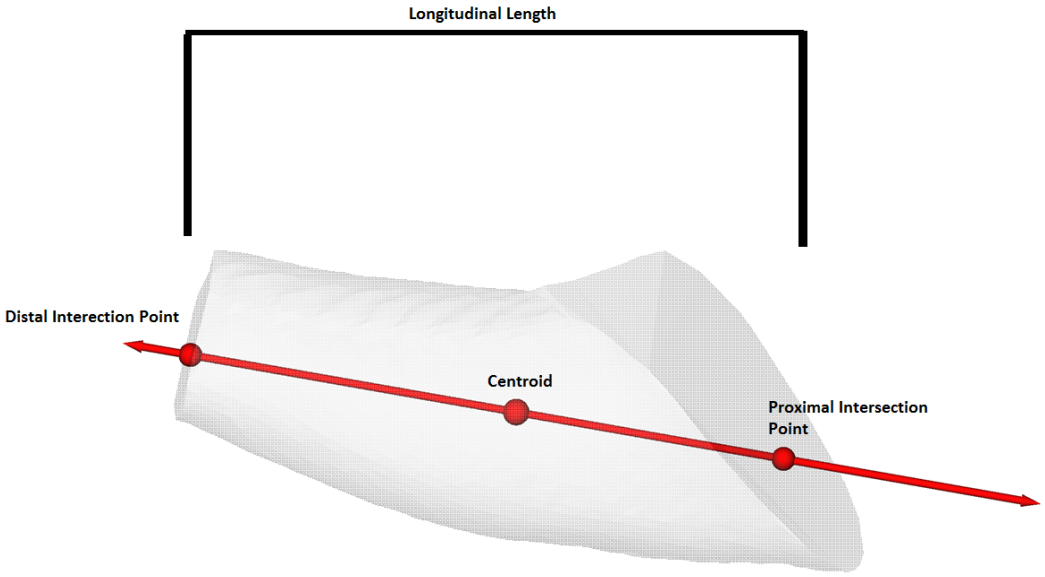

Figure 27: Calculation of segment longitudinal length. An example of the thigh is shown. The intersection points approximate the joints.

Finding the longitudinal length by approximating two segmental endpoints provided a relative distance to be calculated between the proximal/distal location of each segment and the centroid, allowing for the centroid to be represented as percentage distance from an end of the segment. An example of the resultant output from this procedure is shown in Figure 29 where the thick lines represent the distance from the proximal end of each segment to the estimated geometrical center.

3.3.6 Exceptions

The principal axes about the COM of the head, upper trunk, abdomen and pelvis did not coincide with any meaningful anatomical orientation as shown in Figure 28 (left side). To report the BSIPs with respect to a more meaningful orientation, a transformation to a global anatomical axis was performed. This allowed the intersection of the z-axis (coordinate system shown in Figure 28) to define the cranial and caudal ends of these four segments. As all of the subjects were standing in an anatomical posture in the 3D scans, adjusting the axes to coincide with anatomical axes is reasonable. The head and trunk region is approximately symmetric about the midsagittal plane in this orientation. Due to this symmetry it is customarily assumed that the principal axes of inertia of these segments are close to the cardinal anatomic axes through the corresponding COM (Zatsiorsky 2002).

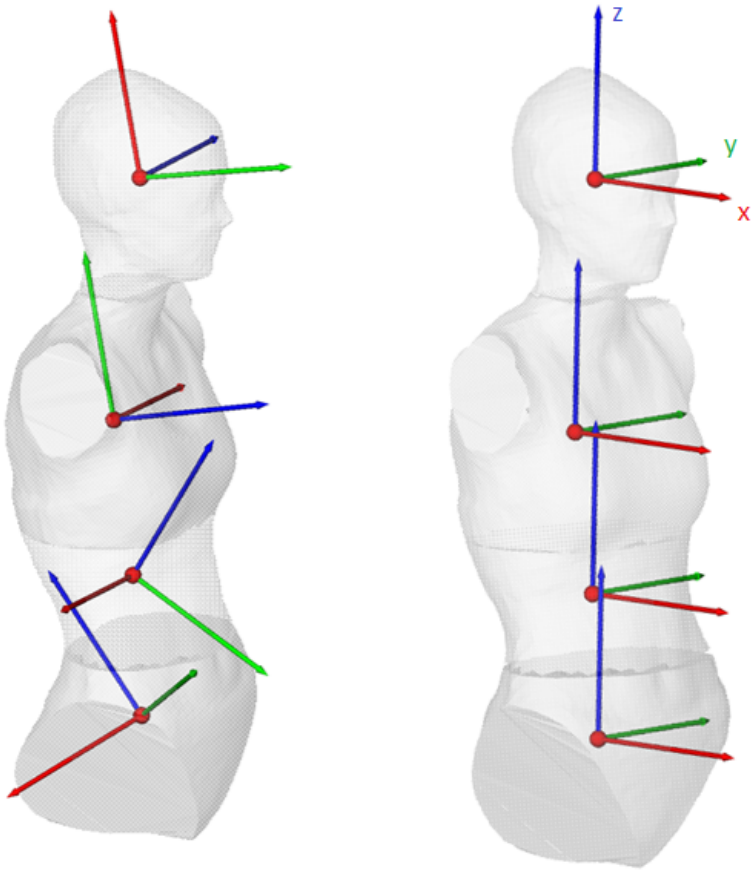

Figure 28: *Left Side:* Principal axis of rotation represented by the Eigenvectors of the MOI about the COM. *Right Side:* Axes Transformed to coincide with global axis. This transformation allowed for reporting the values in cardinal axes with the z-axis representing the cranial-caudal direction.

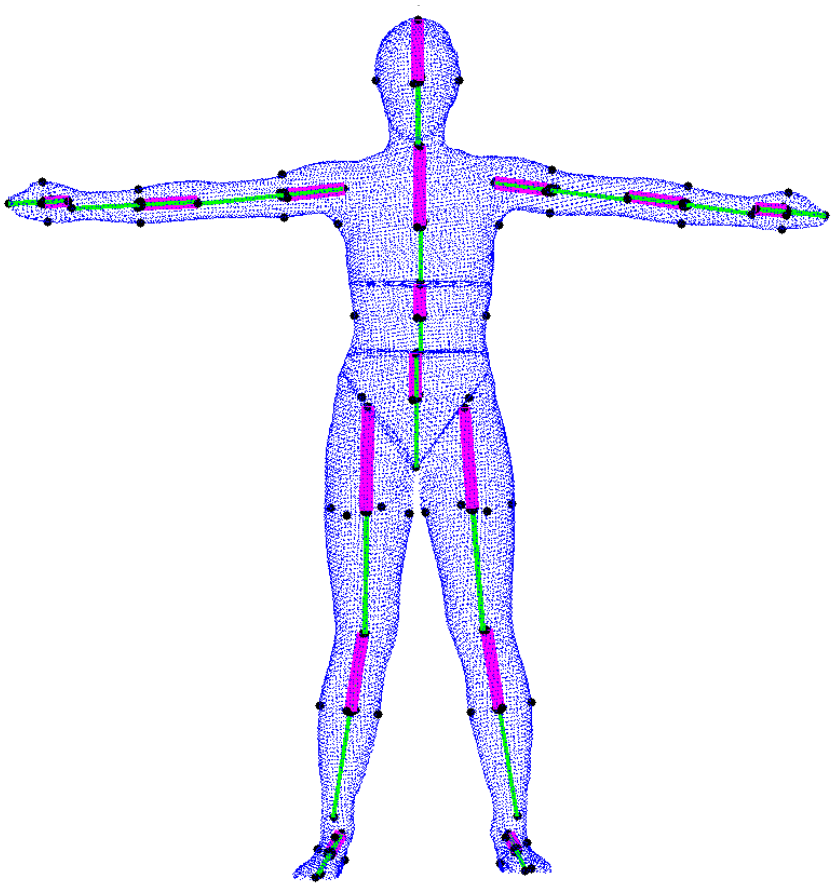

Figure 29: 3D point cloud of human body. Thick lines represent a connection between the centroid of each segment and the proximal end of the segment (cranial endpoints of the head+neck, and torso region).

3.3.7 Coordinate Systems

The coordinate system definitions are shown in Figures 30-32 from all of the respective body segments. The Thigh, Shank, Arm, Forearm, and Hand are all in the principal axes of the body segments. The Head and Torso region is represented in cardinal anatomic axes based on the anatomical upright posture during scanning. Foot axis was adjusted such that the z-axis passes along the length of the foot approximately from the toe to the heel.

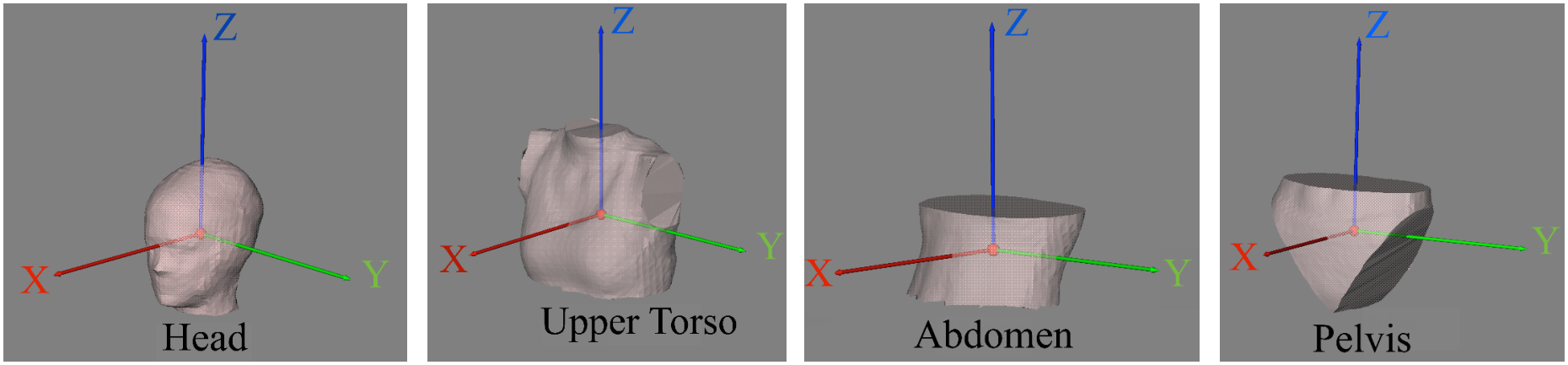

Figure 30: Definitions of coordinate systems of the Head, Upper Torso, Abdomen and Pelvis. The x-axis represents the anteroposterior axis, the y-axis the medial-lateral axis and the z-axis the cranial-caudal axis.

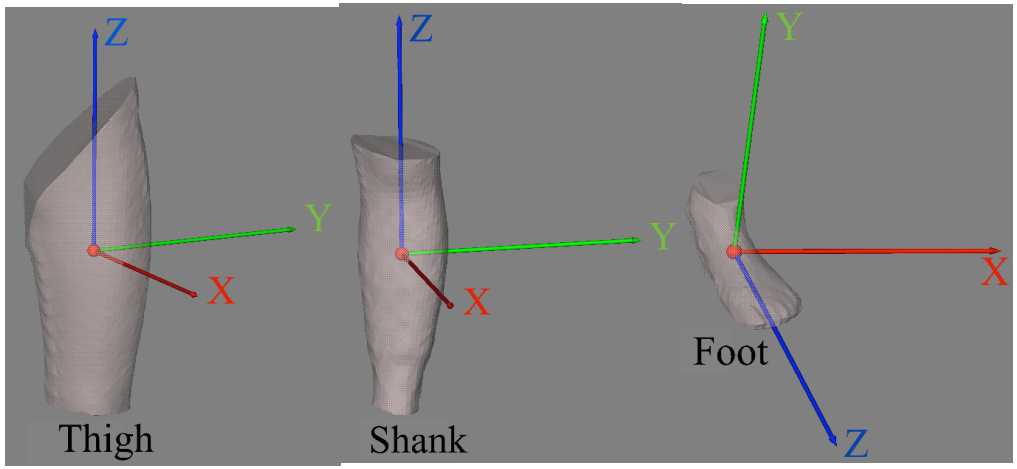

Figure 31: Definitions of coordinate systems of the Thigh, Shank and Foot. The x-axis represents the anteroposterior axis, the y-axis the medial-lateral axis and the z-axis the proximal-distal axis. The foot axes are defined to better match the anatomy of the foot with the z-axis passing from the heel to the toes.

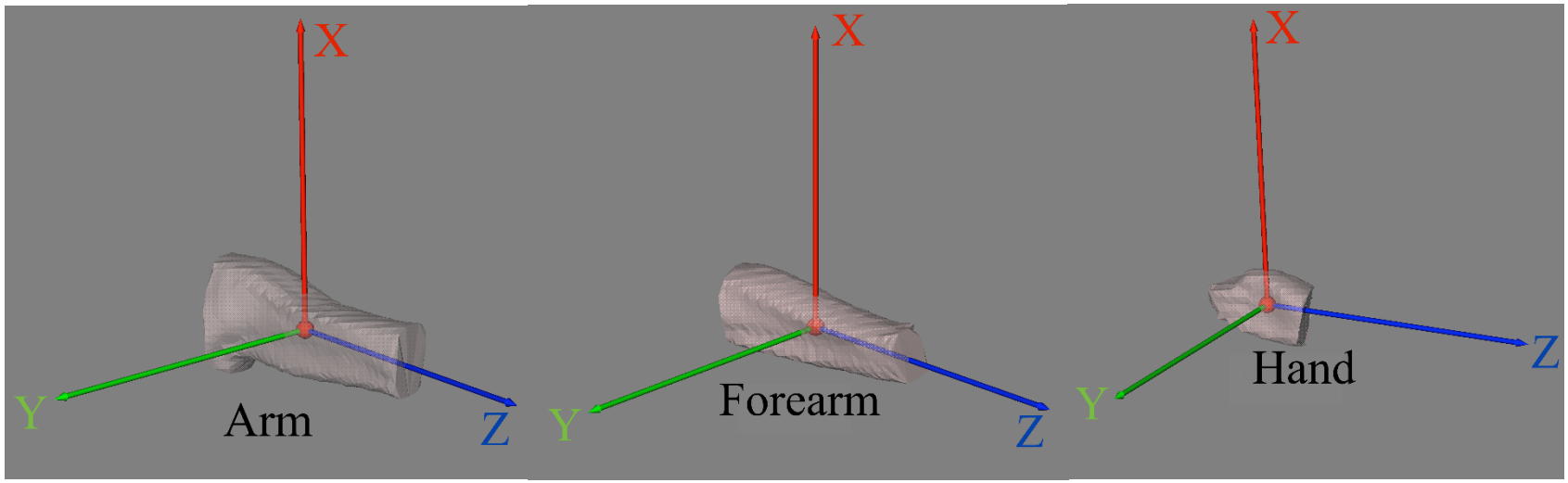

Figure 32: Definitions of coordinate systems of the Arm, Forearm and Hand. The x-axis represents the anteroposterior axis, the y-axis the medial-lateral axis and the z-axis the cranial-caudal axis.

3.4 Scanning of Cylindrical Object

To measure the accuracy and precision of the measurement results of the Kinect V2 used in this experiment a hollow cylinder was scanned 25 times following the proposed protocol. Cylindrical parameters were determined using a tape measure of accuracy ±0.1cm. The longitudinal length was determined as the length from one endpoint to the other. The COM was predicted to be 50% from either endpoint of the cylinder, as it was assumed to be perfectly symmetrical. The BSIPs were determined as detailed in this experiment. Supplementary information is provided in the Appendix C.

3.5 Comparisons to Literature

The estimates obtained using the Kinect and ECM methods were compared to results obtained in literature. Specifically, data compiled by Zatsiorsky and Seluyanov (1983) was used. In their experiment 115 subjects were recruited and analyzed. In their experiment a medical imaging method the Gamma-Scanner was used to estimate BSIPs. Zatsiorsky and Seluyanov (1983) presented regression equations to solve for mass, COM and MOI using subject body weight and height as inputs. The subject pool used in the study closely matched the subject pool from this experiment as well as the large subject pool (Male (n=100), Female (n=15)) were reasons as to why these experimental results were chosen for comparison purposes. The subject data from Zatsiorsky and Seluyanov (1983) is shown in Table 14. The regression equations are shown in the Appendix D.

Table 14: Anthropometric data of subjects from Zatsiorsky and Seluyanov (1983)

Subject	Age (Years)	Height (m)	Mass (kg)
Male (n=100)	23.8±6.2	1.74±0.062	73.0±9.1
Females (n=15)	19.0±4.0	1.74±0.033	61.9±7.3

The data from Zatsiorsky and Seluyanov (1983) is reported with the subjects all standing in an anatomical posture upright with arms straight down at the sides of the body, palms turned forward and head erect. As the segmentation in this project is based on Zatsiorsky and Seluyanov segmentation protocol, the segmentation is as that detailed in Table 10. The MOI are all taken from this position with the anteroposterior axis represented by Ixx the mediolateral axis represented by Iyy and the longitudinal axis represented by Izz. The only exception is the foot with the MOI given for an imaginary position with the foot rotated outward. The axis which is parallel to the flexion axis at the ankle joint is the anteroposterior axis and the axis from the heel to the tip of the second toe is the longitudinal axis (Izz) (defined in : Zatsiorsky & Seluyanov, 1983). The foot axes were adjusted in this experiment to match this definition.

The longitudinal length and COM results, which were used for the comparisons, were based on the definitions shown in Table 15. For the foot, head and torso region the anatomical length was used for comparing the longitudinal length and the COM estimates. This was the case because the anatomical length origin and endpoints were closer related to that of this experiment. For the remainder of the segments the biomechanical lengths were compared. The biomechanical lengths are modified definitions written by Paolo de Leva (1996) based on Zatsiorsky and Seluyanov (1983) (Paolo de Leva, 1996).

Table 15: Segment length definitions used to determine longitudinal length. The longitudinal length is based on the distance between the origin and endpoint of each segment

	Segment	Origin	Endpoint	Length Type
Head + Neck	Head + Neck	Vertex	Cervicale	Anatomical *
Torso	Upper Trunk	Cervicale	Xiphoid	Anatomical
	Abdomen	Xiphoid	Omphalion	Anatomical
	Pelvis	Omphalion	Pubis	Anatomical
Arm	Upper Arm	Shoulder JC	Elbow JC	Biomechanical**
	Forearm	Elbow JC	Wrist JC	Biomechanical
	Hand	Wrist JC	Third Dactylion	Biomechanical
Leg	Thigh	Hip JC	Knee JC	Biomechanical
	Shank	Knee JC	Ankle JC	Biomechanical
	Foot	Heel	Tip of longest toe (Acropodion)	Anatomical

_* From (Zatsiorsky, V. & Seluyanov, 1983)

** Modified version of (Zatsiorsky, V. & Seluyanov, 1983) done by (Paolo de Leva, 1996)

The experimental setup and more details regarding the study, the full results and the subject pool can be found in the book: Kinetics of Human Motion (Zatsiorsky 2002).

3.6 Statistical Analysis

A t-test for dependant means (paired samples t-test) was used to compare the results found for all of the BSIPs across the female and male subjects (Equation 7). A two-tailed hypothesis was assumed. Significance was determined based on three levels: $p<0.05$ (*), $p<0.01$(**), $p<0.001$(***).

$$t = \frac{\left(\frac{\sum D}{N}\right)}{\sqrt{\frac{\left(\sum D^2 - \frac{(\sum D)^2}{N}\right)}{(N-1)N}}}$$

Equation 7: Paired sample t-test where N is the number of samples and D is difference between samples

A Tukey mean-difference plot (Bland-Altman plot) was used to identify if there were differences between the volume estimates between the ECM and Kinect methods. The agreement between the estimates could therefore be determined. Pearson correlation was also used to determine agreement between methods.

To evaluate the reliability of the volume estimates from the 3D scans the intraclass correlation coefficient (ICC) was calculated. This was done for the total volume estimation and the segmentation protocol. For the total volume the volumes from the three Kinect scans were compared with one another for each subject. A single scan from each subject was chosen at random and segmented two times following the protocol. The resultant segmental volumes were compared with one another and the ICC reliability was computed.

Chapter 4
Results

4.0 Acquisition Time

Total experimental acquisition times are shown in Table 16. Lab setup times are based on preparing the equipment necessary to perform the experiment with required software already installed on the computer. Anatomical land marking constitutes the majority of the time with the subject for both the ECM and Kinect methods.

Table 16: Experimental pre and post processing time across three methods.

	Kinect V2	ECM	Zatsiorsky Regression
Lab setup time	~15 minutes	~45 minutes	N/A
Subject Interaction Time	~30 min (Anatomical land marking) ~2 minutes (anthropometrics) ~30 seconds/scan	~20 minutes anatomical land marking ~2 minutes (anthropometrics) ~10 seconds / photo	~2 minutes (acquire weight and height)
Post Processing	~45 minutes/scan	~25 minutes/subject	~5 min
Total Time	**~1.5-2 hours/scan**	**~1.5-2 hours/subject**	**~10 min/subject**

4.1 Test Object Scanning

A plastic cylinder of measured length was scanned 25 times. Inertial parameters estimated using the developed protocol were compared to theoretical values. The results are shown in Table 17. Supplementary data is provided in the Appendix C. The results show that the experimental volume was overestimated on average by 209 cm^3. The longitudinal length and COM% were underestimated by 0.5 cm and 0.2% respectively. The values for the MOI obtained with the experimental method were overestimated by less than 2% for the Ixx (anterior-posterior) and Iyy (medial-lateral) and within 8% of the Izz (longitudinal).

Table 17: Comparison between theoretical and experimentally obtained parameters for a cylindrical tube or radius 4.1±0.1cm and length 97±0.1 cm. Standard Deviation (SD).

		Kinect Data				
Measurement	**Measured**	**Calculated (SD)**	**Max**	**Min**	**Range**	**Mean Difference**
Volume [cm^3]	4964±242	5173 (204)	4927	5550	623	209 cm^3
Length [cm]	94.1 ±0.1	93.6 (2.0)	97.5	89.8	7.7	-0.5 cm
COM [%]	50%	49.8% (0.9)	52.3%	48.2%	4.1%	-0.2%
Ixx [$kgcm^2$]	3676±178	3707 (197)	4049	3449	600	31 $kgcm^2$
Iyy [$kgcm^2$]	3676±178	3702 (196)	4043	3445	598	26 $kgcm^2$
Izz [$kgcm^2$]	42±2	45.3 (4.4)	57.9	39.0	188	3.3 $kgcm^2$

4.2 Reliability

4.2.1 Total Volume

Relative precision of the Kinect total body volume estimation was quantified by calculating the intraclass correlation coefficient (ICC). The ICC for 3 repeated scans across 10 male and 11 female participants was calculated using a two way random effects model and found to be equal

to ICC (2,1) = 0.966 for the males and ICC=(2,1) = 0.982 for the females indicating very high reliability.

4.2.2 Segmentation

The repeated measures of segmental volume were evaluated using the ICC coefficient. To determine the relative repeatability of the segmentation protocol a body scan from each subject was chosen at random and the segmentation protocol was executed twice. The ICC values were above ICC (2, 1)>0.70 with the highest values of ICC (2, 1)>0.9 seen for the torso, and leg for both genders. Full results are shown in Table 18 below.

Table 18: ICC values determined from 2 repeated segmentations of 10 male and 11 female scans. Both segmentations were done on the same scan.

		ICC	
Side	**Segment**	**Male**	**Female**
Upper Body	Head	0.92	0.99
	Upper Torso	0.97	0.99
	Abdomen	0.98	0.99
	Pelvis	0.90	0.98
Right	Arm	0.92	0.81
	Forearm	0.79	0.75
	Hand	0.93	0.72
Left	Arm	0.72	0.89
	Forearm	0.72	0.76
	Hand	0.86	0.74
Right	Thigh	0.96	0.93
	Shank	0.97	0.95
	Foot	0.93	0.90
Left	Thigh	0.95	0.94
	Shank	0.94	0.95
	Foot	0.70	0.79

4.3 Agreement Between methods

A Bland-Altman analysis for the male and female scans reveals the difference between the Kinect and ECM total volume estimates to be greater than zero in all cases except one (Figure 33). Shown in Table 19 are the summary results of the analysis. The results suggest a fixed measurement bias of 0.0023m^3 (2300 cm^3) for the males and 0.0038 m^3 (3800 cm^3) for the females when scanning with the Kinect. Ordinary least product plots are shown in Appendix E with the summary of results shown in Table 19 below.

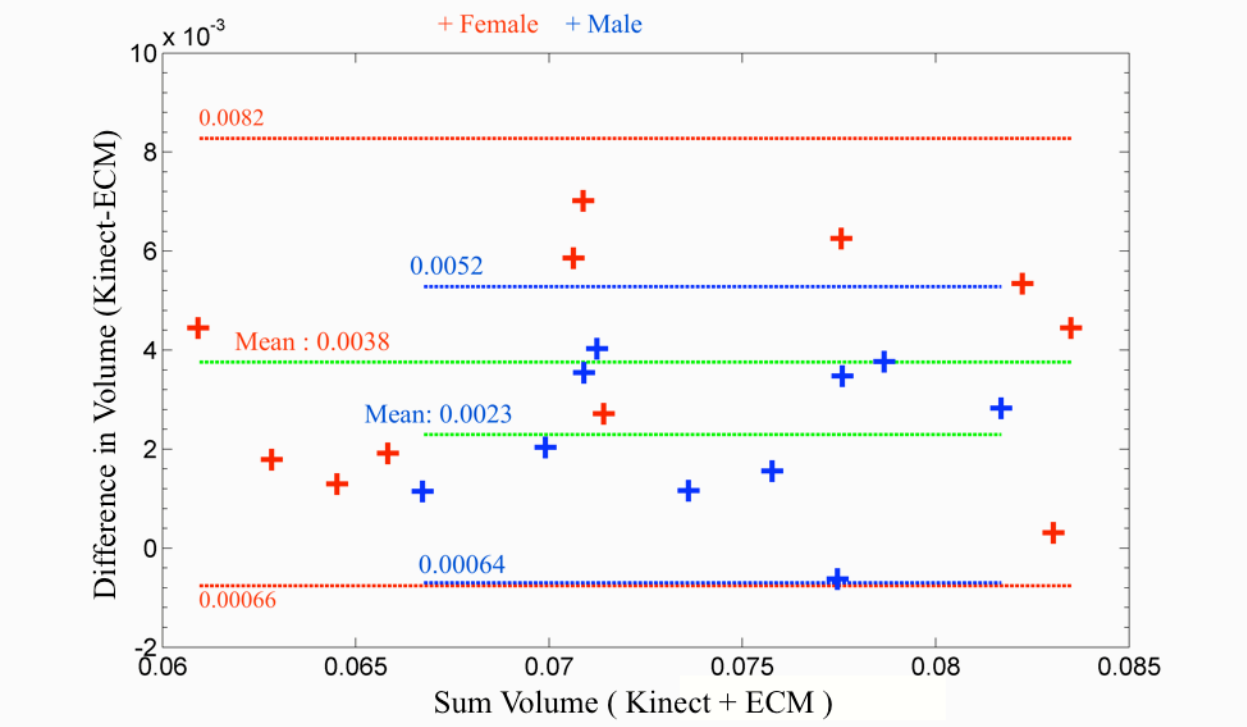

Figure 33: Bland Altman plot of the difference between the Kinect and ECM estimation techniques. Males (n=10) are shown in blue and females (n=11) in red. All units are in m^3

Table 19: Summary of results from Bland Altman analysis and ordinary least products comparing the total volume estimates obatined using the Kinect and the ECM method.

	Bias [m^3]	95 % Confidence interval (Bias) [m^3]	Limits of Agreement [m^3]	r^2
Male (n=10)	0.0023	0.0036-0.0012	0-0.0052	0.90
Female (n=11)	0.0038	0.0026-0.0056	0-0.0082	0.93

4.4 Segmental Volume

The volumes for each body segment for the males and females were compared using the estimated values from the Kinect and ECM acquisition methods. The results for per segment volumes for male subjects are shown in Figure 34 and the female subjects in Figure 35. Cumulative volume calculations, which were obtained by adding the volumes of all of the segments together, show significant differences when comparing the results estimated with ECM and Kinect for both genders with the Kinect consistently estimating a larger volume than ECM (Male $t(9)$: 4.84, $p<0.001$, Females $t(10)$: 5.52, $p<0.001$). For both genders the largest between segment differences are seen in the upper torso (Male $t(9)$: 6.63, $p<0.001$, Female (10), $p<0.001$).

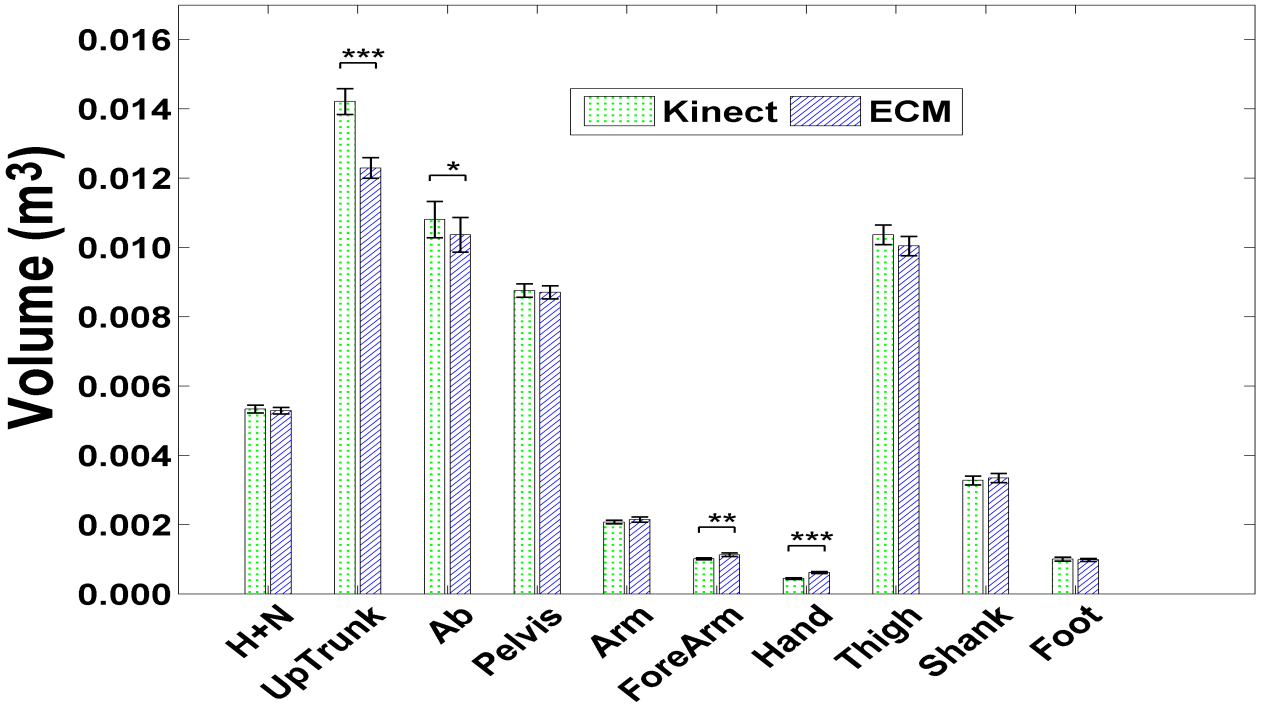

Figure 34: Average volumetric data estimated using Kinect and ECM of 10 body segments for a **male** population (n=10). Error bars represent standard error of the population mean. (***p<0.001, **p<0.01, *p<0.01)

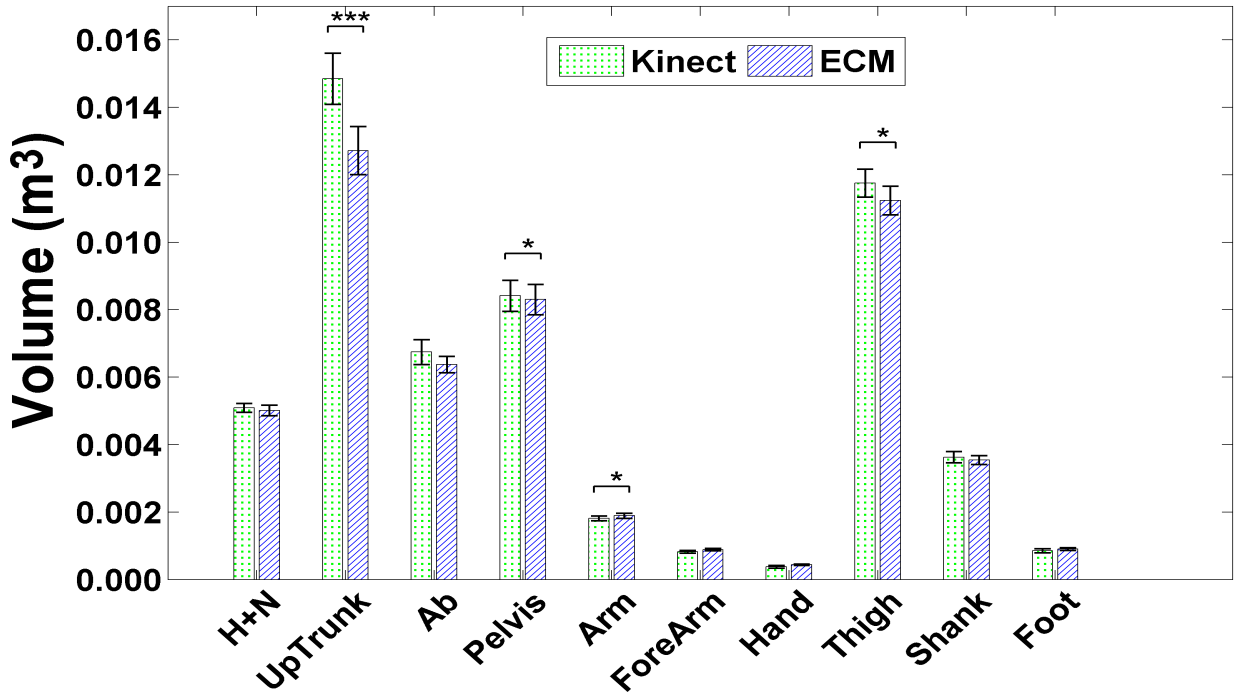

Figure 35: Average volumetric data estimated using Kinect and ECM of 10 body segments for a **female** population (n=10). Error bars represent standard error of the population mean. (***p<0.001, **p<0.01, *p<0.05)

4.5 Total Mass

Results show no significant differences exist between mass estimates estimated using ECM and the scale values for both genders (Male: $t(9) = -1.49$, $p=0.182$, Female: $t(10) = 2.18$, $p=0.054$). However, significant differences were observed for the results obtained using the Kinect (Male: $t(9) = 4.62$, $p<0.01$ Female: $t(10) = 6.98$, $p<0.001$), with an average overestimation of 2.34 kg for male subjects and 3.88kg for females. ECM showed a slight overestimation on the mass, with an average of 0.44kg for males and 0.24kg for the females when compared to the scale values (not significant). Shown in Table 20 and Table 21 are the subject-specific mass comparison for males and females respectively.

Table 20: A comparison of male mass estimates determined from elliptical cylinder model and Kinect compared to scale values. Differences between ECM and Scale (ECM-S) and Kinect and Scale (K-S) are shown. Standard deviation (SD).

Subject	Scale [kg]	ECM [kg]	ECM-S Difference (SD)	Kinect [kg]	K-S Difference (SD)
M1	72.90	73.60	0.70	74.37	1.47
M2	74.95	75.40	0.45	76.86	1.91
M3	79.92	80.82	0.90	83.40	3.48
M4	70.95	69.18	-1.77	70.74	-0.21
M5	69.61	69.77	0.16	73.04	3.43
M6	77.08	78.69	1.61	77.75	0.67
M7	77.88	77.51	-0.37	80.51	2.63
M8	68.72	69.89	1.16	73.48	4.76
M9	75.04	76.07	1.03	79.14	4.11
M10	66.14	66.62	0.48	67.32	1.17
Average Difference			**0.44(0.90)**		**2.34(1.52)**

Table 21: A comparison of female mass estimates determined from elliptical cylinder model and Kinect compared to scale values. Differences between ECM and Scale (E-S) and Kinect and Scale (K-S) are shown. Standard deviation (SD).

Subject	Scale [kg]	ECM [kg]	ECM-S Difference (SD)	Kinect[kg]	K-S Difference (SD)
F1	82.77	83.61	0.84	83.65	0.88
F2	79.30	79.24	-0.07	84.34	5.04
F3	63.92	64.07	0.14	65.17	1.25
F4	69.17	70.43	1.26	72.63	3.46
F5	75.04	74.81	-0.22	80.79	5.75
F6	68.72	68.33	-0.39	73.96	5.24
F7	61.34	62.73	1.39	64.11	2.77
F8	68.55	68.00	-0.55	74.74	6.20
F9	80.55	81.38	0.83	85.28	4.74
F10	58.50	59.23	0.74	63.54	5.04
F11	64.19	65.22	1.03	66.49	2.30
Average Difference			**0.45(0.66)**		**3.88(1.75)**

4.5.1 Segmental Mass

Per segment mass estimates obtained using Kinect and ECM were compared to Zatsiorsky and Seluyanov (1983) regression equations and the published averages from Zatsiorsky and Seluyanov (1983). Shown in Figure 36 are the results for the males and Figure 37 for the females. The mass ratios which are the ratio of the segmental mass to the total body mass are presented in Table 22.

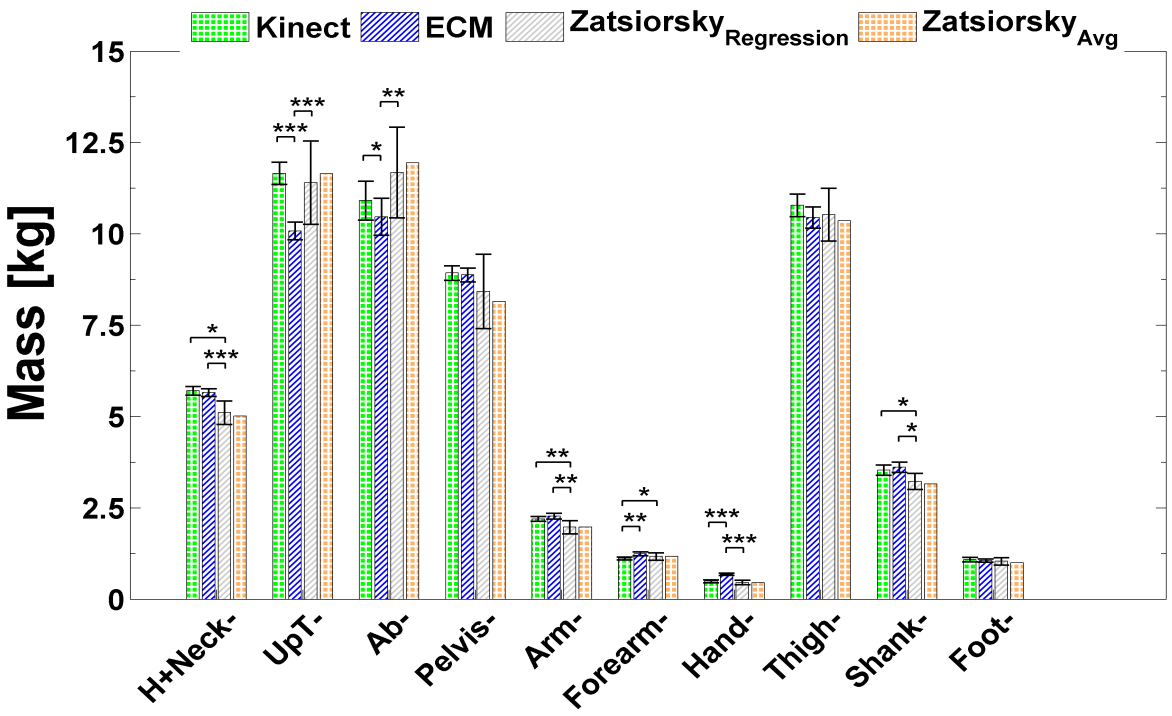

Figure 36: Average estimated segment mass for **male** subjects (n=10). Error bars indicate standard error of the population mean. Regression equations and average values taken from Zatsiorsky and Seluyanov (1983) are based on an n=100 sample size. (***p<0.001, **p<0.01,*p<0.05). Head and Neck (H+Neck), Upper Trunk (UpT), Abdomen (Ab).

Looking at Figure 36 the largest differences are seen between the Kinect and the ECM mass estimation of the upper trunk ($t(9) = 6.64$, $p<0.001$) and hand ($t(9) = 5.12$, $p<0.001$). Comparing the Kinect estimates to the regression values, largest significant differences are seen in the arm ($t(9) = 4.21$, $p<0.01$).

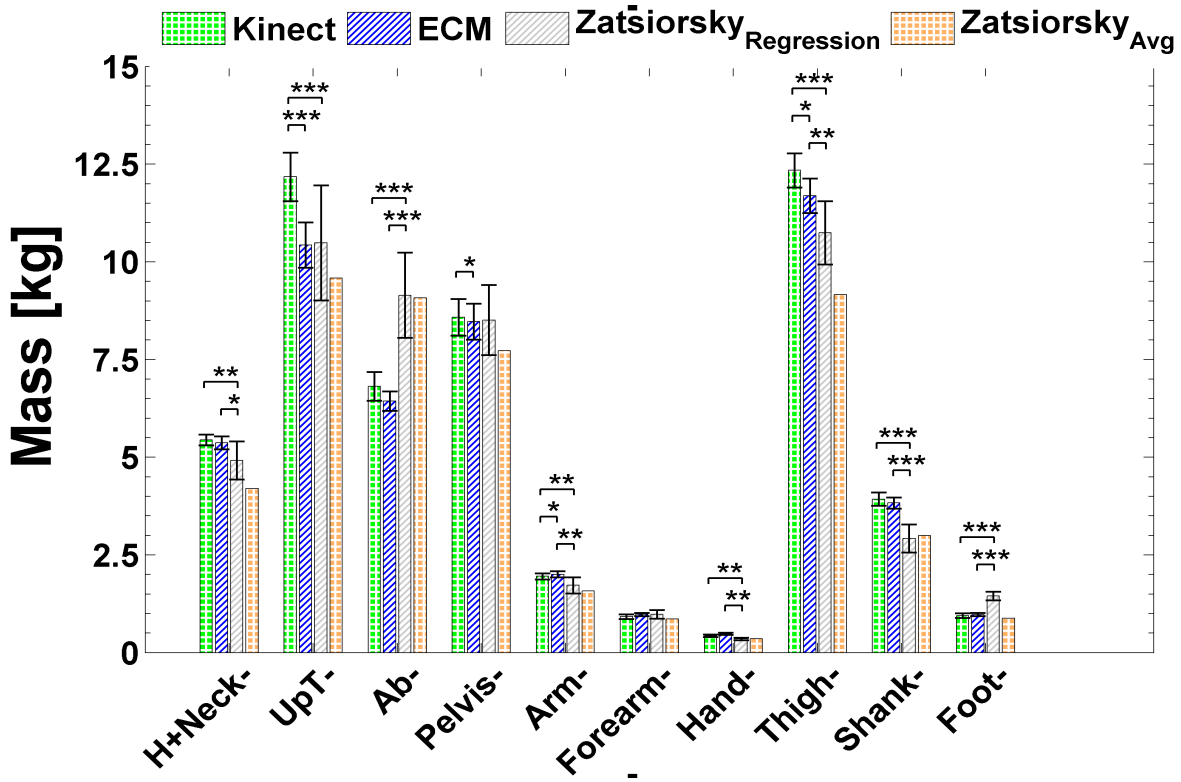

Figure 37: Average estimated segments masses for **female** subjects (n=10). Error bars show standard error of the population mean. Regression equations and average values taken from Zatsiorsky and Seluyanov (1979, 1983) are based on an n=15 sample size. (***p<0.001, **p<0.01,*p<0.05). Head and Neck (H+Neck), Upper Trunk (UpT), Abdomen (Ab).

More differences between segment mass estimates are seen in Figure 37 for the female data than the male data. The largest differences are seen between the Kinect estimates in the abdomen region ($t(10) = 6.77$, $p<0.001$), the upper trunk ($t(10) = 9.55$ (ECM), $t(10) = 4.60$ (Zatsiorsky), $p<0.001$) and the thigh ($t(10) = 2.36$ (ECM), $p<0.01$; $t(10) = 5.9$ (Zatsiorsky), $p<0.001$)

Table 22: Percent total mass shown as the ratio of the average segment mass to the average total body mass for male (n=10) and females (n=11). SD is shown in brackets. Zatsiorsky and Seluyanov (1983) average reported values are shown (Zat). No SD provided for females.

		Mass [%]									
		H+N	**UpT**	**Ab**	**Pelvis**	**Arm**	**FArm**	**Hand**	**Thigh**	**Shank**	**Foot**
Males	**Kinect**	**7.8** (0.7)	**15.9** (1.2)	**14.8** (1.8)	**12.2** (0.9)	**3.0** (0.18)	**1.5** (0.18)	**0.7** (0.2)	**14.7** (0.7)	**4.8** (0.6)	**1.5** (0.3)
	ECM	**7.7** (0.7)	**13.8** (0.8)	**14.2** (1.7)	**12.1** (0.9)	**3.1** (0.3)	**1.7** (0.2)	**0.9** (0.1)	**14.2** (0.8)	**4.9** (0.6)	**1.5** (0.2)
	Zat	**6.9** (0.7)	**15.9** (1.5)	**16.3** (1.7)	**11.2** (1.4)	**2.7** (0.2)	**1.6** (0.1)	**0.6** (0.08)	**14.2** (1.0)	**4.3** (0.3)	**1.4** (0.2)
Females	**Kinect**	**7.8** (0.5)	**17.3** (1.7)	**9.7** (1.0)	**12.2** (1.3)	**2.8** (0.2)	**1.3** (0.3)	**0.6** (0.2)	**17.6** (1.1)	**5.6** (0.8)	**1.4** (0.3)
	ECM	**7.7** (0.4)	**14.8** (1.5)	**9.2** (0.6)	**12.0** (1.3)	**2.9** (0.2)	**1.4** (0.1)	**0.7** (0.1)	**16.7** (1.0)	**5.5** (0.6)	**1.4** (0.2)
	Zat	**6.7**	**15.5**	**14.7**	**12.5**	**2.6**	**1.4**	**0.6**	**14.8**	**4.8**	**1.3**

4.6 Principal Moments of Inertia

The principal MOI results for the male estimates collected using Kinect and ECM alongside estimates using the regression equations from Zatsiorsky and Seluyanov (1983) are shown in Figure 38. Representative MOI information for females is shown Figure 39.

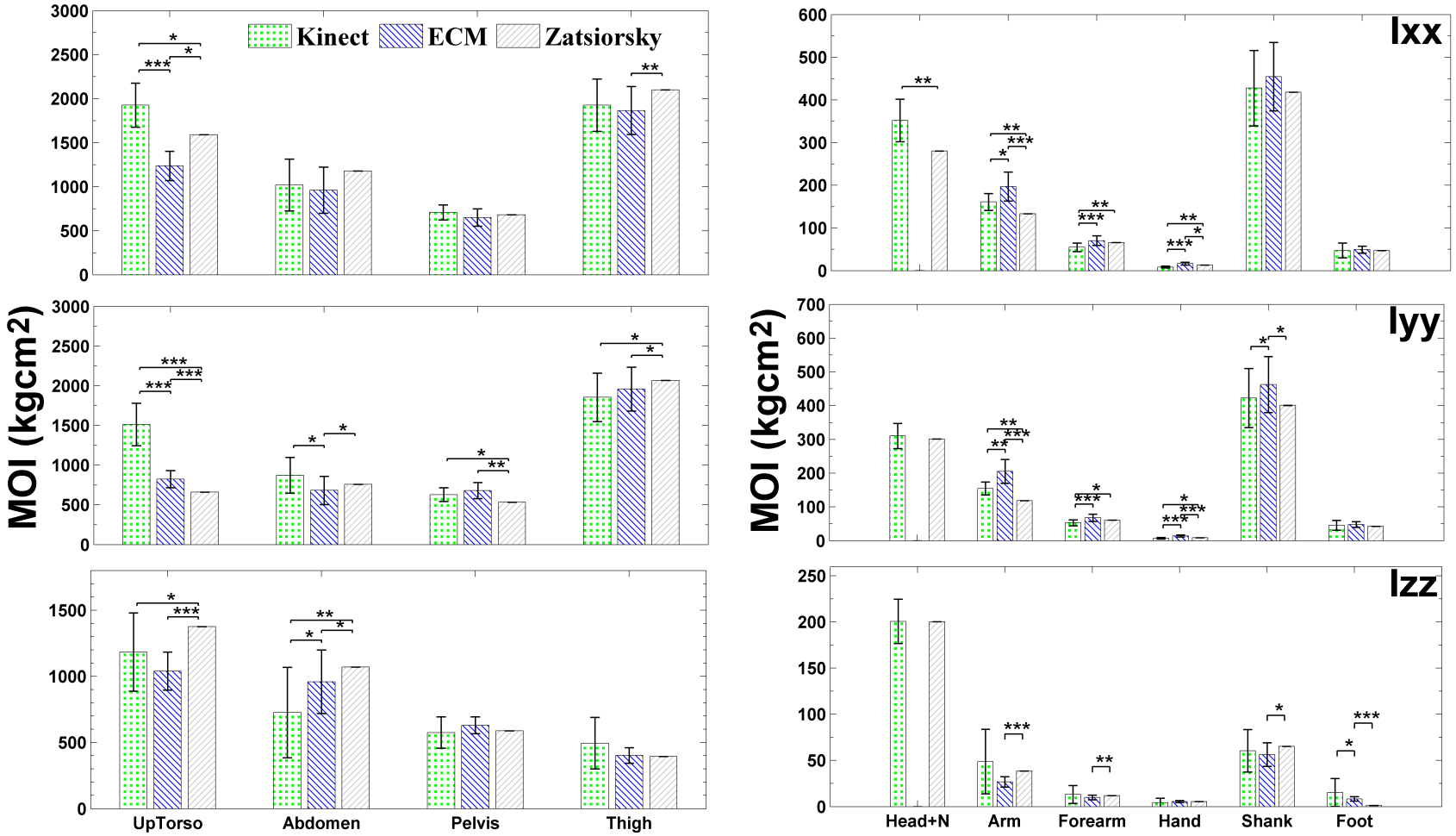

Figure 38: Moment of Inertia results along the principal axes of each of the 10 body segments with Izz representing the longitudinal axis of the segment, Ixx the anterior-posterior and Iyy the medial-lateral. Results shown are for **male** subjects (n=10) obtained from Kinect 3D scans, ECM, and Zatsiorsky and Seluyanov (1979, 1983) regression equations. (***p<0.001, **p<0.01,*p<0.05). Standard deviation shown.

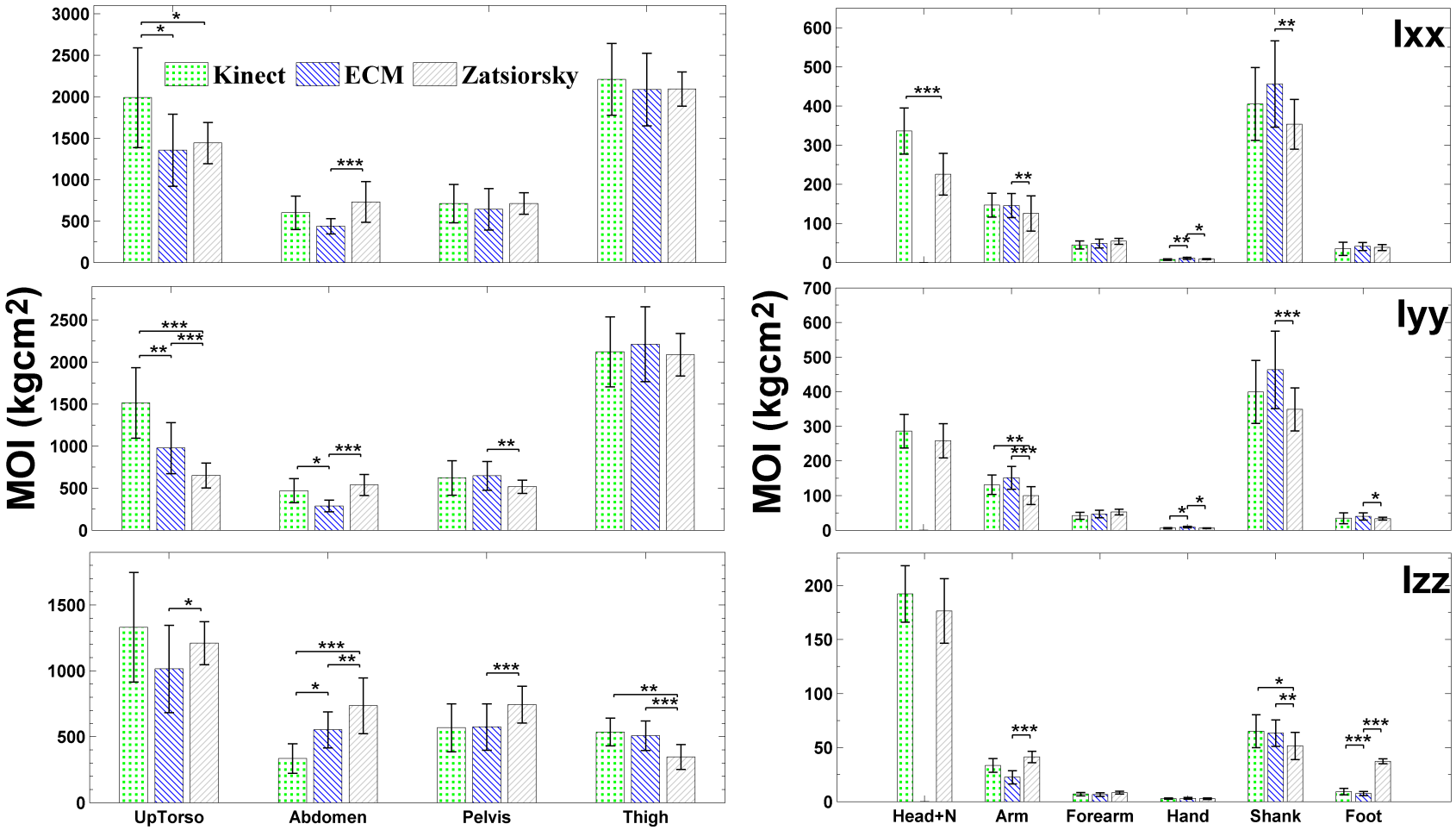

Figure 39 : Moment of Inertia results along the principal axes of each of the 10 body segments with Izz representing the longitudinal axis of the segment, Ixx the anterior-posterior and Iyy the medial-lateral. Results shown are for **female** subjects (n=11) obtained from Kinect 3D scans, ECM, and Zatsiorsky and Seluyanov (1979, 1983) regression equations. (***p<0.001, **p<0.01,*p<0.05). Standard deviation shown.

4.7 Anthropometrics

Length and COM location results estimated using the Kinect and ECM were compared to the average results from Zatsiorsky and Seluyanov (1983). The longitudinal lengths and centers of mass (displayed as a percentage from the proximal end of the segments over the total segment length) are presented in Tables 23-25 with accompanying Figures 40-42. Summary data is shown in Figures 43-46 for the male and female subjects.

Significant differences are seen among many of the segment lengths with the largest observed differences at the hand (M: $t(9)=7.4$; F: $t(10)=9.4$, $p<0.001$) and foot (M: $t(9)=8.3$; F: $t(10)=3.9$, $p<0.001$) for both genders. Differences in the COM for the males and females of the pelvis show the largest difference between the ECM and Kinect with the COM overestimated by 15% for the males and 9% for the females (M: $t(9)=8.8$ F: $t(10)=5.2$, $p<0.001$).

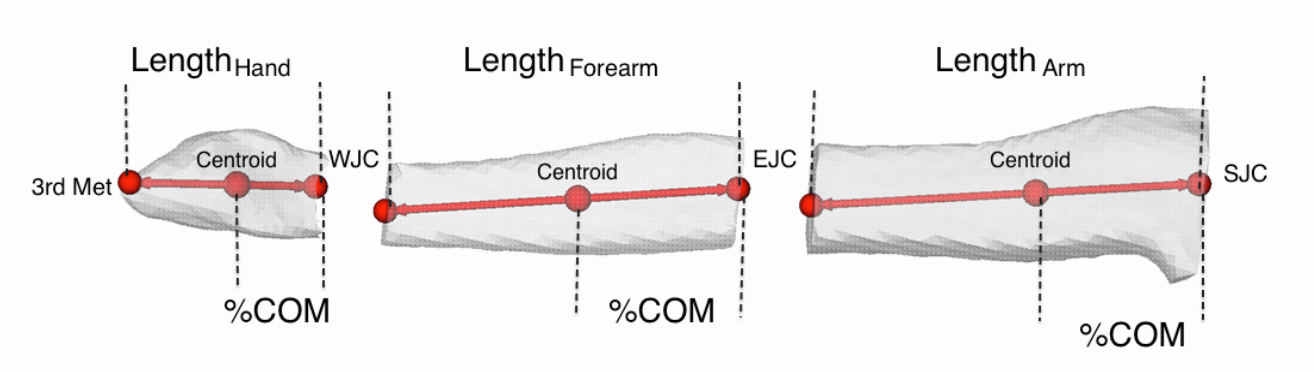

Figure 40: Body arm segmentation showing centre of mass (Centroid), proximal distance of COM as a percentage of the total longitudinal length of the segment (%COM) and longitudinal length of segment (Length). Estimates of the third metatarsal (3rd Met), Wrist joint center (WJC), Elbow joint centre (EJC), and Shoulder joint center (SJC) define the estimated endpoints of each segment.

Table 23: Male and Female longitudinal segment length data and %COM from proximal endpoints for the Arm, Forearm and Hand obtained using the Kinect and ECM. Average values (Avg) published by (Paolo de Leva, 1996) based on (Zatsiorsky & Seluyanov, 1983) subjects. Standard deviation shown in brackets.

			Arm	Forearm	Hand			Arm	Forearm	Hand
Length [mm]	**Male**	**Kinect**	**291.2** (18.9)	**260.1** (10.7)	**152.9** (20.2)	**Female**	**Kinect**	**290.9** (17.4)	**247.2** (21.3)	**147.7** (17.5)
		ECM	**282.8** (17.1)	**273.8** (11.5)	**199.7** (12.0)		**ECM**	**267.4** (24.5)	**261.4** (18.7)	**189.7** (10.4)
		Avg.	**281.7**	**268.9**	**187.9**		**Avg.**	**275.1**	**264.3**	**170.1**
COM [%]		**Kinect**	**41.5** (1.6)	**41.8** (1.0)	**41.8** (2.3)		**Kinect**	**40.4** (1.5)	**43.0** (1.9)	**43.1** (2.4)
		ECM	**38.5** (2.5)	**42.9** (1.5)	**40.7** (2.3)		**ECM**	**41.4** (3.3)	**43.9** (2.4)	**40.6** (3.9)
		Avg.	**57.7**	**45.7**	**36.3**		**Avg.**	**57.5**	**45.6**	**34.2**

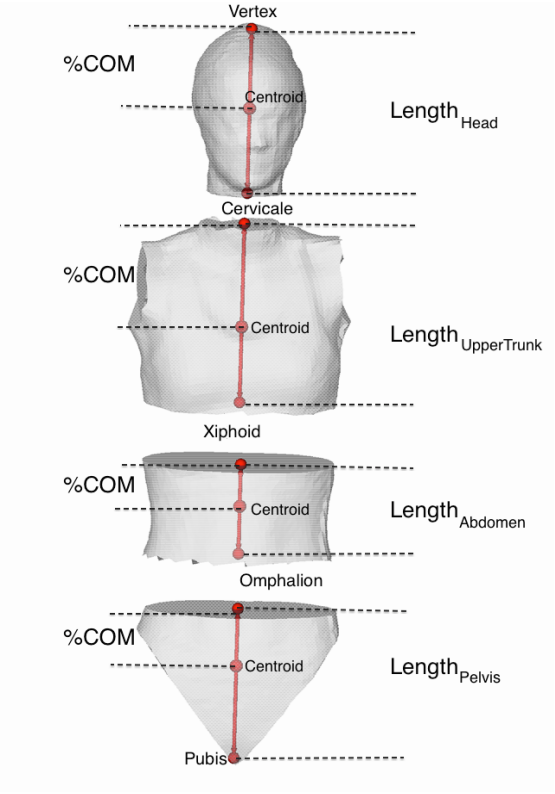

Figure 41: Upper body segments showing centre of mass (Centroid), proximal distance of COM as a percentage of the total longitudinal length of the segment (%COM) and longitudinal length of segment (Length). Estimated Vertex, Cervicale, Xiphoid, Omphalion and Pubis are also shown.

Table 24: Male and Female longitudinal segment length data and %COM for the Head+Neck (H+N), Upper Trunk (UpT), Abdomen (Ab) and Pelvis obtained using the Kinect and ECM. Average values based on (Zatsiorsky & Seluyanov, 1983). Standard deviation shown in brackets.

			H+N	UpT	Ab	Pelvis		H+N	UpT	Ab	Pelvis
Length [mm]	**Male**	**Kinect**	**262.3** (10.1)	**247.8** (17.7)	**195.4** (18.7)	**224.1** (15.3)	**Female**	**264.2** (15.5)	**273.7** (40.7)	**131.5** (11.3)	**224.2** (17.2)
		ECM	**288.8** (8.7)	**237.7** (15.5)	**204.6** (19.7)	**187.6** (16.4)		**284.3** (13.3)	**272.7** (26.1)	**158.8** (43.2)	**214.2** (22.0)
		Avg	**242.9**	**242.1**	**215.5**	**251.7**		**243.7**	**228**	**205.3**	**-***
COM [%]		**Kinect**	**49.4** (0.7)	**54.4** (1.3)	**48.7** (1.1)	**37.0** (1.7)		**48.1** (1.3)	**55.7** (2.6)	**49.6** (1.1)	**36.6** (1.1)
		ECM	**46.5** (1.1)	**58.8** (2.6)	**51.2** (1.5)	**50.8** (3.4)		**45.5** (1.8)	**56.6** (1.8)	**48.6** (8.8)	**45.8** (5.9)
		Avg	**50.0**	**50.6**	**45.0**	**35.4**		**48.5**	**50.5**	**45.1**	**-***

* Data not provided in comparable reference length due to differing endpoints

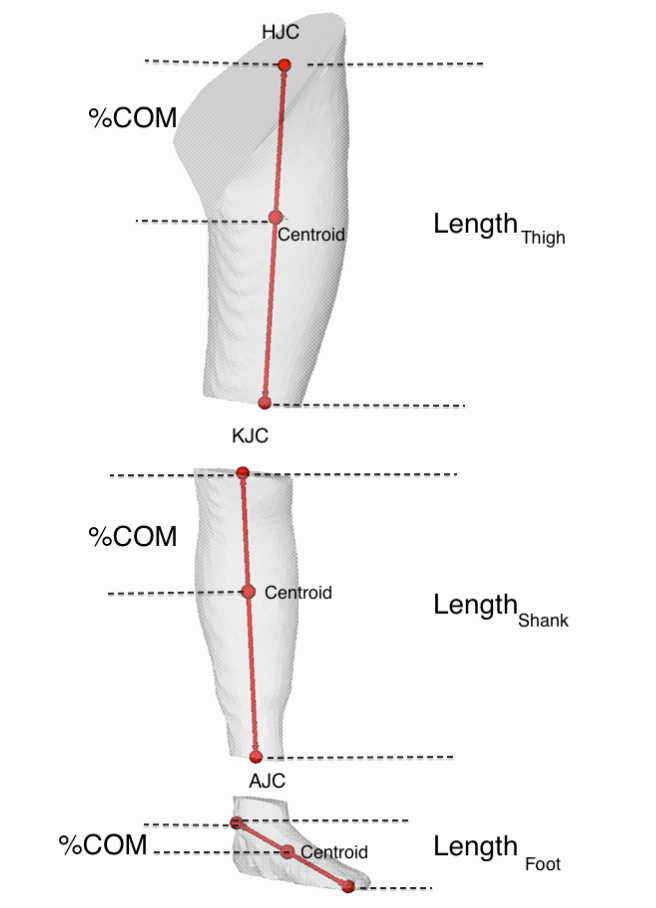

Figure 42: Leg body segments showing centre of mass (Centroid), proximal distance of COM as a percentage of the total longitudinal length of the segment (%COM) and longitudinal length of segment (Length). Estimated Hip joint center (HJC), Knee joint center (KJC), and Ankle joint center (AJC) are shown.

Table 25: Male and Female longitudinal segment length datum and %COM for the Thigh, Shank and Foot obtained using the Kinect and ECM method. Average values adjusted by (Paolo de Leva, 1996) based on (Zatsiorsky, V. & Seluyanov, 1983) except the foot which was not adjusted. Standard deviation shown in brackets.

			Thigh	Shank	Foot*		Thigh	Shank	Foot
Length [mm]	**Male**	**Kinect**	**497.2** (17.4)	**406.3** (16.3)	**246.3** (10.6)	**Female**	**477.1** (26.5)	**386.3** (23.4)	**230.0** (19.2)
		ECM	**475.5** (32.5)	**415.0** (18.8)	**222.7** (3.5)		**426.2** (34.0)	**404.2** (28.8)	**215.8** (12.0)
		Avg	**422.2**	**440.3**	**258.1**		**368.5**	**438.6**	**228.3**
COM [%]		**Kinect**	**43.4** (1.0)	**40.5** (1.3)	**43.5** (2.8)		**44.4** (1.1)	**40.9** (0.9)	**43.4** (2.3)
		ECM	**44.7** (3.3)	**40.0** (1.8)	**39.1** (2.4)		**38.2** (4.6)	**41.2** (1.3)	**38.2** (2.0)
		Avg	**41.0**	**44.0**	**44.2**		**36.1**	**43.5**	**40.1**

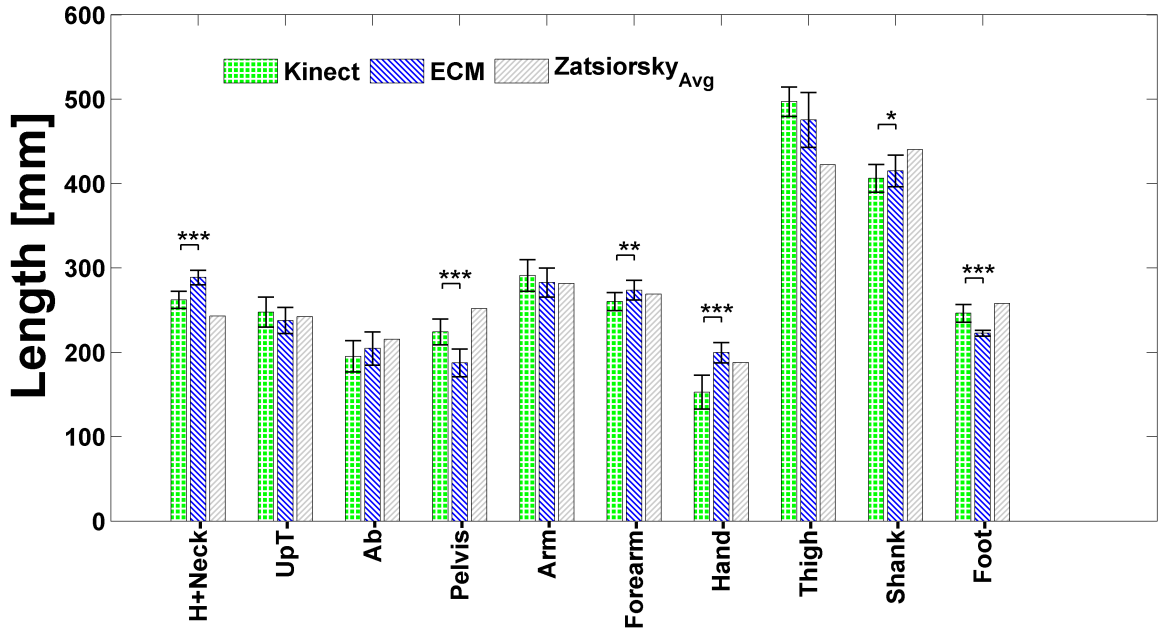

Figure 43 : Summary of longitudinal segment length for **males** comparing estimations obtained using Kinect, ECM and those reported in Zatsiorsky and Seluyanov (1983) Error bars report standard deviation. (***p<0.001, **p<0.01,*p<0.05)

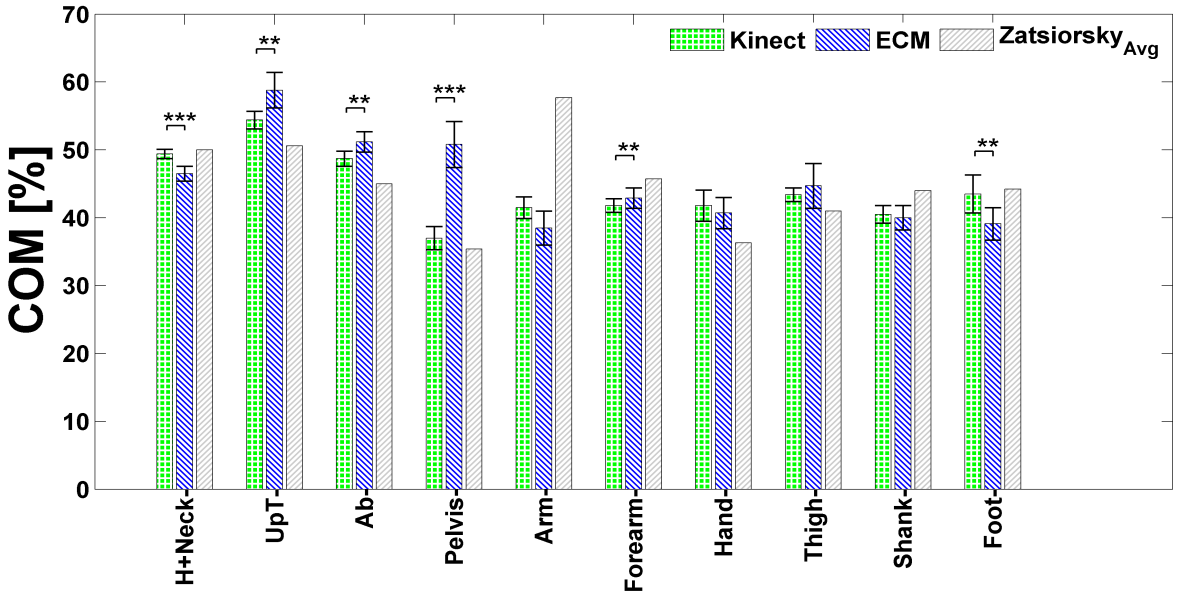

Figure 44: Summary of %COM from proximal endpoint for **males** comparing estimations obtained using Kinect, ECM and those reported in Zatsiorsky and Seluyanov (1983). Error bars report standard deviation. (***p<0.001, **p<0.01,*p<0.05).

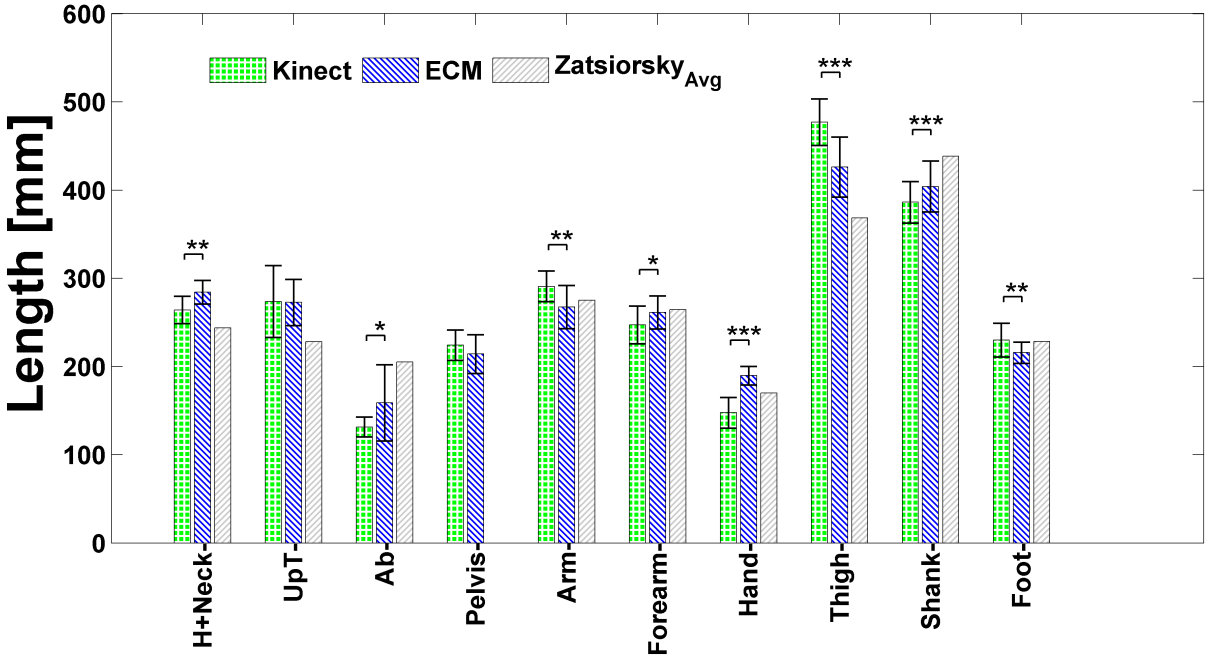

Figure 45: Summary of longitudinal segment length (mm) for **females** comparing estimations obtained using Kinect, ECM and those reported in Zatsiorsky and Seluyanov (1983). Error bars report standard deviation. (***p<0.001, **p<0.01,*p<0.05)

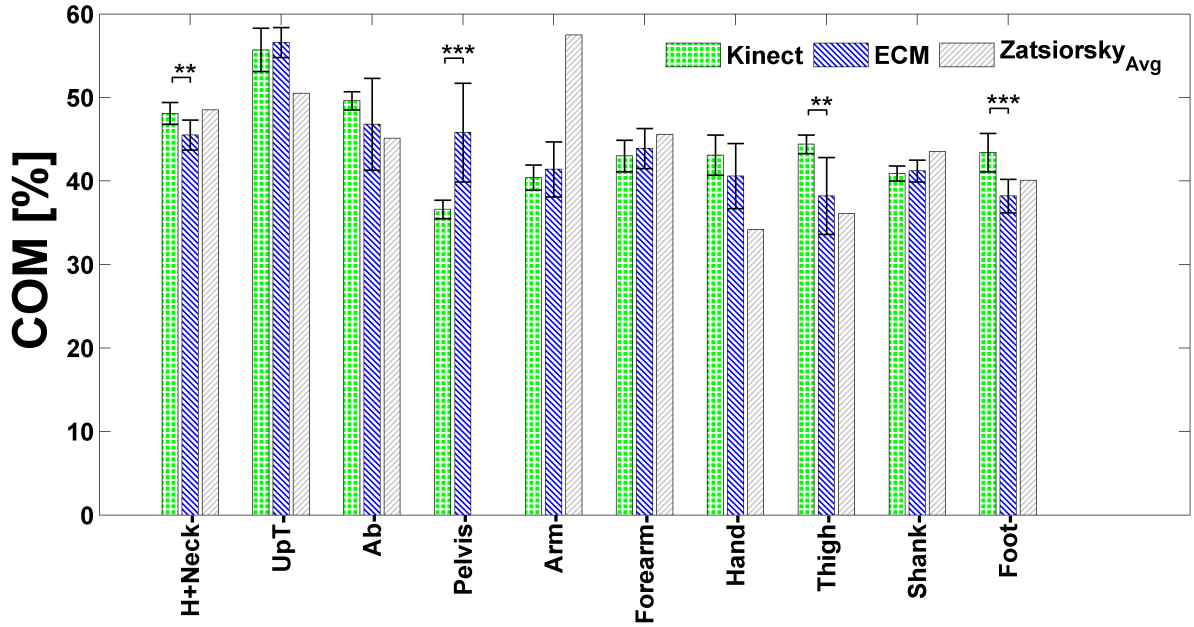

Figure 46: Summary of %COM from proximal endpoint for **females** comparing estimations obtained using Kinect, ECM and those reported in Zatsiorsky and Seluyanov (1983) Error bars report standard deviation. (***p<0.001, **p<0.01,*p<0.05)

4.8 Comparisons of Body Sides

Manual segmentation of the point cloud data resulted in differences seen between opposing segments (left and right). Presented in Table 26 are the average absolute differences between the left and right side segments for males and females for the following estimates: volume, principal MOI (in directions Ixx, Iyy, and Izz), segment length and % COM from proximal endpoint. Large volume differences are seen between sides for the hand (Female= 29.1 % (37.8%), Male= 36.7 % (27.4%)). The large observed standard deviations show that there is a huge spread in this data. The forearm shows the second highest differences between sides (Female = 14 %(15.3%), Male = 14.2 % (8.9%)). Small differences are seen with the thigh, shank and arm with differences of less than 7%.

The MOI results show the highest differences in all three directions for the hand, forearm and foot for both genders. Segment length estimates show low differences (<5%) for all segments except the hand (Female = 9.3 %(9.1%), Male = 11.5 %(9.8%)). Finally, % COM estimates show low differences again (<5%) with the highest variability once again in the hand (Female = 3.7 %(2.5%), Male = 4.4 %(3.3%). A summary of the raw data estimated using the Kinect and ECM methods is provided for in Appendix G.

Table 26: Average absolute differences of left and right side segments for male (n=10) and female (n=11) of estimated BSIP's. Standard deviation is shown in brackets.

		Body Segment					
		Arm	**Forearm**	**Hand**	**Thigh**	**Shank**	**Foot**
Volume	**Female**	**4.7%** (4.7%)	**14.0%** (15.3%)	**29.1%** (37.8%)	**4.1%** (2.2%)	**6.3%** (5.3%)	**10.2%** (8.8)
	Male	**6.5%** (4.6%)	**14.2%** (8.9%)	**36.7%** (27.4%)	**3.1%** (2.7%)	**4.0 %** (2.7%)	**6.1%** (4.9%)
Ixx	**Female**	**8.4%** (4.4%)	**22.7%** (20.1%)	**46.1%** (46.9%)	**4.0%** (2.5%)	**8.5%** (6.3%)	**21.3%** (20.6%)
	Male	**9.6%** (5.9%)	**15.7%** (7.3%)	**64.4%** (45.1%)	**8.2%** (6.4%)	**7.7%** (4.8%)	**10.9%** (9.5%)
Iyy	**Female**	**15.4%** (11.1%)	**23.4%** (24.8%)	**46.2%** (48.6%)	**4.6%** (2.9%)	**9.0%** (7.0%)	**21.0%** (12.0%)
	Male	**8.47%** (6.2%)	**14.61%** (8.3%)	**53.8%** (42.8%)	**8.04%** (5.7%)	**6.25%** (4.6%)	**14.65%** (10.3%)
Izz	**Female**	**9.5%** (4.9%)	**23.9%** (20.9%)	**44.7%** (50.2%)	**7.3%** (3.6%)	**13.3%** (11.5%)	**20.0%** (12.6%)
	Male	**18.7%** (15.4%)	**24.9%** (20.9%)	**48.6%** (34.6%)	**7.3%** (6.4%)	**9.5%** (6.6%)	**13.3%** (8.5%)
Length	**Female**	**2.8%** (1.9%)	**2.6%** (2.8%)	**9.3%** (9.1%)	**0.8%** (0.5%)	**1.6%** (0.9%)	**4.1%** (2.9%)
	Male	**1.9%** (1.4%)	**2.3%** (1.7%)	**11.5%** (9.8%)	**1.9%** (0.6%)	**1.9%** (1.4%)	**3.2%** (2.7%)
COM	**Female**	**2.4%** (1.7%)	**3.1%** (2.5%)	**3.7%** (2.5%)	**1.3%** (0.8%)	**1.1%** (0.8%)	**3.2%** (3.8%)
	Male	**2.5%** (2.2%)	**1.9%** (1.1%)	**4.4%** (3.3%)	**1%** (0.6%)	**1.1%** (0.9%)	**2.6%** (2.2%)

Chapter 5
Discussion

5.0 Introduction

As a primary goal, this experiment sought to investigate whether the 3D data attained using the Microsoft Kinect V2 could be used to estimate subject specific BSIPs. Ten male and 11 female subjects were recruited from the Queen's University student population. Each subject had three full body 3D scans taken using a developed protocol. Each full body scan was manually segmented in Meshlab into 16 segments according to the segmentation protocol of Zatsiorsky and Seluyanov (1983). Data from the body segmentation process were imported into custom MATLAB code, which quantified the resultant BSIP outputs. Also using ECM, developed by Jensen (1978), BSIPs were determined with this subject specific geometric method. The output BSIPs obtained using the Kinect V2 protocol was compared to those from the ECM. Data obtained using Zatsiorsky and Seluyanov (1983) regression equation, which used subject height and mass as input parameters, was compared to the values estimated using the Kinect and ECM methods. This specific set of regression equations was chosen as they were developed using

medical imaging technology with a large subject pool that closely resembled that of this study (Zatsiorsky & Seluyanov, 1983; Zatsiorsky, 2002).

5.1 Comparison of Results

5.1.1 Total Body and Segment Volume

The total body volume estimates were consistent among repeated scans (3 scans per person) with male and female results showing ICC (2, 1) ≥ 0.95. Results estimated using the Kinect were on average 0.0023 m^3 (3%) and 0.0038m^3 (5.1%) higher for males and females respectively when compared to ECM volumetric estimates. The overestimation is consistent with the findings from scanning the cylindrical object, where the Kinect overestimated total volume by approximately 4.2%. The Bland-Altman analysis suggests a fixed measurement bias. All but one case shows the differences were above zero as seen in Figure 33. There is no evidence of any proportional bias suggesting larger volume does not mean larger difference.

In the study by Clarkson et al. (2014) 12 male torsos were scanned and segmented. The author observed a systematic measurement offset of 0.001 m^3 when comparing to the volumes predicted using Yeadon's (1990) geometric model. Clarkson et al. (2014) used an older version of the Kinect device (Version 1), which has a lower depth resolution than the Kinect V2 (Clarkson et al., 2014; Microsoft Corporation, 2015). However, the observations were similar as to those observed in this experiment. The Kinect overestimated the upper torso by approximately 0.0019m^3 and 0.002 m^3 for males and females respectively. The upper torso volume overestimation accounted for 83% of the volume overestimation seen in the total volume of the males and 53% for the females.

The accuracy results of the Kinect V2 from Yang et al. (2015) suggest that based on the distance away the subject was during this experimental protocol, the average depth accuracy error would be around 2mm (Yang et al., 2015). For a scanning volume of $1m^3$ (as an example) this would equate to a scanning error of approximately $0.006m^3$ or about 0.6%. The total scanning volume for the subjects was much lower; therefore, the overestimation cannot be fully attributed by the device measurement errors suggested by Yang et al. (2015).

Concave surfaces and high radius edges (of 90° and greater) have shown to be problematic with the older generation Kinect V1 and are a known issue with many other 3D scanning technologies (Meister et al., 2012). The scanning of concave surfaces or steep edges on the body can result in volume inaccuracies. Although subjects were asked to keep their hands extended during scanning (to prevent cupping) it would appear that the hand/palm region was not estimated in high detail during the scans. Similar observations were seen for the head/ neck region as well as in-between the thighs and under the arms (regions of steep edges). Examples of the head and hands is shown in Figure 47 showing select scans of varying degree of deformity.

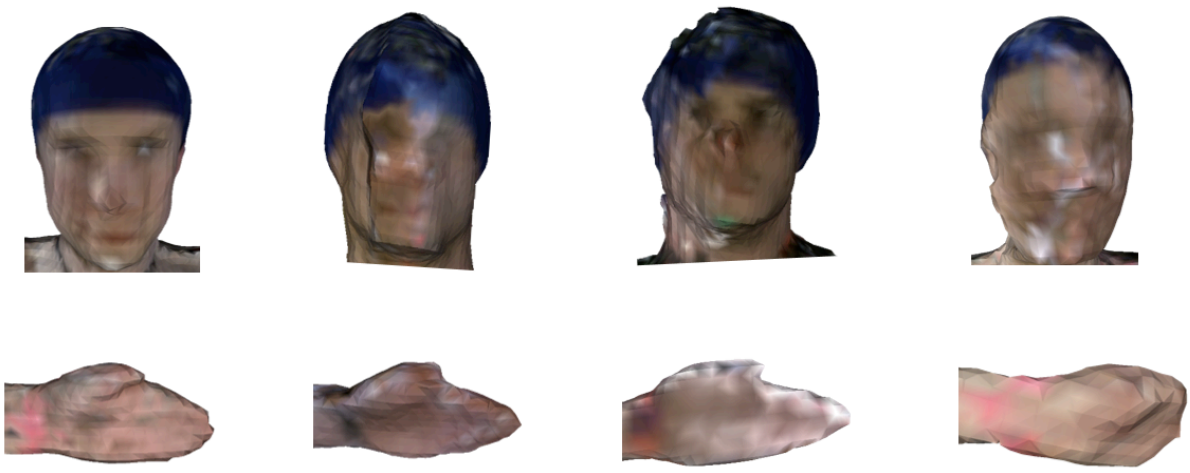

Figure 47: Head and hand scans. Varying degree of detail in the head region with concave surfaces appeared as filled in. Further to the right head suggests subject sway, as facial features are distorted.

Per segment volume results (Figure 34 and Figure 35) suggest that there is the largest significant difference in the estimation of the volume of the upper torso, for both genders (Male t (9): 6.6, $p<0.001$, Female: t (10) = 9.1, $p<0.001$)). This was consistent amongst all of the segmented torsos for males and females. The experiment was designed to limit any error associated with data collection but the manual nature of segmentation performed in the ECM and the 3D segmentation protocol is a factor, which cannot be disregarded. The segmentation of the trunk region required proximal and distal as well as lateral and medial cuts, making the upper trunk section cumbersome to segment. Although every precaution was taken to keep segmentation error to a minimum, errors resulting from the digitization of the trunk (ECM) and planar segmentation of the 3D scans (performed in Meshlab) could explain some of the observed differences. A close up of the segmentation of the torso is shown in Figure 48.

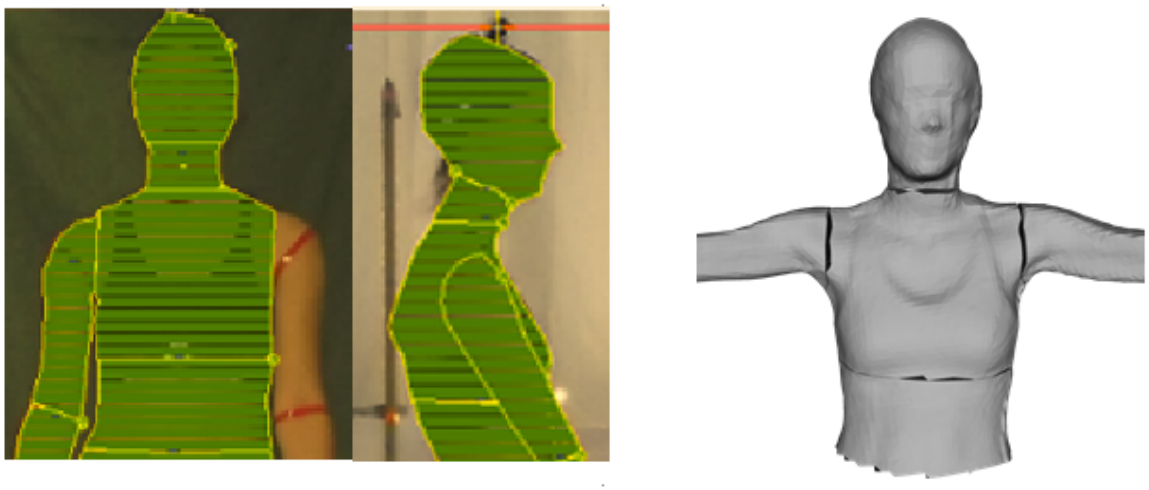

Figure 48: *Left:* Digitization of the trunk region *Right*: Planar segmentation of trunk region

Other possibilities for a larger observed volume could be attributed to the scanning posture. In the ECM protocol subjects stood with their arms closer to the body, whereas in the Kinect protocol the subjects had their arms abducted approximately 90°. The modified pose for the

Kinect was to minimize scanning errors that were observed when the subject had their arms too close to the trunk (Figure 16). The pose could have contributed to a larger observed volume in the scans of the torso. From the 3D scans it appears that this pose extended the chest muscles resulting in the possibility that a larger volume was attributed to upper torso during segmentation. This would mean that the arms would lose volume. In both genders the arms were, on average, estimated to be lower in volume with the Kinect. The torso is highly sensitive to any chest movement resulting from breathing. If the subjects chest was moving during the scanning this could have also attributed to the observed volume discrepancies. In the protocol subjects were asked to take only very shallow breaths during the scanning to minimize this effect.

Deviations from the contours of the body in digitization with ECM could account for errors of volumetric data attained with ECM (Wicke & Lopers, 2003). However, variability was minimized as a single trained operator performed the digitization over 50 times. Wicke and Lopers (2003) stressed the importance of ensuring that the participant was properly aligned with the camera axes during the photo acquisition portion of ECM. Although this was highly enforced in the data collection sessions, slight movement during collection was possible. Wicke and Lopers (2003) commented that the general overestimation seen in the ECM method may have been due to cavities in the shapes of the hand, chest and head (Wicke & Lopers, 2003). Cavities in these regions could have perhaps been less pronounced with the ECM method but picked up with the Kinect, resulting in volume discrepancy.

Additionally, motion artifact during 3D scanning may have contributed to unwanted 3D points, which could result in a discrepancy in the total volume. Although visual inspection made it possible to see when a subject had moved (example: large swaying of the arms resulted in obvious deformations in the scan as shown in Appendix F), it was very difficult to see small

movements. Movements could have contributed to extra points in the cloud resulting in volume overestimation (such as Figure 47, furthest right images). The head scans shown in Figure 47 demonstrate how a slight movement of the head would appear in the scan. Meunier et al. (2000) scanned the heads of subjects with a 3D laser scanner and noted that involuntary movement was unavoidable but could be mitigated with a head rest (Meunier et al., 2000). Goktruk et al. (2004) noticed that the motion artifact in scanning simple objects was mostly observed around the edges of the objects. He proposed an increase in frame rate would minimize the problem (Gokturk et al., 2004). In this protocol the scanning frequency of 30Hz was at the maximum range capability of the Kinect V2 (Microsoft Corporation, 2015). The scan duration of approximately 30 seconds in this experiment is long and standing with your arms raised for this amount of time will almost certainly lead to small vibrations of the body, making this a major limitation. If this pose is to be adapted, allowing support for the arms perhaps by using a string hanging from the ceiling could minimize involuntary movement of the limb.

5.1.2 Mass

The scale mass values provide the closest approximation to the true mass of the subjects. The estimates obtained with ECM show an average body mass overestimation of 0.44kg for the males and 0.45 kg for the females, corresponding to an average error of (M:0. 59%, F:0.64%) when comparing to the scale. The Kinect overestimated mass by 2.34kg for males and 3.88 kg on average for females, corresponding to an average error of (M: 3.11%, F: 5.23%). There appears to be a wide range in mass estimation with Kinect differences ranging from -0.21→4.76kg (Males SD: 1.52) and 0.88→6.20kg (females SD: 1.75) (Table 20 & Table 21). It appears as if

the over/under estimations are random. No correlation between the subjects BMI values, weight, or height is seen when investigating these differences (Appendix F).

The larger discrepancies seen in the female subjects suggest that morphological differences play a role. The thigh, pelvis and upper trunk for the females were estimated to be of larger volume using the Kinect, compared to ECM estimates in turn leading to larger mass predictions. This could have been a result of the breasts and larger hips. The abdomen region for the females shows no significant differences between Kinect and ECM methods however a large average difference is seen when comparing to the regression equation results. It is possible that this is a result of the 12% larger BMI in the female subject pool in this experiment when compared to that of the pool of which the regression equation are based on. The segment mass means compared well for the males across all of the methods (6.4% higher BMI when compared to regression subject pool). On average the per segment results compare well with the Kinect acquired data showing segment mass averages which are also quite similar to the regression equation results. The segmental mass values shown as a percentage of the total weight (Table 22) show trends similar to those mentioned above.

The mass estimates in this experiment were based on density inputs derived from cadavers of a much older population (Chandler et al., 1975) and from CT trunk estimates of a more closely related population (Pearsall et al., 1996). Using a surface scanning technique such as the one proposed here, there is a large amount of versatility with the inputs. For example, Rossi et al. (2013) captured 3D scans of subjects using an Artec 3D Scanner (V0.6) (Price: $5-20k) and with subject specific DEXA scans derived density inputs which were inputted into the 3D scans (Rossi & Lyttle, 2013). The possibility of substituting a highly expensive not widely available camera like the Artec with the Kinect appears promising. Alternatively, carefully selecting

density values to appropriately match the criteria of the subjects being measured from literature is possible reducing the need for expensive medical imaging.

5.1.3 Mass Moments of Inertia

The estimated principal MOI from the 3D scans show measurement means that are comparable to those estimated with ECM and those estimated using the regression equations from Zatsiorsky and Seluyanov (1983). The largest mean differences seen in the Kinect data were in all three principal MOI for the upper torso of the males and females. This was not surprising as this part of the trunk had already shown to be overestimated in volume and consequently, had a larger mass. Calculating the MOI can be challenging to obtain accurately due to the squaring of the moment arm (Wicke & Dumas, 2014). The experimental results observed in this experiment show comparable means for the MOI across the three methods of acquisition. This suggests that the findings show potential.

The Kinect scans deliver consistent outputs amongst repeated scans (25 scans) without visible deviations. From scanning the cylinder, a volume overestimation of 209 cm^3 (4.2%) with a standard deviation of 204 cm^3, was observed which resulted in less than 1% error in calculating the MOI about the Ixx and Iyy axis of the cylinder (coordinate system show in Appendix C). A 7% error was seen in the MOI about the longitudinal (Izz axis). This suggests that the scans were accurately portraying the physical geometry but with a larger radius than measured. This would result in estimating a larger total volume and in turn the MOI about the longitudinal axis Izz would also be larger, as observed. Although larger volumes were observed with scanning the body, this likely did not have a larger effect on the MOI values presented here. The results

suggest that overestimation would be spread evenly (every point slightly overestimated), which would have a small effect on the MOI.

In early studies, only Chandler et al. (1975) presented the MOI data along the principal axes of the body segments. The technique involved supporting each cadaver segment rigidly in a specific orientation and estimating the MOI about several axes during rotation (Chandler et al., 1975). This allowed for computation of the principal axes and an estimation of the inertial tensor. However, the data has been disputed and deemed incorrect as the findings did not satisfy the inequality depicted by **Equation** 8 (Zatsiorsky 2002).

$$I_{yy} + I_{zz} \geq I_{xx}$$

Equation 8: Principal MOI inequality equation. Where Izz is the longitudinal axis Iyy is the medial lateral axis and Ixx is the anteroposterior axis

The MOI data presented in this experiment satisfies the inequity. With the computerized nature of the project it is simple to evaluate this. A major advantage of the MOI estimates taken from 3D scans is that they are highly adjustable. There is a large amount of versatility because the data is programmable. Therefore, the morphology of the subject does not limit the possible outputs. Studies which used cadavers or living body segments (quick release method) are difficult to manipulate once the data is collected, because the collection is highly dependent on the specimen available (examples: (Chandler et al., 1975; Dempster, 1955)). With medical imaging such as DEXA, the MOI is restricted to two planes, limiting the output estimates (Wicke & Dumas, 2008). With the MOI being highly dependent on the orientation, morphology and mass, reporting in various coordinate systems and orientations of the body would not be difficult with

this technique. This suggests potential of the Kinect in future applications, which require MOI estimates.

5.1.4 Segment Length and Center of Mass

The digitization and segmentation were done separately for both methods and could explain some of the mean differences (<5%) seen in the segment lengths. Using ECM, Sanders et al. found a variability of <5% for the longitudinal segment except for the neck (5.2%) (Sanders et al. 2015) Differences in the length of the hand (+25%) with the Kinect (M: $t(9) = 7.43$, $p>0.001$, F: $t(9) = 9.39$, $p>0.001$) may be a result of poor scanning quality of the 3D point cloud (as shown in Figure 47) resulting in possibly a weak definition of the longitudinal vector. There were no observed statistical differences ($p>0.05$) in the longitudinal length of the upper trunk, abdomen, arm, and thigh for the males and the upper trunk for the females. Differences between ECM and Kinect may be attributed to the definitions of the segment endpoints. In ECM anatomical landmarks placed by the operator are manually selected in the Slicer software to define segment endpoints. In the Kinect the longitudinal vector is defined as the inertial axis of each segment (Figures 30-32 show all of the coordinate systems). The length of the vector is based on the proximal and distal intersection of this axis for each segment (passing through the centroid). Although the developed protocol was only a proposed approximation of the segment endpoints, the results validate the method, as the means across both genders do not suggest large differences.

Slight deviations of the location of the joint centers could easily contribute to differences seen in the COM estimates. There was good agreement between Kinect and ECM with differences between methods of fewer than 2% except for the pelvis. The pelvis COM was estimated to be

higher with the ECM by approximately 15% for the males and 9.1% for the females. The lower pelvis length seen with the ECM model suggests that the pelvis length is estimated from the Omphalion to an estimated hip joint centre, whereas in the Kinect protocol this length is from the Omphalion to the pubis. This could however not be verified but the results suggest it to be the case. Although differences are seen for the COM estimates between methods, the results validate that the proposed protocol can estimate the COM of the body segments. With further work this can be further verified and improved upon.

5.2 Segmentation

Segmentation of the 3D scans showed ICC estimates for the segment volumes across two separate segmentations of a single scan to be on average ICC (2,1) ≥0.80 with the foot, arm, forearm and hand showing the lowest values (Male: ICC (2,1) = 0.70 (foot), ICC (2,1) = 0.72 (Forearm and Arm), Female: ICC (2,1) = 0.79 (Foot), ICC (2,1) = 0.74, 0.72 (Left-hand, Right-hand))). The values indicate a high repeatability with ICC ≥ 0.70 considered as adequate (de Vet et al., 2006). The lower ICC values for the foot and arms could be due to the distortion of the anatomical landmark markers present in these regions. The landmarks, which were approximately 2cm in diameter, had a high contrast between the subject and their skin, which acted as segmentation boundaries. Unclear landmarks on the scan could have resulted in less accurate segmentation repeatability. Although tape was used to better define the segmentation boundaries (detailed in Methods 3.1.1), this also was not always clear, as shown in Figure 51. Color scanning requirements, which helped to define the landmarks, is a limitation in the segmentation method of this experiment because the segmentation fully depended on clear color scans.

Another limitation is the scan alignment. Each body scan prior to segmentation was aligned so that the body was positioned along anatomical planes. This was done by aligning the scan about a principal axes (as detailed in the Methods 3.2.3). Segmentations cuts were made about a plane perpendicular to this orientation. Therefore, any misalignment of the scan would result in the perpendicular cut being angled, with the possibility of the segment being sliced on a slant. This would inadvertently affect the inertial estimates.

The time required in post processing is largely due to the segmentation protocol. Each 3D scan took about 45min-1 hour to manually segment following the developed protocol. This suggests the potential for developing a quicker segmentation protocol alongside dedicated segmentation software. One future approach to this could be using the Kinect V2 Skeleton available with the Kinect. This approach could eliminate the land marking reducing the subject interaction time and post processing time (Microsoft Corporation, 2015). Eliminating the manual anatomical land marking and manual segmentation would make it possible for the system to be fully automated.

The Kinect V2 skeleton is capable of estimating up to 25 joints (Microsoft Corporation, 2015). The major difficulty would be in simultaneously capturing the skeleton and the 3D data then overlaying them onto each other (Skeleton and 3D data are in different coordinate systems). A suggested approach to this is shown in Figure 49-50. However, the accuracy of using the Kinect V2 Skeleton in estimating joints which are subject specific has yet to be evaluated in literature. Based on preliminary testing, the capabilities are promising but work still needs to be done.

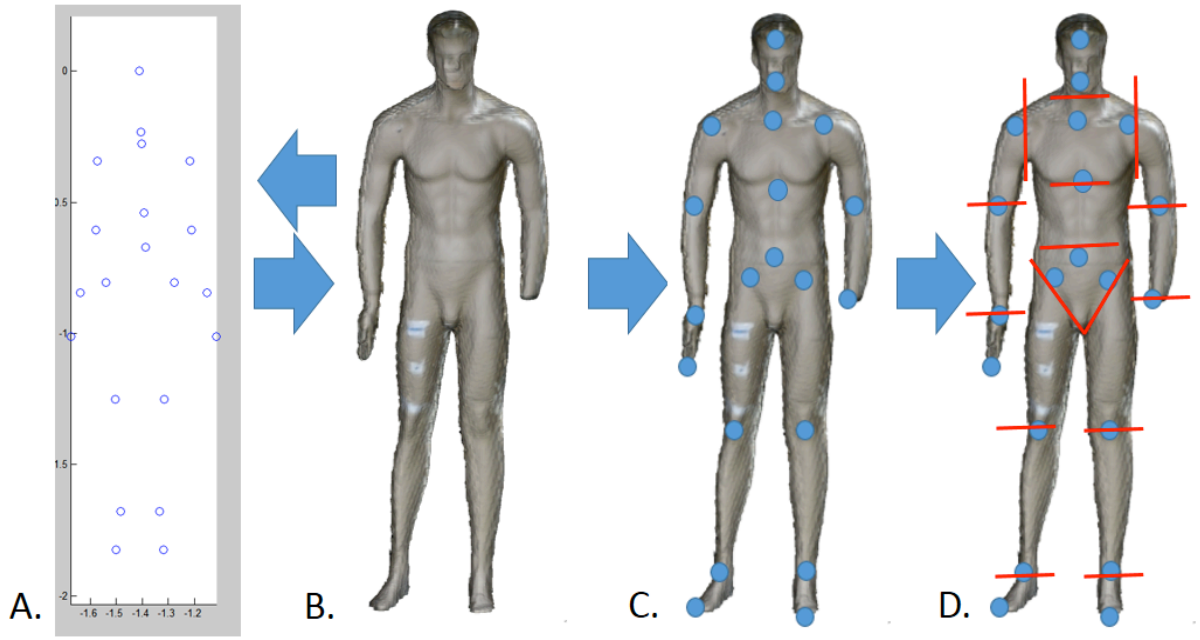

Figure 49: **A:** Kinect Skeleton imported into Matlab. **B:** 3D scans of test manikin. **C.** Hypothetical merging of 3D data with Kinect Skeleton. **D.** Planar segmentation along estimated joints

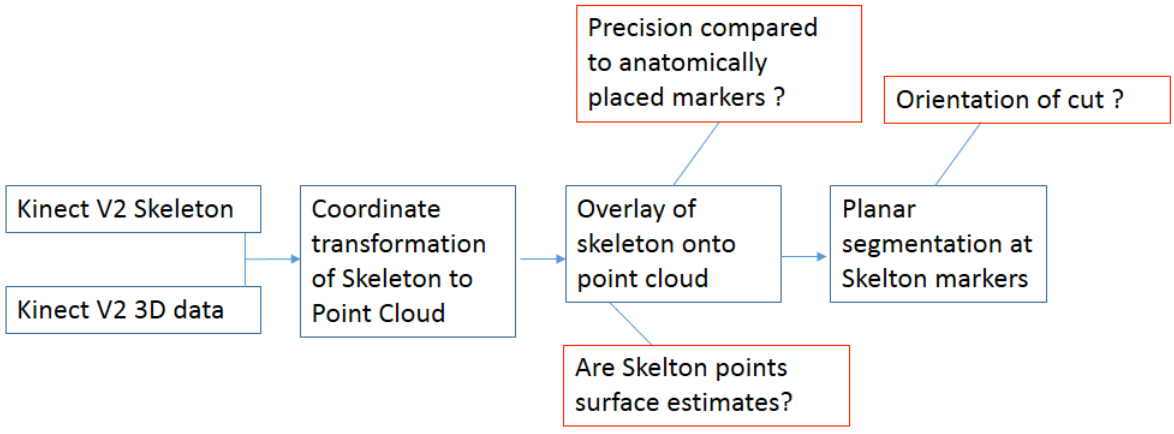

Figure 50: Flow Chart of proposed future segmentation protocol and proposed questions

5.3 Scanning

A major drawback of the scanning protocol was circling the Kinect around the subject. Due to the orientation of the subject (with the arms abducted at 90° to the torso), the Kinect device would come significantly closer to the subject's hands than any other body part (Figure 52-A). It is possible that this could have contributed to errors and explains some of the poor quality scans of the hands (shown in Figure 47). If a subjects arm span was at or above 1 meter then this would mean the Kinect would be viewing the subject's arms at a distance that it reportedly cannot track (Lachat et al., 2015; Microsoft Corporation, 2015; Yang et al., 2015). The exact implications of this are not known. However, as can be seen in Figure 51 it would appear that this could contribute to the consistent discoloration seen along the arms of the subject resulting in loss of landmarks.

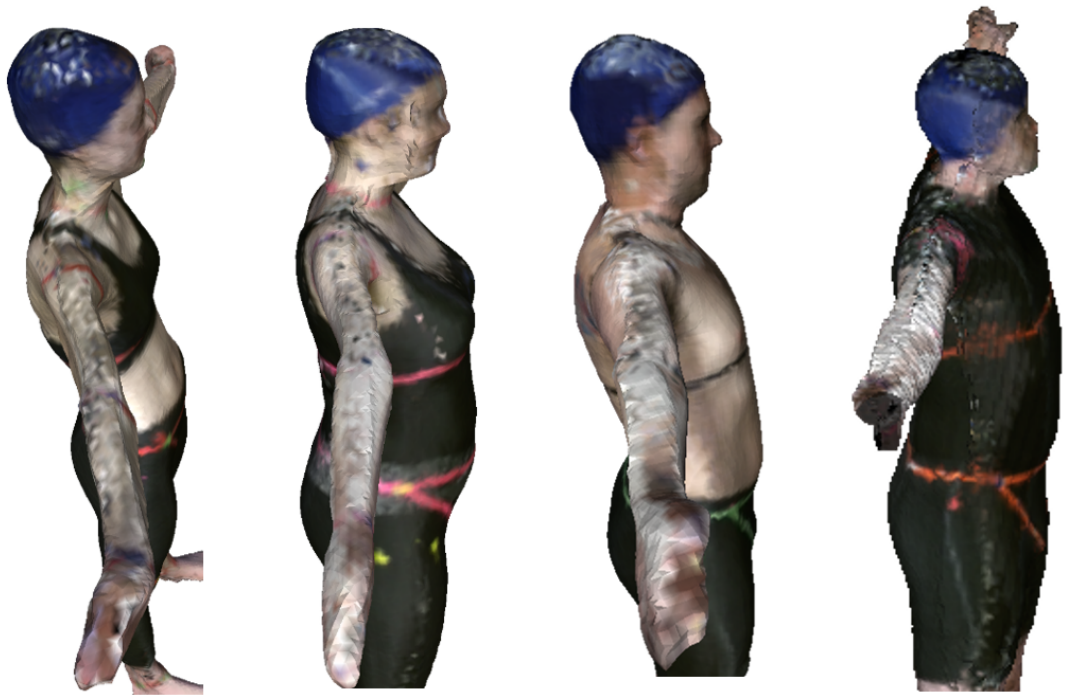

Figure 51: Scans of subjects showing arm discoloration and potential inaccuracies as a result of physical Kinect distance or subject movement.

Figure 52 provides an example of adjusting the subject's arms to optimize the Kinect viewing distance. Alternatively, a larger radius within the area of lowest error (Figure 12) could be used to encircle the subject (Yang et al., 2015). However, due to the limitations imposed by the physical room this experiment took place, this was not possible. As seen in Figure 53, by bending the arm at the elbow and keeping the hands extended and forearms internally rotated it is hypothesized this could minimize the scanning error by increasing the scanning distance.

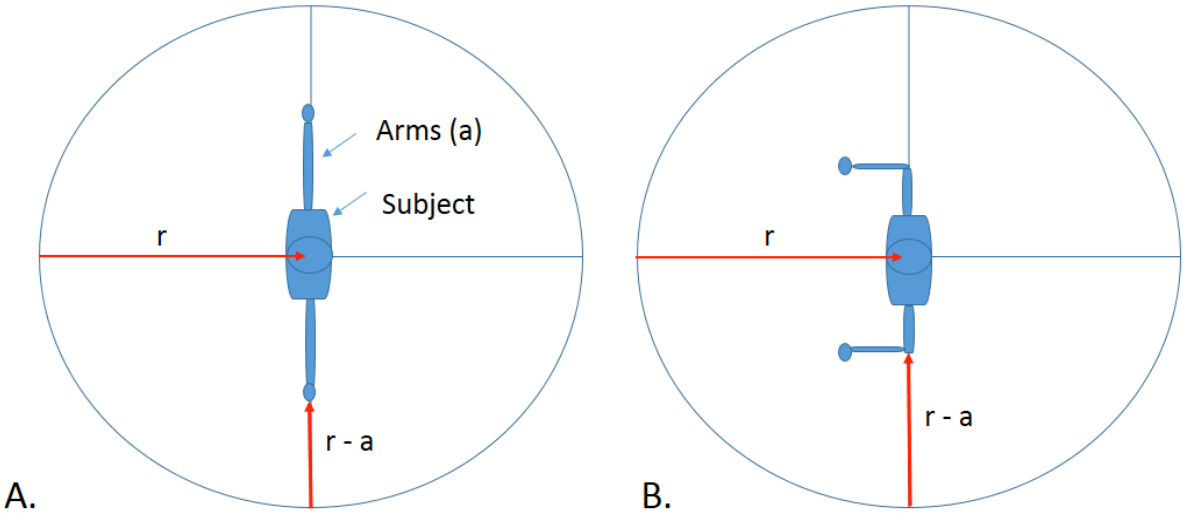

Figure 52: A: The current experimental setup with subject's arms abducted 90 away from torso. The Radius (r) which was 1.5m significantly decrease when the Kinect is near the hands. B. Suggested modified pose to increase radius.

It is possible that the scanning protocol also resulted in the differences seen amongst the both sides of the body (right side versus left side) for the body segments. These differences were highest for the hands and forearms. With the distortion seen from the discoloration poorer visibility of the landmarks also lead to lower repeatability in the segmentation further explaining the results.

5.4 Advantages and Limitations of the Method

The proposed experimental setup is low cost (~$300), simple to use and widely available. As shown, the system is capable of estimating a variety of BSIPs and anthropometric measures, which are specific to the subject of interest. This allows for the measurements to be specific to the subject and not reliant on any prior assumptions on the geometry of the body. In addition, there is the possibility of obtaining data such as segment circumferences even when the subject has already left the data collection. 3D body scans provide the flexibility of archiving the scans if

future subject information needs to be quantified. Another noteworthy advantage of the system is the ease of use, as there is only limited training required. Methods which are subject specific methods can require skilled technicians (Hatze 1980; Yeadon 1990).

The dedicated MATLAB code served as a means of rapidly calculating the desired outputs. However, Meshlab, which is open-source, and freely available software, is capable of estimating all of the parameters, which were estimated in this experiment. If a researcher desires only a couple of measures from a small number of subjects it is definitely possible to acquire volume and MOI parameters from Meshlab (Peyer et al., 2015; Shin et al., 2013). This could keep the associated costs quite low and allow the setup to be very feasible for a wide range of laboratories without excessive programing requirements or high setup times.

The Kinect appears to overestimate volume but almost entirely in the trunk. Further studies should investigate different body types and see if these observations are consistent. Yang et al (2015) proposed techniques to increase the accuracy of the Kinect by using multiple sensors however, further investigation into the hardware technology of the Kinect V2 has yet to be carried out (Yang et al., 2015).

The findings in this experiment suggest that the Kinect V2 setup could be used to acquire BSIP information of subjects without restrictions. Subjects such as: children, high/low BMI subjects, pregnant woman, and amputees to name a few could be better represented by using the proposed setup. Applying generalized models to these populations is not representative and could affect experimental outcomes (Kwon 1996; Pataky et al., 2003). Damavandi et al. (2009) showed that subject morphology is directly related to changes in MOI estimates (Damavandi et al., 2009). Challis and Kerwin (1996) showed joint moments are sensitive to the COM estimation. The limitation however is the density values. This method only acquires the morphological surface

information and not the internal compositions of the body. Therefore, density inputs should be selected based on similar populations for highest accuracy.

The current space requirements suggest a room size of 4mx4m to comfortably carry out the protocol. Although this is not a lot of space it can be a limitation in labs with limited space. Rotating the subject and having the Kinect stationary is a possibility, which was only experimented with to a minor extent. This could be something, which can be invested for further study. Secondly, the posture proposed in this protocol could be difficult for children or patients who are unable to remain still for a longer period of time. In such cases, modifications can easily be made. Researchers wishing for solving BSIPs of only certain segments of the body can develop a modified protocol by simply scanning the segments, which are of interest.

Chapter 6
Conclusions and Recommendations

6.0 Conclusion

The first objective of the project was to determine if it was possible to acquire subject specific BSIP estimates using a Kinect V2 and if so to develop a protocol. A 3D scanning protocol was designed using the Microsoft Kinect V2 as the main acquisition tool. Ten male and 11 female subjects were recruited from the Queen's University student population. Each subject had three full body 3D scans taken following a developed protocol. The protocol used freely available software. 3D Builder, Microsoft's 3D acquisition tool designed for the Kinect V2, was used as the interface to capture point cloud data. Meshlab and Netfabb Basic were used to manipulate, triangulate the points and segment the subject appropriately. Custom written Matlab code, was used to approximate the volume, mass, MOI, COM and longitudinal segment lengths of each of

the body segments. Although it was possible to calculate these this manually in Meshlab, using Matlab the process could be automated and the outputs better tailored. The volumetric results obtained with the Kinect were consistent among 3 repeated scans (ICC (2, 1) ≥0.95).

The second objective was to make comparisons between the estimates obtained using the Kinect V2 system to those obtained with a geometrical model which has been validated in literature Results were compared to predicted values from the ECM (elliptical cylinder model), a geometrical model developed by Jensen (Jensen 1978). The Kinect overestimated total volume on average by 0.0023 m^3 (3%) and 0.0038m^3 (5.1%) for males and females respectively when compared to ECM volumetric estimates. This would appear as a systematic bias because static scanning of a measured cylinder showed volume overestimation of approximately 4.3%. However, the overestimation could be attributed to a variety of factors. Movement of the subject during the scanning protocol, physical distance of the Kinect and the manual segmentation are all factors that may contribute to error in the total segmental volumes.

Total body mass was overestimated on average 2.34 kg for male subjects and 3.88kg for females using the Kinect. ECM showed a slight overestimation on the mass, with an average of 0.44kg for males and 0.24kg. The MOI values across all three estimation techniques were comparable with largest differences seen in the upper torso region. Similar observations were seen for the longitudinal length measures.

The final objective of the project was to conclude on the finding with respect to the value of this device in this field of research. The results suggest great potential for a low cost system (~$300) for acquiring subject specific BSIPs. Without gold standard data it is difficult to conclude whether the observed differences were systematic however the findings show similar results too two other methods performed in this experiment. Although those methods have their own

attributed errors it is promising to see comparable results across all of the BSIP parameters for this specific subject pool. The potential of using the device on subjects of varying morphology and age still needs to be investigated but there is no reason to suggest that the errors would substantially differ from what was observed in this experiment. .

Considering these factors, the Kinect offers the potential of acquiring a wide range of subject segment information at a very low cost. There is flexibility with the segmentation definitions and density inputs, allowing for highly tailored BSIP calculations of subjects of interest. The results suggest that the device would be well accepted in this field.

6.2 Future Recommendations

1. It is proposed to use the Kinect Skeleton V2 to automate the manual segmentation protocol presented in this experiment. By simultaneously capturing the skeleton alongside 3D data one could overlay the data and use the Skeleton joint estimations as the regions of planar segmentation. The Skeleton would need to be further evaluated as to the accuracy of estimating subject specific joint estimates. This could be done by comparing the results obtained from manual land marking to those estimated with the Skeleton.
2. The scanning posture could be modified to reduce the chance of movement during scanning protocol and increase the distance at which the Kinect device is when scanning the arms. This could potentially lead to improved results of the hand and forearm region. Changing the posture could also lead to reducing the chance of subject sway; in turn increasing the quality of the outputs. Reducing sway could also lead to increased view of the anatomical landmarks used for segmentation in the arms.

3. The use of multiple Kinect V2 devices could be investigated to reduce the data acquisition time, minimizing any chance of subject movement. Using multiple devices could also lead to a fully automated system requiring only a single computer operator. If the cameras were position in such a way that they could capture the features of the subject in 360°, this would reduce acquisition time sensationally.

References

Andrews, James G., & Mish, Sean P. (1996). Methods for investigating the sensitivity of joint resultants to body segment parameter variations. *Journal of Biomechanics*, *29*, 651–654.

Baca, Arnold. (1996). Precise determination of anthropometric dimensions by means of image processing methods for estimating human body segment parameter values. *Journal of Biomechanics*, *29*(4), 563–567.

Barmpoutis, Angelos. (2013). Tensor body: real-time reconstruction of the human body and avatar synthesis from RGB-D. *IEEE Transactions on Cybernetics*, *43*(5), 1347–56.

Barter, James T. (1957). *Estimation of the mass of body segments*. Wright Air Development Center, Air Research and Development Command, United States Air Force, Wright-Patterson Air Force Base, Ohio.

Bauer, Jeremy J., Pavol, Michael J., Snow, Christine M., & Hayes, Wilson C. (2007). MRI-derived body segment parameters of children differ from age-based estimates derived using photogrammetry. *Journal of Biomechanics*, *40*(13), 2904–10.

Bjørnstrup, J. (1996). Estimation of human body segment parameters: statistical analysis of results from prior investigations. Aalborg University, Laboratory of Image Analysis.

Bonnechère, B., Jansen, B., Salvia, P., Bouzahouene, H., Sholukha, V., Cornelis, J., Van Sint Jan, S. (2014). Determination of the precision and accuracy of morphological measurements using the Kinect™ sensor: comparison with standard stereophotogrammetry. *Ergonomics*, *57*(4), 622–31.

Brooks, C. B., & Jacobs, A. M. (1975). The gamma mass scanning technique for inertial anthropometric measurement. *Medicine and Science in Sports*, *7*(4), 290–294.

Challis, J. H., & Kerwin, D. G. (1996). Quantification of the uncertainties in resultant joint moments computed in a dynamic activity. *Journal of Sports Sciences*, *14*(3), 219–231.

Chandler, R. F., Clauser, C. E., McConville, J. T., Reynolds, H. M., & Young, J. W. (1975). Investigation of inertial properties of the human body. *Traffic Safety*, (March), 1–169.

Chang, H., Li, Y.W., Chen, H. T., Feng, S.Y. & Chien, T. T. (2013). A dynamic fitting room based on microsoft kinect and augmented reality technologies. In *Human-Computer Interaction. Interaction Modalities and Techniques (*pp. 177-185). Springer Berlin Hedielberg.

Cheng, C. K., Chen, H. H., Chen, Chen S. L., Chen L., & Chen, C. Y. (2000). Segment inertial properties of Chinese adults determined from magnetic resonance imaging. *Clinical Biomechanics*, *15*(8), 559–566.

Choppin, Simon B., Probst, Heidi, Goyal, Amit, Clarkson, Sean, Wheat, Jonathan, & Hospitals, Derby. (2013). Breast volume calculation using a low-cost scanning system. In *4th International Conference Exibition on 3D Body Scanning*. (pp. 11–14).

Cignoni, P., Callieri, M., Corsini, M., Dellepiane, M., Ganovelli, F., & Ranzuglia, Guido. (2008). MeshLab: An Open-Source Mesh Processing Tool. *Sixth Eurographics Italian Chapter Conference*, 129–136.

Clarkson, Sean, Choppin, Simon, Hart, John, Heller, Ben, & Wheat, Jon. (2012). Calculating Body Segment Inertia Parameters from a Single Rapid Scan Using the Microsoft Kinect. In *Proceedings of the 3rd International Conference on 3D Body Scanning Technologies* (pp. 153–163). Ascona, Switzerland: Hometrica Consulting - Dr. Nicola D'Apuzzo.

Clarkson, Sean, Wheat, Jon, Heller, Ben, & Choppin, Simon. (2014). Assessing the Suitability of the Microsoft Kinect for Calculating Person Specific Body Segment Parameters. In *Computer Vision-ECCV 2014 Workshops* (pp. 372-385). Springer International Publishing.

Clarys, J. P., & Marfell-Jones, M. J. (1986). Anatomical segmentation in humans and the prediction of segmental masses from intra-segmental anthropometry. *Human Biology; an International Record of Research*, *58*(5), 771–782.

Clauser, CE, McConville, JT, & Young, JW. (1969). *Weight, volume, and center of mass of segments of the human body*. ANTIOCH Coll Yellow Springs, Ohio.

Damavandi, Mohsen, Barbier, Franck, Leboucher, Julien, Farahpour, Nader, & Allard, Paul. (2009). Effect of the calculation methods on body moment of inertia estimations in individuals of different morphology. *Medical Engineering & Physics*, *31*(7), 880–6.

De Vet, Henrica C. W., Terwee, Caroline B., Knol, Dirk L., & Bouter, Lex M. (2006). When to use agreement versus reliability measures. *Journal of Clinical Epidemiology*, *59*(10), 1033–1039.

Dempster, Wilfred. (1955). Space Requirements of the Seated Operator: Geometrical, kinematic, and mechanical aspects of the body with special reference to the limbs (Wright Air Development Center Tech. Rep. No. 55-159) *Dayton, Ohio: Wright Patterson Air Force Base, WADC (National Technical Information Service No. AD-087892)*

Doumanoglou, Alexandros, Asteriadis, Stylianos, Alexiadis, Dimitrios S., Zarpalas, Dimitrios, & Daras, Petros. (2013). A dataset of Kinect-based 3D scans. *2013 IEEE 11th IVMSP Workshop: 3D Image/Video Technologies and Applications, IVMSP 2013 - Proceedings*.

Drillis, Rudolfs, Contini, Renato, & Bluestein, Maurice. (1964). Body segment parameters: A survey of measurement techniques. *Artificial Limbs*. 8(1), 44-66.

Dumas, Geneviève, Diesbourg, Tara, Budd, Ryan, Labaj, Adam, & Meyer, Florence. (2013). Comparison Between a Subject-Specifc Model to Estimate Moments in the Low back and 3D-SSP. In *XXIV Congress of the International Scoiety of Biomechanics* (pp. 2–3).

Durkin, J., Dowling, J., & Andrews, D. (2002). The measurement of body segment inertial parameters using dual energy X-ray absorptiometry. *Journal of Biomechanics*, *35*(12), 1575–80.

Durkin, J. L. (2008). Measurement and estimation of human body segment parameters. In *Routledge Handbook of Biomechanics and Human Movement Science*. Routledge, Oxford, UK, 197-213.

Durkin, Jennifer. (2003). *Development of a Geometric Modelling Approach for Human Body Segment Inertial Parameter Estimation*. (Doctoral Dissertation, McMaster University)

Durkin, Jennifer L., Dowling, James J., & Scholtes, Laura. (2005). Using Mass Distribution Information to Model the Human Thigh for Body Segment Parameter Estimation. *Journal of Biomechanical Engineering*, *127*(3), 455.

Erdmann, Włodzimierz S. (1997). Geometric and inertial data of the trunk in adult males. *Journal of Biomechanics*, *30*, 679–688.

Espitia-Contreras, Alvaro, Sanchez-Caiman, Pedro, & Uribe-Quevedo, Alvaro. (2014). Development of a Kinect-based anthropometric measurement application. *Proceedings - IEEE Virtual Reality*, 71–72.

Ganley, Kathleen J., & Powers, Christopher M. (2004). Determination of lower extremity anthropometric parameters using dual energy X-ray absorptiometry: The influence on net joint moments during gait. *Clinical Biomechanics*, *19*, 50–56.

Gittoes, Marianne, Bezodis, Ian, & Wilson, Cassie. (2008). An image-based approach to obtaining anthropometric measurements for interia modelling. Journal of applied biomechanics, 25(3), 265-270.

Gokturk, S. B., Yalcin, H., & Bamji, C. (2004). A Time-Of-Flight Depth Sensor - System Description, Issues and Solutions. *2004 Conference on Computer Vision and Pattern Recognition Workshop*.

Hanavan, E. P. (1964). *A mathematical model of the human body. AMRL-TR-64-102. Aerospace*.

Hatze, H. (1975). A new method for the simultaneous measurement of the movement of inertia, the damping coefficient and the location of the centre of mass of a body segment in situ. *European Journal of Applied Physiology and Occupational Physiology*, *34*(4), 217–226.

Hatze, H. (1980). A mathematical model for the computational determination of parameter values of anthropomorphic segments. *Journal of Biomechanics*, *13*(10), 833–843.

Hatze, Herbert, & Baca, Arnold. (1992). Contact-free determination of human body segment parameters by means of videometric image processing of an anthropomorphic body model. In *Applications of Digital Image Processing* (Vol. 1771, pp. 536–546).

Henseler, Helga, Kuznetsova, Alina, Vogt, Peter, & Rosenhahn, Bodo. (2014). Validation of the Kinect device as a new portable imaging system for three-dimensional breast assessment. *Journal of Plastic, Reconstructive and Aesthetic Surgery*, *67*(4), 483–488.

Heymsfield, Steven, Ross, Robert, Wang, ZiMian, & Frager, David. (1997). Imaging Techniques of Body Composition: Advantages of Measurement and New Uses. In *Emerging Technologies for Nutrition Research: Potential for Assessing Military Performance Capability* (pp. 127–150).

Ho, Wei Hua, Shiang, Tzyy Yuang, Lee, Chan Chin, & Cheng, Shiou Yuan. (2013). Body segment parameters of young Chinese men determined with magnetic resonance imaging. *Medicine and Science in Sports and Exercise*, *45*(9), 1759–1766.

Huang, H. K., & Suarez, F. R. (1983). Evaluation of cross-sectional geometry and mass density distributions of humans and laboratory animals using computerized tomography. *Journal of Biomechanics*, *16*, 821–832.

Huang, H. K., & Wu, S. C. (1976). The evaluation of mass densities of human body in vivo from CT scans. *Computers in Biology and Medicine*, *6*(4), 337–343.

Huang, Zhenhao, Xu, Zeke, Li, Zhiyuan, Zhao, Zhuoxiong, & Tao, Dapeng. (2013). Depth and Skeleton Information Model for Kinect Based Hand Segmentation. *Proceedings of the 2013 International Conference on Advanced ICT*, 622–626.

Jensen, Robert K. (1978). Estimation of the biomechanical properties of three body types using a photogrammetric method. *Journal of Biomechanics*, *11*(8), 349–358.

Jensen, R. K. (1993). Human morphology: Its role in the mechanics of movement. *Journal of Biomechanics*, *26*, 81–94

Jensen, RK, & Fletcher, Paula. (1994). Distribution of mass to the segments of elderly males and females. *Journal of Biomechanics*, *21*(1), 89–96.

Kibble, T. W. B., & Berkshire, F. H. (2004). *Classical mechanics*. Imperial College Press.

Kingma, Idsart, Toussaint, Huub M., De Looze, Michiel P., & Van Dieen, Jaap H. (1996). Segment inertial parameter evaluation in two anthropometric models by application of a dynamic linked segment model. *Journal of Biomechanics*, *29*, 693–704.

Kolb, A, Barth, E., Koch, R., & Larsen, R. (2009). Time-of-Flight Sensors in Computer Graphics. *Eurographics 2009 - State of the Art Reports*, 119–134.

Kramer, J., Burrus, N., Echtler, F., Daniel, H. C., & Parker, M. (2012). *Hacking the Kinect*. Vol. 268. New York, NY, USA.

Kwon, Y. H. (2001). Experimental simulation of an airborne movement: Applicability of the body segment parameter estimation methods. *Journal of Applied Biomechanics*, *17*(3), 232–240.

Kwon, Young H. (1996). Effects of the method of body segment parameter estimation on airborne angular momentum. *Journal of Applied Biomechanics*, *12*(4), 413–430.

Lachat, E., Macher, H., Mittet, M. -a., Landes, T., & Grussenmeyer, P. (2015). First Experiences With Kinect V2 Sensor for Close Range 3D Modelling. *ISPRS - International Archives of the Photogrammetry, Remote Sensing and Spatial Information Sciences*, *XL-5/W4*(February), 93–100.

Lee, Mei Kay, Le, Ngoc Sang, Fang, Anthony C., & Koh, Michael T. H. (2009). Measurement of body segment parameters using dual energy X-ray absorptiometry and three-dimensional geometry: an application in gait analysis. *Journal of Biomechanics*, *42*(3), 217–22.

Lephart, SA, IV, JH Bolte, & Albery, CB. (2014). the Inertial Properties of Cadaver Segments, a Comparison of Frozen and Thawed Densities, and Segment Densities Related to Endomorphy and Ectomorphy. *Journal of Sports*, (June), 119–136.

Liu, Y. K., & Wickstrom. (1972). Estimation of the Intertial Property Distribution of the Human Torso from Segmented Cadaveric Data. *Perspectives in Biomedical Engineering*.

Lu, J., & Wang, M. (2008). Automated anthropometric data collection using 3D whole body scanners. *Expert Systems with Applications*, *35*(1-2), 407–414.

Ma, Yanzhao, Kwon, Junghoon, Mao, Zhihong, Lee, Kunwoo, Li, Linlin, & Chung, Hayoung. (2011). Segment inertial parameters of Korean adults estimated from three-dimensional body laser scan data. *International Journal of Industrial Ergonomics*, *41*(1), 19–29.

Martin, P. E., Mungiole, M., Marzke, M. W., & Longhill, J. M. (1989). The use of magnetic resonance imaging for measuring segment inertial properties. *Journal of Biomechanics*, *22*(4), 367–376.

Mcconville, John T., & Churchill, Thomas. (1980). Anthropometric Relationships of Body and Body Segment Moments of Inertia. Anthropology Reasearch Project Inc. Yellow Springs, Ohio.

Meister, Stephan, Izadi, Shahram, & Kohli, Pushmeet. (2012). When can we use KinectFusion for ground truth acquisition? *Proceedings Workshop Color-Depth Camera Fusion Robot.*, 3–8.

Meunier, P., Tack, D., Ricci, a, Bossi, L., & Angel, H. (2000). Helmet accommodation analysis using 3D laser scanning. *Applied Ergonomics*, *31*(4), 361–369.

Microsoft Corporation. (2015). Kinect for Windows Features. Retrieved from http://www.microsoft.com/en-us/kinectforwindows/discover/features.aspx

Mungiole, Michael, & Martin, Philip E. (1990). Estimating segment inertial properties: Comparison of magnetic resonance imaging with existing methods. *Journal of Biomechanics*, *23*(10), 1039–1046.

Nikolova, G. S. (2010). Anthropometric Measurements and Model Evaluation of Mass-Inertial Parameters of the Human Upper and Lower Extremities.

Nikolova, Gergana Stefanova, & Toshev, Yuli Emilov. (2007). Estimation of male and female body segment parameters of the Bulgarian population using a 16-segmental mathematical model. *Journal of Biomechanics*, *40*(16), 3700–7.

Ning, Xiaopeng, Guo, Guodong, & Member, Senior. (2013). Assessing Spinal Loading Using the Kinect Depth Sensor: A Feasibility Study. *IEEE Sensors Journal*, *13*(4), 2012–2013.

Norton, Jonathan, Donaldson, Nicholas, & Dekker, Laura. (2002). 3D whole body scanning to determine mass properties of legs. *Journal of Biomechanics*, *35*(1), 81–86.

Ogeng, Julius. (2014). The Research Value ofthe Cadaver, *3*(3), 366–367.

Oh, Baek-Lok, Kim, Jongmin, Kim, Jongshin, Hwang, Jeong-Min, & Lee, Jehee. (2014). Validity and reliability of head posture measurement using Microsoft Kinect. *The British Journal of Ophthalmology*, 1560–1564.

Paolo de Leva. (1996). Adjustments to Zatsiorsky-Seluyanov's Segment Interia Parameters. *Journal of Biomechanics*, *29*(9), 1223–1230.

Pataky, Todd C., Zatsiorsky, Vladimir M., & Challis, John H. (2003). A simple method to determine body segment masses in vivo: reliability, accuracy and sensitivity analysis. *Clinical Biomechanics*, *18*(4), 364–368.

Pearsall, David J., & Reid, J. Gavin. (1994). The Study of Human Body Segment Parameters in Biomechanics An Historical Review and Current Status Report. *Sports Medicine*, *18*(2), 126–140.

Pearsall, D., & Costigan, P. (1999). The effect of segment parameter error on gait analysis results. *Gait and Posture*, *9*(3), 173–183.

Pearsall, D. J., Reid, J. G., & Livingston, L. a. (1996). Segmental inertial parameters of the human trunk as determined from computed tomography. *Annals of Biomedical Engineering*, *24*(26), 198–210.

Pearsall, D. J., Reid, J. G., & Ross, R. (1994). Inertial properties of the human trunk of males determined from magnetic resonance imaging. *Annals of Biomedical Engineering*, *22*, 692–706.

Peyer, Kathrin E., Morris, Mark, & Sellers, William I. (2015). Subject-specific body segment parameter estimation using 3D photogrammetry with multiple cameras. *PeerJ*, *3*, e831.

Pope, Malcolm H. (2005). Giovanni Alfonso Borelli--the father of biomechanics. *Spine*, *30*(20), 2350–2355.

Rao, Guillaume, Amarantini, David, Berton, Eric, & Favier, Daniel. (2006). Influence of body segments' parameters estimation models on inverse dynamics solutions during gait. *Journal of Biomechanics*, *39*(8), 1531–6.

Reid, J. Gavi., & Jensen, RK. (1990). Human body segment inertia parameters: a survey and status report. *Exercise and Sport Sciences Reviews*.

Reinbolt, J. a., Haftka, R. T., Chmielewski, T. L., & Fregly, B. J. (2007). Are patient-specific joint and inertial parameters necessary for accurate inverse dynamics analyses of gait? *IEEE Transactions on Biomedical Engineering*, *54*(5), 782–793.

Robertson, William S. P. (2013). A modern take on the theoretical modelling of inertial properties of a human body for biomechanical simulations. In *20th International Congress on Modelling and Simulation* (pp. 768–774).

Rossi, Marcel, & Lyttle, Andrew. (2013). Body segment inertial parameters of elite swimmers using DXA and indirect methods. *Journal of Sports(*February), 761–775.

Sanders, Ross H., Chiu, Chuang-yuan, Gonjo, Tomohiro, Thow, Jacki, Oliveira, Nuno, Psycharakis, G., … Mccabe, Carla B. (2015). Reliability of the Elliptical Zone Method of Estimating Body Segment Parame- ters of Swimmers. *Journal of Sports Science and Medicine*, *14*(March), 215–224.

Sarfaty, Ori, & Ladin, Zvi. (1993). A Video-Based System for the Estimation of the Inertial Properties of Body Segments. *Journal of Biomechanics*, *26*(8), 1011–1016.

Shin, Berthold, Venkatramani, Rajkumar, Borker, Priya, Olch, Arthur, Grimm, John, & Wong, Kenneth. (2013). Spatial Accuracy of a Low Cost High Resolution 3D Surface Imaging Device for Medical Applications. *International Journal of Medical Physics,Clinical Engineering and Radiation Oncology*, *02*(02), 45–51.

Silva, Miguel P. T., & Ambrósio, Jorge a C. (2004). Sensitivity of the results produced by the inverse dynamic analysis of a human stride to perturbed input data. *Gait and Posture*, *19*, 35–49.

Smisek, Jan, Jancosek, Michal, & Pajdla, Tomas. (2011). 3D with Kinect. *2011 IEEE International Conference on Computer Vision Workshops (ICCV Workshops)*, 1154–1160.

Staden, H. Von. (1992). The discovery of the body: human dissection and its cultural contexts in ancient Greece. *The Yale Journal of Biology and Medicine*, *65*, 223–241.

Stancic, I., Supuk, Tamara, & Cecic, Mojmil. (2009). Computer vision system for human anthropometric parameters estimation. *WSEAS Transactions on Systems*, *8*(3), 430–439.

Sun, H., & Jensen, R. K. (1993). Body segment growth curves during infancy. *Journal of Biomechanics*, *26*(3), 294.

Tong, Jing, Zhou, Jin, Liu, Ligang, Pan, Zhigeng, & Yan, Hao. (2012). Scanning 3D full human bodies using Kinects. *IEEE Transactions on Visualization and Computer Graphics*, *18*(4), 643–50.

Wall-Scheffler, Cara M. (2012). Size and Shape: Morphology's Impact on Human Speed and Mobility. *Journal of Anthropology*, *2012*, 1–9.

Weber, Immanuel, Koch, Johannes, Meskemper, Joshua, & Friedl, Kim. (2011). Is the MS Kinect system suitable for motion analysis? *Researchgate.net*, 53242.

Weinbach, A. (1938). Contour Maps, Center of Gravity, Moment of Inertia and Surface Area of the Human Body. *Human Biology*, *10*(3), 356–371.

Wheat, Jon, Fleming, Reuben, Burton, Maria, & Penders, Jacques. (2011). Establishing the accuracy and feasibility of Microsoft Kinect in various multi-disciplinary contexts.

Whitsett, Charles Edward. (1963). Some Dynamic Response Characteristics of the Weightless Man. United States Air Force, Wright Patterson, Ohio.

Wicke, Jason, & Dumas, Genevieve a. (2010). Influence of the volume and density functions within geometric models for estimating trunk inertial parameters. *Journal of Applied Biomechanics*, *26*(1), 26–31.

Wicke, Jason, & Dumas, Geneviève a. (2014). A new geometric-based model to accurately estimate arm and leg inertial estimates. *Journal of Biomechanics*, *47*(8), 1869–75.

Wicke, Jason, & Dumas, Genevieve a. (2008). Estimating segment inertial parameters using fan-beam DXA. *Journal of Applied Biomechanics*, *24*, 180–184.

Wicke, Jason, & Lopers, Becky. (2003). Validation of the volume function within Jensen's (1978) elliptical cylinder model. *Journal of Applied Biomechanics*, 3–12.

Williams, Genevieve, Irwin, Gareth, Kerwin, David G., & Newell, Karl M. (2009). Accuracy of Body Mass Prediction using Segmental Inertia Parameters Modelled from Photographic Images. In *ISBS- Conference Proceedings Archive* (Vol. 1, No.1).

Winter, David. (1990). Biomechanics and motor control of human movement (3rd ed.). John Wiley & Sons.

Yang, Lin, Zhang, Longyu, Member, Student, Dong, Haiwei, Alelaiwi, Abdulhameed, & Saddik, Abdulmotaleb El. (2015). Evaluating and Improving the Depth Accuracy of Kinect V2 for Windows, *15*(8), 4275–4285.

Yeadon, M. R., & Morlock, M. (1989). The appropriate use of regression equations for the estimation of segmental inertia parameters. *Journal of Biomechanics*, *22*(617), 683–689.

Yeadon, MR. (1990). The simulation of aerial movement—II. A mathematical inertia model of the human body. *Journal of Biomechanics*, *21*(1), 67–74.

Yessoufou, L., Lawani M.M, & Dumas, G. (2014). Study of the Inertial Parameters Segments among 30 Women of Porto / Novo (Benin) by the Application of the Method of Jensen. Gynecol Obstet (Sunnyvale), 4(241), 2161-0932.

Yokoi, T., Shibukawa, K., Ae, M., Ishijima, M., & Hashihara, Y. (1986). Body segment parameters of Japanese children. *Japanese Journal Physical Education*, (31), 53–66.

Young, J.W., Chandler, R.F., & Snow, C.C. (1983). Anthropometric and mass distribution characteristics of the adult female. (No. FAA-AM-83-16).

Zatsiorsky, V., & Seluyanov, V. (1983). The mass and inertia characteristics of the main segments of the human body. In *Biomechanics VIII-B: Proceedings of the Eight International Congress of Biomechanics* (pp. 1152–1159).

Zatsiorsky, Vladimir M. (2002). Kinetics of Human Motion, *Champaign, IL.*

Appendix A

A.1 Queen's University Ethics Approval

March 09, 2015

Mr. Pawel Kudzia
Master's Student
Department of Mechanical and Materials Engineering
Queen's University
Room 319, McLaughlin Hall
130 Stuart Street
Kingston, ON, K7L 3N6

GREB Ref #: GMECH-033-15; Romeo # 6014999
Title: "GMECH-033-15 Estimating Body Inertial Parameters Using Microsoft Kinet"

Dear Mr. Kudzia:

The General Research Ethics Board (GREB), by means of a delegated board review, has cleared your proposal entitled **"GMECH-033-15 Estimating Body Inertial Parameters Using Microsoft Kinet"** for ethical compliance with the Tri-Council Guidelines (TCPS) and Queen's ethics policies. In accordance with the Tri-Council Guidelines (article D.1.6) and Senate Terms of Reference (article G), your project has been cleared for one year. At the end of each year, the GREB will ask if your project has been completed and if not, what changes have occurred or will occur in the next year.

You are reminded of your obligation to advise the GREB, with a copy to your unit REB, of any adverse event(s) that occur during this one year period (access this form at https://eservices.queensu.ca/romeo_researcher/ and click Events - GREB Adverse Event Report). An adverse event includes, but is not limited to, a complaint, a change or unexpected event that alters the level of risk for the researcher or participants or situation that requires a substantial change in approach to a participant(s). You are also advised that all adverse events must be reported to the GREB within 48 hours.

You are also reminded that all changes that might affect human participants must be cleared by the GREB. For example you must report changes to the level of risk, applicant characteristics, and implementation of new procedures. To make an amendment, access the application at https://eservices.queensu.ca/romeo_researcher/ and click Events - GREB Amendment to Approved Study Form. These changes will automatically be sent to the Ethics Coordinator, Gail Irving, at the Office of Research Services or irvingg@queensu.ca for further review and clearance by the GREB or GREB Chair.

On behalf of the General Research Ethics Board, I wish you continued success in your research.

Yours sincerely,

Joan Stevenson, Ph.D.
Chair
General Research Ethics Board

c: Dr. Genevieve Dumas, Faculty Supervisor

A.2 Letter of Information and Consent Form

Project title: Estimating Body Segment Inertial Parameters using a Microsoft Kinect

Researchers: Pawel Kudzia B.Eng , Geneviève Dumas PhD

Background information: You are being invited to participate in a research study directed by Mr. Pawel Kudzia and overseen by Dr. Geneviève Dumas as part of Mr. Kudzia's Master's thesis to evaluate the feasibility in using a Kinect in estimating morphological parameters of the body. These parameters are necessary in biomechanics specially in estimating loads on joints. We will read through this consent form with you in order to describe procedures in detail and answer any questions you might have. This study is funded by the NSERC Discovery Grant program and has been reviewed for ethical compliance by the Queen's University General Research Ethics Board.

Details of the study:

Purpose: The aim of this study is to evaluate the feasibility and practicality of using a Kinect camera to capture morphological features of the body. Specifically, by using a Kinect, the manual measurement aspects of other methods could be reduced. By reducing manual input in body model, the participant interaction time could be reduced, error can be minimized, and the technical status within the field of anthropometrics and biomechanical analysis can be advanced.

Commitment: Your participation in the current study will consist of a one-hour session in which information regarding the morphology of your body will be captured. Anatomical markers (reflective tape) will be placed on bony landmarks of your body to help the researcher identify these important features in the post processing stage of the experiment. Identification of anatomical landmarks will require the researcher to palpate various locations on your body some of which include: the spine, arms, shoulder and hipbones. You have been asked to wear tight and forming clothing as a means of reducing errors associated with measurement and marker placement. Specifically, male volunteers will have the option to wear forming shorts and either a tight forming shirt or no shirt at all. Female volunteers will be given the option between wearing long or short forming pants and a sports bra or a tight forming workout shirt. Each subject will have their weight taken and their height measured and a few other body measurements.

Once the markers have been placed on you, you will be asked to stand in a designated area of the room with your palms open facing forward. When ready, the researcher will do a quick count down and ask you to stand still for about 3 seconds. Two photographs, snapped at the exact same time, will be taken of you. One photograph will be from the front and one from the right side. The photographs will later be used in a software that helps to estimate 3D volumes and body properties. Next, the researcher will do a second count down and ask you to stand as still as possible for approximately 30 seconds. The researcher will walk around you while holding the Kinect camera. The device will capture your position on the computer and display a cloud of

points that represent your body as a 3D color image. This full process will be repeated three times to ensure that there are no gaps in the data collection or gaps in the 3D reconstruction.

The data acquired from this experiment will be used to understand and evaluate the feasibility of using a Kinect in estimating physical body parameters. If at any point you the subject are uncomfortable with the researcher coming in contact with you even after the full procedure has been briefed to you and the strategies identified in the "Risks" section below are implemented, you will be withdrawn from the study.

Risks: The only known risk you may face in this study is shyness or embarrassment when anatomical landmarks are determined by the researcher. For example, when the researcher must identity landmarks such as the hip bones or greater trochanter of your thigh they will notify you that that area will be identified. To reduce any discomfort the procedure will be very verbally announced as the researcher goes through the process of placing anatomical landmarks on you. To further help with any discomfort the researcher will point to the landmark being identified and verbally ask each time before proceeding to place a marker there.

Benefits: While you may not benefit directly from this study, results from this study may improve our understanding of the feasibility of using the Kinect for collecting physical body parameters.

In/Exclusions: Female and male adults (18-30y) are the target audience for this study. If you are pregnant you do not qualify to be in the study.

Confidentiality: All information obtained during the course of this study is strictly confidential and your anonymity will be protected at all times. You will be identified by a study code so that the data collected will be not be associated with your name. Data will be stored in locked folders accessible only by the researchers listed above. Any photos or images that may be collected will also be stored in protected folders and/or locked cabinets, located in a locked office and locked computer. You will not be identified in any publication or reports.

Payment: Every participant will receive $10 after completing their participation in this study as well as a complementary 3D scan. Your participation is voluntary and you are free to withdraw at any time. There are no consequences for withdrawal from this study. Your signature below indicates that you understand that your participation is voluntary and that you are free to withdraw at any time. If at any time you choose to withdraw all data that was collected from you previously will be destroyed.

Dissemination of findings: Research results will be presented at a conference and/or in an open access publication relevant to the digital library community. The results of this study will be used to assess the repeatability and feasibility in estimating morphological parameters using a Kinect. There are no foreseeable secondary uses of the data.

Any questions about study participation may be directed to Pawel Kudzia at pawel.kudzia@queensu.ca or Professor Geneviève Dumas at Dumas@me.queensu.ca or at 613-533-2648. Any ethical concerns about the study may be directed to the Chair of the General Research Ethics Board at chair.GREB@queensu.ca or 613-533-6081.

This study has been granted clearance according to the recommended principles of Canadian ethics guidelines, and Queen's policies.

Your signature below indicates that you have read this Letter of Information and have had any questions answered to your satisfaction. Please keep a copy of this letter for your records.

"I understand what is being asked of me when participating in this study. I understand that participation in this study is voluntary in nature and that I am free to withdraw at any time. I also understand that every measure will be taken to ensure that my confidentiality is protected. Lastly, I understand that should I have any concerns, questions, or comments regarding my participation in this study, I will contact the researchers (Professor Geneviève Dumas) or the Chair of the General Research Ethics Board."

Name: _____

Date: _____

Signature: _____

A.3 Subject Data Sheet

Date and Time: _____ **Identification Code:**

Private and Confidential: Biomechanics Research Lab
Queen's University, Mechanical and Materials Engineering, Kingston, ON

Subject Name: _____ **Age(y):** _____ **Weight (lbs):** _____ **Height (cm)**_____

Step 1: Experimental Set up

Kinect connected and working	
Cameras set up	
Software ready	
Anatomical Markers ready	
ECM set-up correct	
Consent Form ready	
Folder made for subject	

Step 2: Subject

Subject Briefed	
Consent Form signed	
Tight clothing put on	
Age, Weight, Height	
Anatomical markers (right side)	
Anatomical tape	

Step 3: Data Acquisition

Direct subject to platform for 3D scanning protocol	
Advise to take shallow breaths	
Scan subject until 3 scans have been complete (check list)	
Check scans before saving	
Direct Subject to location of Jensen's protocol	
Acquire Photographs	
Check Photographs	

Final Checklist:

Subject Morphological Information ☐	Frontal and Sagittal Plane photographs acquired ☐	3D body scans with no visible surface error and markers visible	Scan 1 ☐ Scan 2 ☐ Scan 3 ☐

Appendix B

Project Code

Project code is located in an own Cloud File share under the following URL:

https://myfiles.engineering.queensu.ca/public.php?service=files&t=a1b33542acc193d243edc56af12e067a

Password: Kinect

Sample data is provided as well as explicit instructions one how to execute the file. This is included in the read me file.

Appendix C

Measuring Cylinder

$$\text{Volume}_{\text{cylinder}} = \pi r^2 h$$

Equation A-1: Volume of cylinder where r is the radius and h is the height

$$\begin{bmatrix} \frac{1}{12}mh^2 + \frac{1}{4}mr^2 & 0 & 0 \\ 0 & \frac{1}{12}mh^2 + \frac{1}{4}mr^2 & 0 \\ 0 & 0 & \frac{1}{2}mr^2 \end{bmatrix}$$

Equation A-2: MOI along a principal axis of a cylinder with radius r and height h. The mass was calculated based on a cylindrical density of $0.001 kg/cm^3$

Table A-27: Measured cylindrical values

Parameter	Measurement
Radius	4.1cm±0.1cm
Height	94.0cm ±0.1cm
Volume	4964.2cm^3±242.0 cm^3

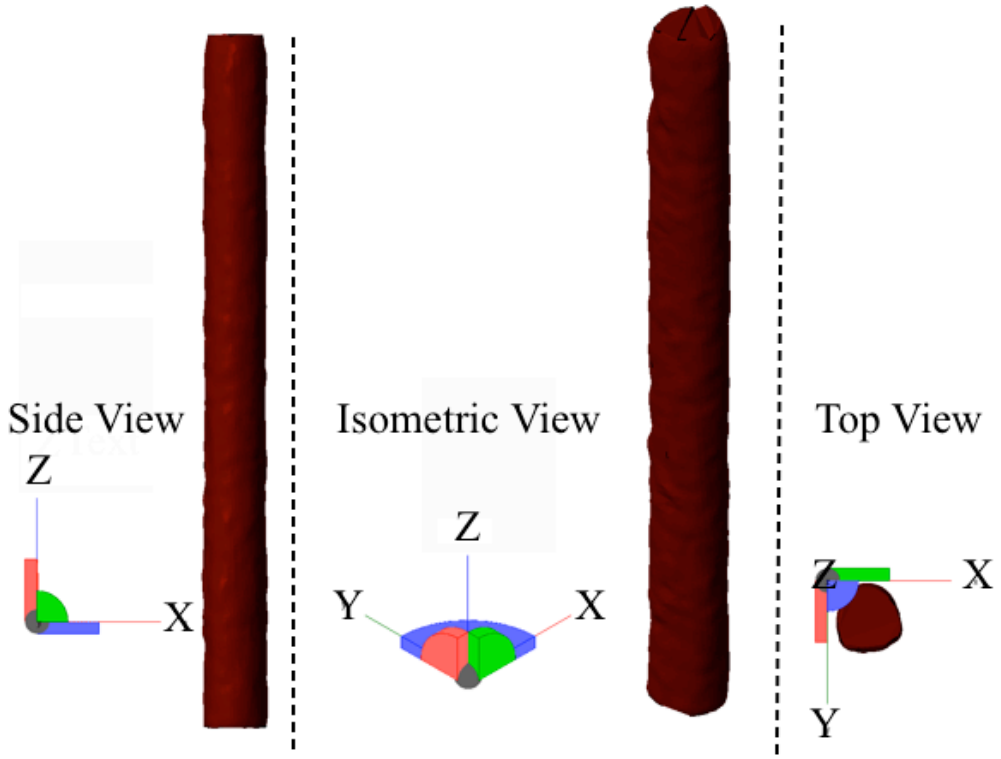

Figure 53: Scanned cylinder showing side, isometric and top view. Coordinate system shown.

Appendix D

Regression Equations

The equations below are in the form of $Y = B_0 + B_1X_1 + B_2X_2$ where X_1 is the body weight in kilograms and X_2 is the height in centimeters. The data is taken from (Zatsiorsky 2002). The axes definitions are shown in 3.3.7 Coordinate Systems.

Table E- 1: Female MOI regression equations with output units ($kgcm^2$)

	Longitudinal axis			Mediolateral axis			Anteroposterior axis		
	B0	**B1**	**B2**	**B0**	**B1**	**B2**	**B0**	**B1**	**B2**
Head	-35.48	2.43	0.237	66.4	-0.447	1.29	217.8	-0.032	0.059
UpperTorso	-2823.2	25.8	12.8	-2075	15.6	9.4	-4038.5	28.6	20
Abdomen	-672.9	1.47	7.53	-546	2.87	5.1	-368.7	-6.22	8.86
Pelvis	-715.9	23.5	-1.106	-633	10.8	2.26	-987.6	14.9	3.76
Thigh	1339.8	6.3	-8.28	-2659.4	50.35	6.96	-4033.4	44.99	17.08
Shank	-53.2	0.284	0.489	-943.3	-2.51	8.47	-963.1	-3.57	9.04
Foot	23.9	0.337	-0.059	-61.4	0.348	0.406	-92.24	0.486	0.558
Arm	-118.6	1.19	0.44	-330.4	-0.461	2.67	-151.4	0.107	1.554
Forearm	7.4	0.21	-0.08	-138.5	0.533	0.887	-132.1	0.62	0.825
Hand	-2.138	0.053	0.0073	-5.79	0.087	0.034	-5.71	0.122	0.035

Table E- 2: Male MOI regression equations with output units ($kgcm^2$)

	Longitudinal axis			Mediolateral axis			Anteroposterior axis		
	B0	**B1**	**B2**	**B0**	**B1**	**B2**	**B0**	**B1**	**B2**
Head	61.6	1.72	0.0814	-112	1.43	1.73	-78	1.171	1.519
UpperTorso	561	36.03	-9.98	367	18.3	-5.73	81.2	36.73	-5.97
Abdomen	1501	43.14	-19.8	263	26.7	-8	618.5	39.8	-12.87
Pelvis	-775	14.7	1.685	-934	11.8	3.44	-1568	12	7.741
RightThigh	-13.5	11.3	-2.28	-3690	32.02	19.24	-3557	31.7	18.61
RightShank	-70.5	1.134	0.3	-1152	4.594	6.815	-1105	4.59	6.63
RightFoot	-15.48	0.0144	0.088	-97.09	0.414	0.614	-100	0.48	0.626
RightArm	-16.9	0.662	0.0435	-232	1.525	1.343	-250.7	1.56	1.512
RightForearm	5.66	0.306	-0.088	-67.9	0.855	0.376	-64	0.95	0.34
RightHand	-6.26	0.0762	0.0347	-13.68	0.088	0.092	-19.5	0.17	0.116

Appendix E

Least squares plots

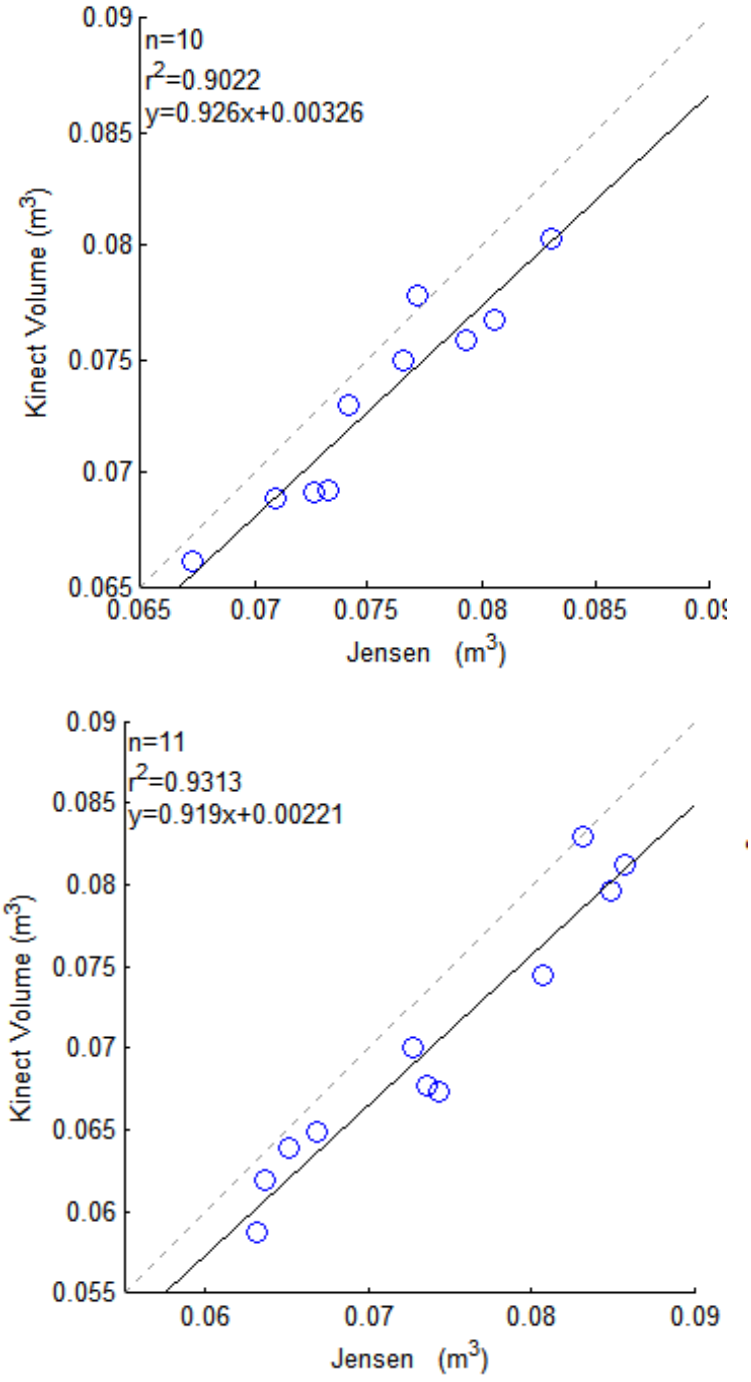

Figure 54: Ordinary least squares plots comparing the Jensen (ECM) against the Kinect volume estimates. Top: Males (n=10). Bottom: Females (n=11).

Appendix F

ECM Outputs

Sample ECM digitization and output data

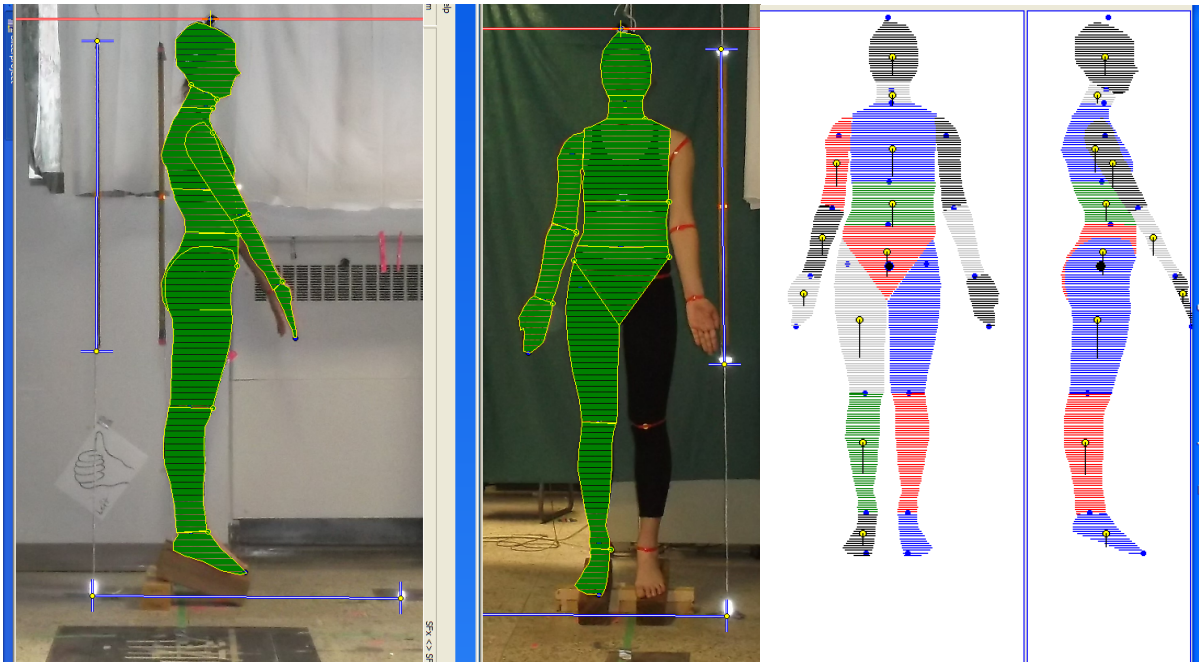

Figure 55: *Left Side*: Manual Digitization of subject in the Slicer software. *Right Side*: ECM output diagram showing COM, segment endpoints and slicing.

Kinect: Examples of Subject Sway

Figure 56: Two scans showing 3D scans which have evidence of the subject swaying or moving during the scan. The hands and the head are most noticeable in distortion

Kinect Differences

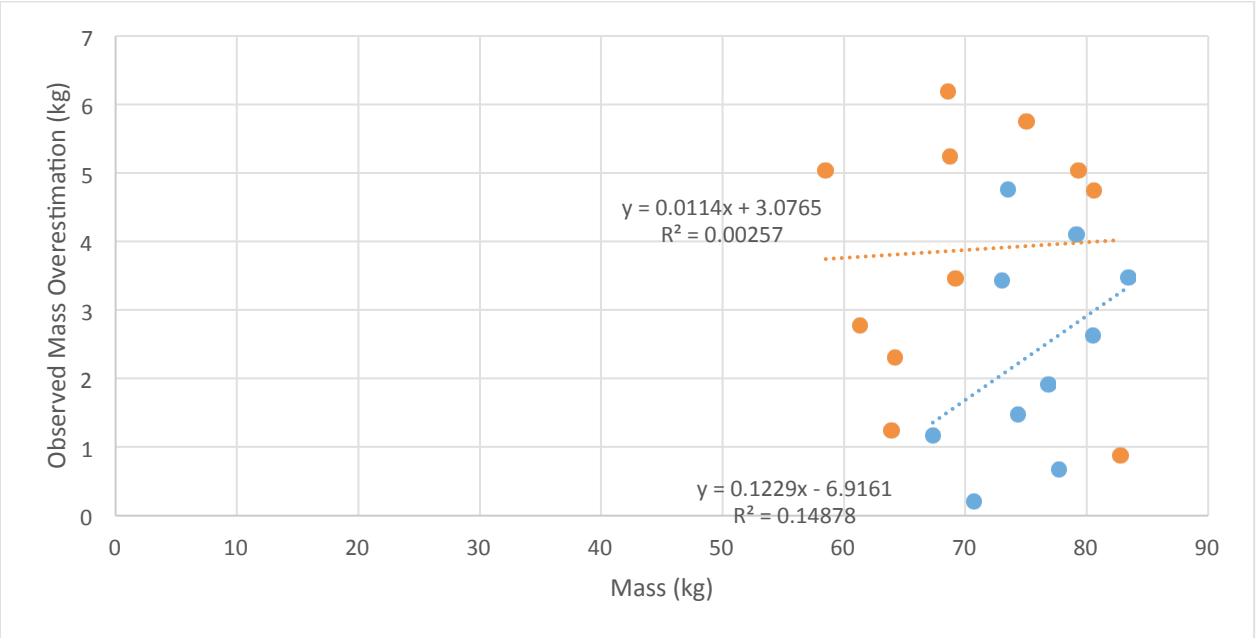

Figure 57: Plot showing subjects mass(kg) against the differences between the scale and Kinect mass estimates for males (blue) and females (orange).

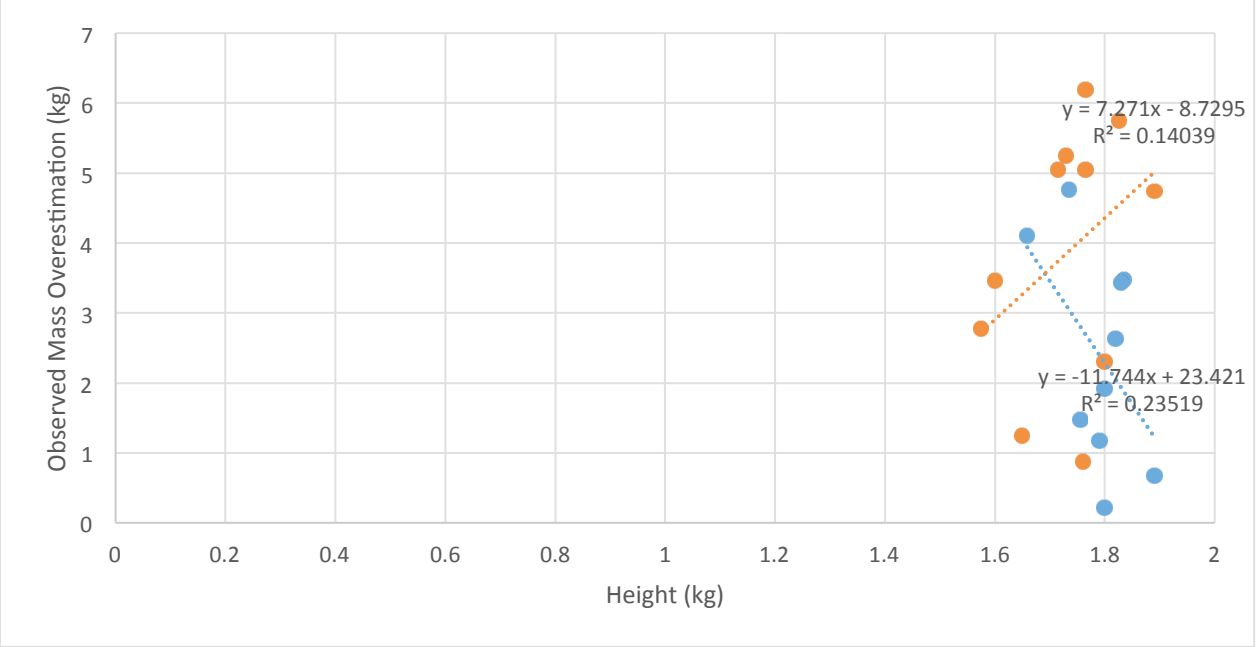

Figure 58: Plot showing subject height (m) against the differences between the scale and Kinect estimates for males (blue) and females (orange).

Appendix G

Kinect Data

Body Segment Volume

Females

Table G-3: Raw Body Segment volume values of 11 female participants as determined using Kinect. A total of 16 segments are shown.

		Female (n =11) VOLUME ESTIMATES $[cm^3]$										
		Subjects										
	Seg	F1	F2	F3	F4	F5	F6	F7	F8	F9	F10	F11
Upper Body	H	5996	5134	4561	4890	5602	4899	4885	4730	5608	4692	4977
	T1	14725	19044	13182	15399	16254	13351	11333	14064	19426	11586	15011
	T2	8602	9373	5858	6605	7462	6903	6079	5851	6539	5192	5752
	T3	8991	11087	7597	8004	8009	7514	6794	7492	11772	7200	8124
Right Side	A	2345	1802	1742	2019	2000	1911	1773	1634	2205	1521	1588
	F	748	730	604	894	1465	727	828	764	922	859	808
	H	343	377	414	383	515	398	443	414	395	348	404
	T	14577	12456	10677	11856	13550	12398	10790	12673	12827	9669	10259
	S	3641	3665	3408	3733	4397	3810	2577	4259	4024	3510	3060
	F	820	780	731	676	959	867	834	1142	1356	924	818
Left Side	A	2364	1736	1617	1723	1794	1904	1802	1729	2171	1553	1566
	F	1078	746	470	815	881	789	868	836	894	909	801
	H	725	382	100	387	289	402	439	354	269	389	408
	T	13974	13095	10199	11613	12771	12690	10650	12719	11934	10121	9569
	S	3575	3780	3284	3149	3823	4014	2715	4795	4020	3736	3041
	F	692	729	724	619	910	983	907	930	1361	936	604

Males

Table G-4: Raw Body Segment Volume values of 10 male participants as determined using Kinect. A total of 16 segments are shown.

	Male (n =10) VOLUME ESTIMATES [$kgcm^2$]										
		Subjects									
	Seg	M1	M2	M3	M4	M5	M6	M7	M8	M9	M10
Upper Body	H	4779	5198	4836	5520	5547	5531	6010	5049	5384	5501
	T1	13398	13482	14603	14886	13311	13002	16240	13339	16316	13594
	T2	12734	11735	13926	10205	8474	10508	10886	10567	10993	8056
	T3	8369	9233	9547	8258	8888	8184	8540	9480	9421	7670
Right Side	A	2095	1939	2658	2001	1952	2071	2251	1787	2195	2068
	F	1009	1004	1260	992	910	1175	1309	931	956	820
	H	468	393	756	477	426	563	607	447	476	272
	T	10318	11288	11761	8825	9904	11380	11478	9961	10569	9003
	S	2995	3408	3537	2697	3787	4034	3228	3406	2952	2724
	F	796	1009	871	911	1215	1486	997	901	824	910
Left Side	A	2005	2056	2264	1956	1931	1897	2124	1821	2101	2360
	F	1158	975	986	1054	847	989	1021	939	1031	1002
	H	460	320	525	467	353	251	287	371	559	450
	T	9972	10153	11529	8975	9782	10862	11235	9815	11459	9125
	S	2851	3321	3189	2745	4033	3925	3310	3383	3111	2880
	F	778	1032	854	959	1318	1289	1029	1058	983	870

Body Segment Moments of Inertia

Females

Table G-5 : Raw Body Segment Data for MOI about the inertial anteroposterior axis (Ixx) of 11 Females subjects determined using Kinect.

		Female (n =11) MOI Ixx $[kgcm^2]$										
		Subjects										
	Seg	F1	F2	F3	F4	F5	F6	F7	F8	F9	F10	F11
Upper Body	H	300	275	371	292	306	321	347	336	383	471	416
	T1	2106	1326	3149	1936	1219	1602	2038	1925	2928	1791	2399
	T2	409	379	582	527	510	604	623	634	1089	861	637
	T3	626	529	1137	582	489	600	733	689	1193	793	690
Right Side	A	131	122	180	143	114	141	144	125	137	200	148
	F	41	52	54	48	39	39	45	34	42	58	44
	H	8	6	5	6	8	7	7	5	6	20	4
	T	1855	1688	2855	2491	1752	2356	2311	1964	2541	2901	2704
	S	321	367	574	490	217	444	413	422	401	385	505
	F	30	42	79	57	32	38	40	20	30	30	44
Left Side	A	137	134	213	149	107	150	154	139	139	230	141
	F	50	51	60	46	33	34	49	42	36	44	98
	H	6	5	9	8	9	7	7	6	7	7	9
	T	1670	1711	2643	2525	1685	2400	2248	1862	2620	2825	2541
	S	325	403	544	573	245	467	415	325	440	366	463
	F	20	40	81	41	36	46	36	16	22	21	34

Table G-6 : Raw Body Segment Data for MOI about the inertial mediolateral axis (Iyy) of 11 Females subjects determined using Kinect.

		Female (n =11) MOI Iyy $[kgcm^2]$										
		Subjects										
	Seg	F1	F2	F3	F4	F5	F6	F7	F8	F9	F10	F11
Upper Body	H	254	236	288	250	255	274	356	249	303	388	311
	T1	1492	991	1555	1378	989	1307	1660	1658	2246	1554	2279
	T2	355	314	493	448	416	482	523	455	806	699	435
	T3	553	466	635	493	427	506	590	588	997	689	1043
Right Side	A	133	130	146	143	101	142	132	131	130	218	201
	F	49	49	48	45	32	33	96	41	36	42	58
	H	5	4	6	7	8	6	8	5	6	6	8
	T	1767	1609	2192	2379	1652	2232	2545	1852	2443	2731	2708
	S	318	361	405	480	215	436	482	416	399	383	565
	F	29	39	38	54	30	36	41	19	28	29	75
Left	A	128	117	137	137	108	131	139	119	130	187	169
	F	40	50	44	47	38	38	42	33	41	56	52

	H	6	6	7	6	7	6	4	5	5	17	4
	T	1614	1629	2149	2432	1588	2309	2443	1764	2479	2709	2521
	S	323	399	410	567	243	454	458	322	435	360	537
	F	20	37	34	38	34	42	33	15	21	20	76

Table G-7**:** Raw Body Segment Data for MOI about the inertial longitudinal axis (Izz) of 11 Females subjects determined using Kinect.

	Female (n =11) MOI Izz [$kgcm^2$]										
		Subjects									
	Seg	**F1**	**F2**	**F3**	**F4**	**F5**	**F6**	**F7**	**F8**	**F9**	**F10**	**F11**
Upper Body	**H**	188	164	195	165	178	175	210	198	193	250	226
	T1	1366	850	1342	1179	789	1027	1582	1332	1939	1226	2132
	T2	233	193	325	212	246	325	379	321	568	465	310
	T3	519	425	568	472	397	467	483	483	831	622	981
Right Side	**A**	16	15	25	18	24	27	27	30	26	35	32
	F	4	5	6	4	5	4	13	6	4	5	6
	H	3	2	2	2	3	2	3	2	2	2	2
	T	392	356	551	566	473	566	676	568	584	752	579
	S	47	61	66	84	37	69	96	65	63	65	71
	F	7	9	8	11	7	7	9	5	6	6	14
Left Side	**A**	15	16	24	19	24	26	22	21	22	39	31
	F	5	6	5	5	6	5	6	5	4	8	6
	H	2	2	2	2	3	2	1	2	2	6	1
	T	346	391	535	583	463	610	598	539	634	677	506
	S	47	67	65	103	40	76	69	49	65	65	70
	F	4	9	8	8	7	9	8	4	6	5	16

Males

Table G-8**:** Raw Body Segment Data for MOI about the inertial anteroposterior axis (Ixx) of 10 males subjects determined using Kinect.

	Male (n =10) MOI Ixx [$kgcm^2$]										
		Subjects									
	Seg	**M1**	**M2**	**M3**	**M4**	**M5**	**M6**	**M7**	**M8**	**M9**	**M10**
Upper Body	**H**	263	300	260	313	299	345	388	262	308	326
	T1	1754	1552	1944	1927	1804	1674	2459	1614	2130	1685
	T2	1363	1148	1498	904	729	1006	1023	899	1032	611
	T3	531	660	683	477	654	548	562	675	665	468
Right Side	**A**	138	149	237	170	167	191	164	143	150	183
	F	54	53	64	61	49	74	75	50	52	42
	H	8	7	23	10	8	10	13	8	9	4
	T	1793	2063	2066	1510	1552	2343	1984	1622	1743	1507
	S	358	405	466	296	478	550	371	399	335	353

	F	6	12	11	10	17	23	12	9	8	10
Left Side	**A**	130	182	218	165	155	160	158	129	140	215
	F	66	59	57	65	46	59	60	54	49	54
	H	9	4	13	9	5	3	3	7	12	10
	T	1686	1664	2134	1504	1397	1996	1810	1531	1823	1508
	S	334	404	447	312	543	611	427	405	336	382
	F	6	12	12	11	20	18	12	12	11	9

Table G-9**:** Raw Body Segment Data for MOI about the inertial mediolateral axis (Iyy) of 10 males subjects determined using Kinect.

	Male (n =10) MOI Iyy [$kgcm^2$]										
		Subjects									
	Seg	**M1**	**M2**	**M3**	**M4**	**M5**	**M6**	**M7**	**M8**	**M9**	**M10**
Upper Body	**H**	325	349	302	368	361	391	449	311	343	377
	T1	866	993	1035	1191	1003	958	1348	993	1365	1032
	T2	1007	855	1097	675	469	731	691	709	715	429
	T3	629	694	763	575	592	573	629	739	758	526
Right Side	**A**	118	145	231	167	160	189	144	138	136	176
	F	52	53	66	60	49	73	73	50	50	41
	H	6	6	21	9	7	9	11	7	8	3
	T	1860	2125	2179	1611	1602	2417	2095	1731	1830	1566
	S	358	410	469	297	480	556	373	404	340	351
	F	29	45	35	37	60	78	42	36	34	41
Left Side	**A**	117	173	202	162	146	159	145	122	132	191
	F	64	58	55	63	45	57	56	52	47	52
	H	7	3	11	8	5	2	2	6	10	9
	T	1720	1734	2225	1572	1446	2076	1907	1625	1930	1588
	S	330	409	442	307	542	610	425	407	338	383
	F	24	46	27	34	67	54	40	45	39	37

Table G-10**:** Raw Body Segment Data for MOI about the inertial longitudinal axis (Izz) of 10 males subjects determined using Kinect.

	Male (n =10) MOI Izz [$kgcm^2$]										
		Subjects									
	Seg	**M1**	**M2**	**M3**	**M4**	**M5**	**M6**	**M7**	**M8**	**M9**	**M10**
Upper Body	**H**	171	193	175	219	229	210	240	191	205	213
	T1	1673	1535	1935	1664	1404	1409	2022	1402	2027	1391
	T2	1203	1129	1530	888	668	870	1051	1009	1125	663
	T3	710	791	872	659	682	650	748	833	865	611
Right Side	**A**	47	29	41	27	27	32	46	23	43	32
	F	9	8	14	7	6	9	12	7	8	5
	H	4	3	7	3	3	5	6	3	3	1
	T	423	507	536	325	402	487	535	409	461	342

	S	47	65	61	40	70	79	54	62	45	39
	F	29	45	34	38	54	70	40	36	36	37
Left Side	**A**	38	32	39	28	32	32	34	27	33	57
	F	10	8	8	13	5	7	8	7	9	8
	H	3	2	5	3	2	1	2	2	4	3
	T	395	421	493	327	389	423	523	398	541	342
	S	46	57	48	44	78	68	56	59	50	38
	F	24	41	26	35	59	57	39	46	36	33

Raw ECM Data

Body Segment Volume

Females

Table G-11: Raw Body Segment Volume values of 11 Females participants as determined using ECM.

	Female (n =11) VOLUME ESTIMATES [cm^3]										
		Subjects									
	Seg	**F1**	**F2**	**F3**	**F4**	**F5**	**F6**	**F7**	**F8**	**F9**	**F10**	**F11**
Upper Body	**H**	6183	5482	4782	4995	5380	4809	4587	4312	5295	4491	4851
	T1	13695	17232	12343	12866	13828	11107	9247	11427	16356	9902	11941
	T2	7755	7429	5862	6532	7508	6518	5852	5649	6163	5149	5720
	T3	8935	10841	7529	7916	7789	7493	6769	7086	11653	7193	8135
Right Side	**A**	2382	1767	1814	1877	2031	1926	1841	1767	2295	1536	1580
	F	1036	820	693	873	1047	974	872	786	1106	726	851
	H	486	334	407	543	451	337	533	431	557	305	456
	T	14667	12202	9625	11050	11373	11556	10899	11360	11799	9174	9964
	S	3552	3377	3355	3778	4171	3383	2709	4164	4027	3328	3153
	F	1035	795	783	750	887	712	882	939	1121	914	1111

Males

Table G-12: Raw Body Segment Volume values of 11 Females participants as determined using ECM.

	Male (n =10) VOLUME ESTIMATES [cm^3]										
		Subjects									
	Seg	**M1**	**M2**	**M3**	**M4**	**M5**	**M6**	**M7**	**M8**	**M9**	**M10**
Upper	**H**	4779	5384	4916	5231	5644	5627	5601	4928	5284	5498
	T1	11857	13022	13207	12650	11374	12077	12512	10738	14040	11506

	T2	10965	11606	13903	10061	8053	10379	9909	10313	10351	8117
	T3	8392	8845	9359	8281	8890	8124	8540	9527	9445	7658
Right Side	**A**	2062	1979	2776	2086	1989	2153	2254	1833	2210	2133
	F	1186	1163	1198	1239	869	1232	1405	926	1118	983
	H	708	706	659	640	551	697	683	485	567	504
	T	10757	10068	10383	8563	9522	11119	11314	9085	10498	9148
	S	2905	3205	3582	2871	3787	4264	3366	3448	3049	2993
	F	896	943	849	936	867	1317	1090	1081	923	927

Body Segments Moments of Inertia

Females

Table G-13: Raw Body Segment Data for MOI about the inertial anteroposterior axis (Ixx) of 11 Females subjects determined using ECM.

	Female (n =11) MOI Ixx [$kgcm^2$]										
		Subjects									
	Seg	**F1**	**F2**	**F3**	**F4**	**F5**	**F6**	**F7**	**F8**	**F9**	**F10**	**F11**
Upper Body	**H**	0	0	0	0	0	0	0	0	0	0	0
	T1	1393	2235	1220	1306	1561	988	798	1198	2087	890	1228
	T2	591	589	378	459	546	429	381	391	393	311	353
	T3	616	1126	471	525	486	563	414	459	1178	566	651
Right Side	**A**	180	126	133	117	170	127	112	158	217	131	131
	F	51	45	30	46	57	49	38	48	77	43	49
	H	13	6	8	13	12	9	12	10	16	7	12
	T	2914	2536	1411	1719	2211	2187	1715	2204	2505	1576	1970
	S	422	428	380	449	574	453	243	607	654	418	393
	F	44	34	31	27	43	33	36	44	61	41	58

Table G-14: Raw Body Segment Data for MOI about the inertial mediolateral axis (Iyy) of 11 Females subjects determined using ECM.

	Female (n =11) MOI Iyy [$kgcm^2$]										
		Subjects									
	Seg	**F1**	**F2**	**F3**	**F4**	**F5**	**F6**	**F7**	**F8**	**F9**	**F10**	**F11**
Upper Body	**H**	0	0	0	0	0	0	0	0	0	0	0
	T1	1003	1514	962	954	1081	739	547	825	1559	659	908
	T2	396	397	242	302	376	305	236	210	294	193	236

	T3	803	915	617	632	630	501	489	511	996	466	561
Right Side	A	189	21	138	126	175	24	117	162	231	133	135
	F	50	44	30	44	55	8	37	47	75	42	48
	H	11	5	7	11	10	2	11	8	14	6	10
	T	3029	571	1506	1857	2336	2342	1865	2339	2645	1673	2071
	S	426	431	387	462	584	459	245	617	659	432	398
	F	42	33	30	27	42	33	35	42	59	39	59

Table G-15: Raw Body Segment Data for MOI about the inertial longitudinal axis (Izz) of 11 Females subjects determined using ECM.

	Female (n =11) MOI Izz [$kgcm^2$]										
	Subjects										
	Seg	F1	F2	F3	F4	F5	F6	F7	F8	F9	F10	F11
Upper Body	H	0	0	0	0	0	0	0	0	0	0	0
	T1	1205	1756	886	1061	1159	809	617	815	1409	625	825
	T2	749	833	444	606	632	557	464	450	553	375	423
	T3	693	851	499	529	540	478	396	440	967	419	508
Right Side	A	35	130	20	25	24	132	23	18	31	14	15
	F	9	6	4	6	9	46	7	5	9	4	6
	H	4	2	3	4	3	8	4	3	4	2	3
	T	790	2678	416	524	508	537	515	499	521	341	378
	S	67	57	58	73	83	56	43	80	72	57	50
	F	10	6	6	6	7	5	7	8	11	8	10

Males

Table G-16: Raw Body Segment Data for MOI about the inertial anteroposterior axis (Ixx) of 10 males subjects determined using ECM.

	Male (n =10) MOI Ixx [$kgcm^2$]										
		Subjects									
	Seg	M1	M2	M3	M4	M5	M6	M7	M8	M9	M10
Upper Body	H	0	0	0	0	0	0	0	0	0	0
	T1	1180	1347	1418	1286	1103	1164	1303	963	1542	1068
	T2	1118	1039	1600	929	671	1000	919	851	916	580
	T3	543	611	703	655	755	544	692	820	691	484
Right Side	A	163	171	276	186	178	225	211	158	186	217
	F	75	74	77	82	49	77	86	60	61	64
	H	20	21	20	17	12	20	18	11	15	12
	T	1956	1857	2043	1404	1674	2433	2059	1582	1912	1742
	S	355	419	543	382	541	614	444	442	381	422
	F	43	43	43	47	42	70	55	55	48	47

Table G-17: Raw Body Segment Data for MOI about the inertial mediolateral axis (Iyy) of 10 males subjects determined using ECM.

	Male (n =10) MOI Iyy [$kgcm^2$]										
		Subjects									
	Seg	M1	M2	M3	M4	M5	M6	M7	M8	M9	M10
Upper Body	H	0	0	0	0	0	0	0	0	0	0
	T1	731	936	880	897	740	754	854	639	1025	792
	T2	752	821	1091	642	436	700	608	685	651	445
	T3	711	753	802	571	633	631	602	731	853	516
Right Side	A	169	176	288	193	185	235	220	165	199	225
	F	73	70	74	80	47	74	82	58	58	63
	H	17	17	17	15	10	16	16	9	12	10
	T	2014	1952	2151	1514	1734	2526	2176	1668	2024	1830
	S	360	429	548	389	551	634	452	448	388	428
	F	41	43	41	45	40	69	56	52	46	46

Table G-18: Raw Body Segment Data for MOI about the inertial longitudinal axis (Izz) of 10 males subjects determined using ECM.

	Male (n =10) MOI Izz [$kgcm^2$]										
		Subjects									
	Seg	M1	M2	M3	M4	M5	M6	M7	M8	M9	M10
Upper Body	H	0	0	0	0	0	0	0	0	0	0
	T1	1041	1083	1232	1031	854	1080	1058	856	1297	864
	T2	947	1243	1469	867	590	857	858	990	1057	717
	T3	619	652	714	558	605	562	593	703	734	566
Right Side	A	26	23	41	25	23	25	29	20	31	25
	F	11	10	11	11	6	12	15	6	10	7
	H	7	7	6	6	5	7	6	4	5	4
	T	447	415	421	315	366	442	502	339	446	331
	S	46	53	58	41	67	87	57	59	49	45
	F	7	8	6	7	7	14	10	10	7	7